Non-Linear Dynamics - Phenomenology

Yannis PAPAPHILIPPOU
Accelerator and Beam Physics group
Beams Department
CERN

CERN Accelerator School

Advanced Accelerator Physics Course 2024

Spa, Belgium

10-22 November 2024

Summary

- Phase space dynamics – fixed point analysis
- Poincaré map
- Motion close to a resonance
- Onset of chaos
- Chaos detection methods
  - Dynamic Aperture
  - Lyapunov exponent
  - Frequency map analysis
  - Numerical applications

Phase space dynamics - Fixed point analysis

Phase space dynamics

- Valuable description when examining trajectories in **phase space** (u, p_u)
- Existence of integral of motion imposes geometrical constraints on phase flow
- For the simple **harmonic oscillator**

$$H = \frac{1}{2}\left(p_u^2 + \omega_0^2 u^2\right)$$

phase space curves are **ellipses** around the equilibrium point parameterized by the Hamiltonian (energy)

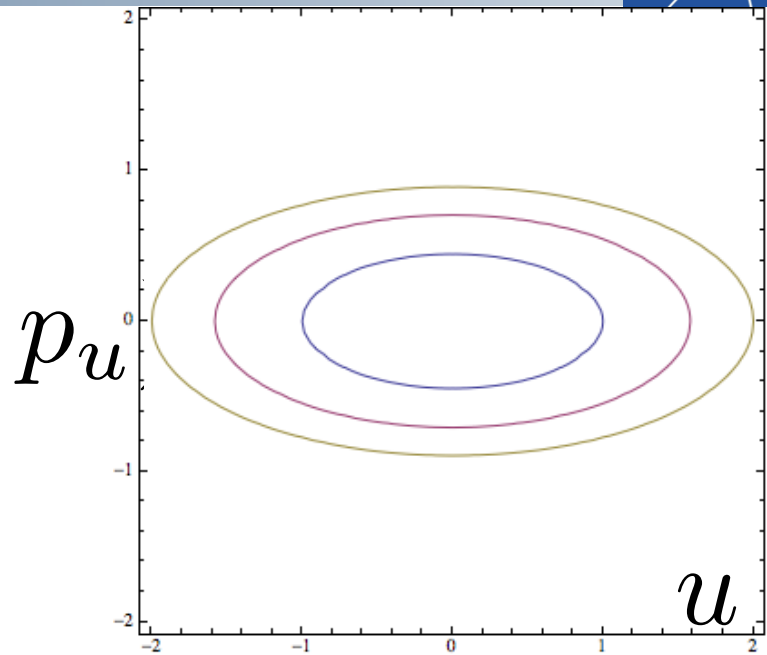

Phase space dynamics

- Valuable description when examining trajectories in **phase space** (u, p_u)
- Existence of integral of motion imposes geometrical constraints on phase flow
- For the simple **harmonic oscillator**

$$H = \frac{1}{2}\left(p_u^2 + \omega_0^2 u^2\right)$$

phase space curves are **ellipses** around the equilibrium point parameterized by the Hamiltonian (energy)

- By simply **changing** the **sign** of the potential in the harmonic oscillator, the phase trajectories become **hyperbolas**, symmetric around the equilibrium point where two straight lines cross, moving towards and away from it

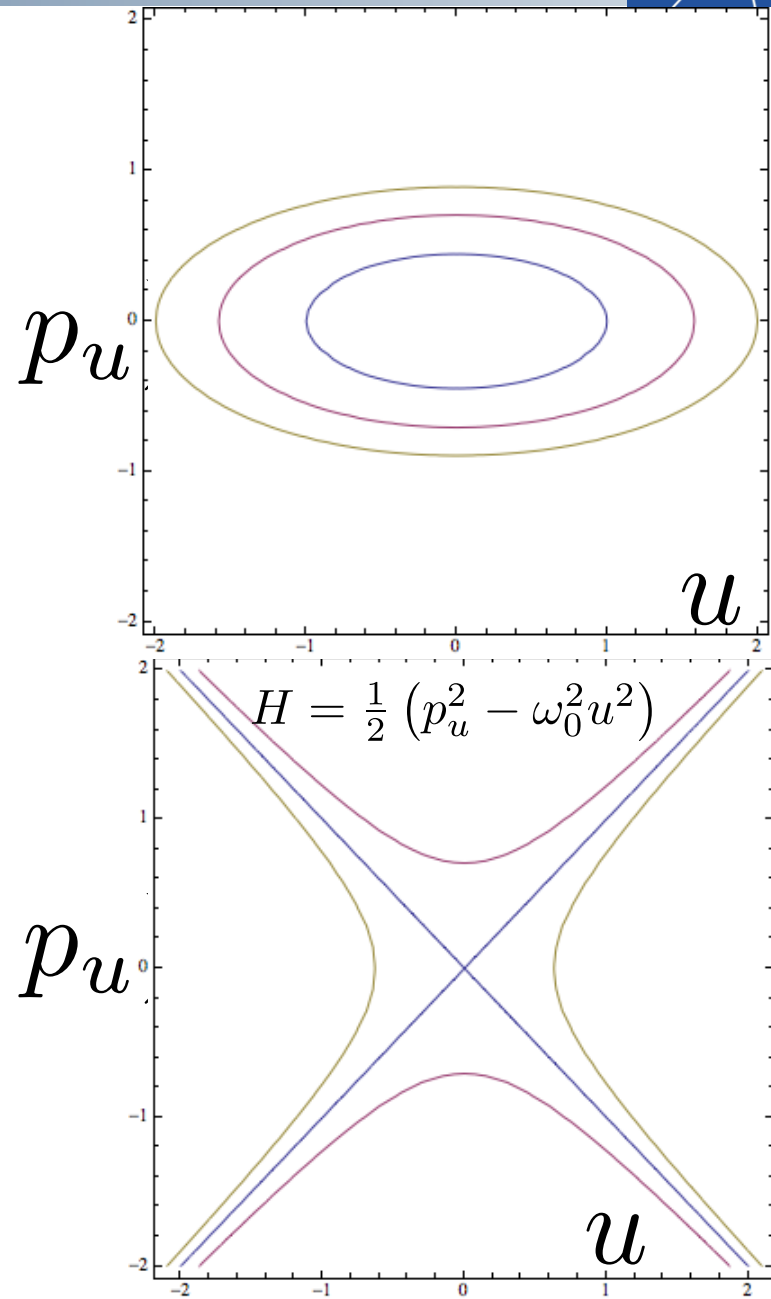

Non-linear oscillators

- Conservative non-linear oscillators have Hamiltonian

$$H = E = \frac{1}{2}p_u^2 + V(u)$$

  with the potential being a general (polynomial) function of positions
- **Equilibrium points** are associated with extrema of the potential

Non-linear oscillators

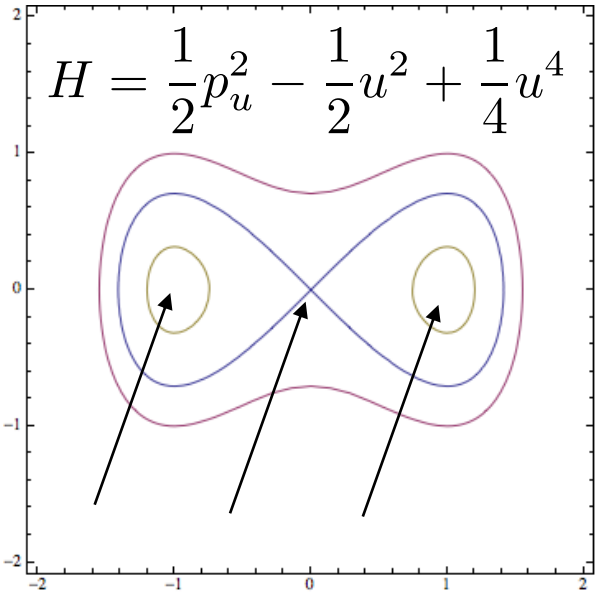

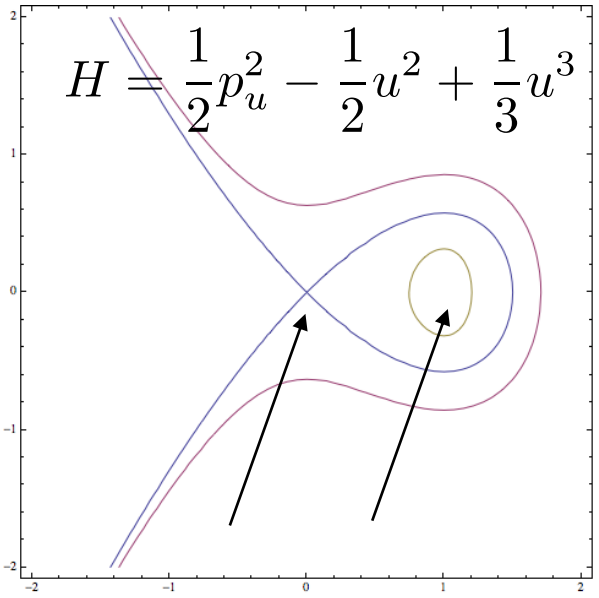

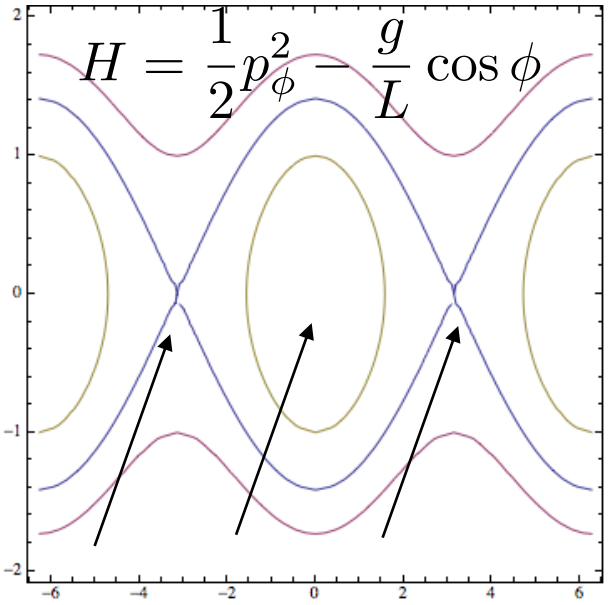

- Conservative non-linear oscillators have Hamiltonian

$$H = E = \frac{1}{2}p_u^2 + V(u)$$

with the potential being a general (polynomial) function of positions

- **Equilibrium points** are associated with extrema of the potential
- Considering three non-linear oscillators
  - **Quartic** potential (left): two minima and one maximum
  - **Cubic** potential (center): one minimum and one maximum
  - **Pendulum** (right): periodic minima and maxima

Fixed point analysis

- Consider a general second order system
$$\frac{du}{dt} = f_1(u, p_u)$$
$$\frac{dp_u}{dt} = f_2(u, p_u)$$
- Equilibrium or "**fixed**" points $f_1(u_0, p_{u0}) = f_2(u_0, p_{u0}) = 0$ are determinant for topology of trajectories at their vicinity

Fixed point analysis

- Consider a general second order system $\begin{aligned} \frac{du}{dt} &= f_1(u, p_u) \\ \frac{dp_u}{dt} &= f_2(u, p_u) \end{aligned}$
- Equilibrium or "**fixed**" points $f_1(u_0, p_{u0}) = f_2(u_0, p_{u0}) = 0$ are determinant for topology of trajectories at their vicinity
- The **linearized equations** of motion at their vicinity are

$$\frac{d}{dt}\begin{bmatrix}\delta u \\ \delta p_u\end{bmatrix} = \mathcal{M}_J \begin{bmatrix}\delta u \\ \delta p_u\end{bmatrix} = \underbrace{\begin{bmatrix} \frac{\partial f_1(u_0, p_{u0})}{\partial u} & \frac{\partial f_1(u_0, p_{u0})}{\partial p_u} \\ \frac{\partial f_2(u_0, p_{u0})}{\partial u} & \frac{\partial f_2(u_0, p_{u0})}{\partial p_u} \end{bmatrix}}_{\textbf{Jacobian matrix}} \begin{bmatrix}\delta u \\ \delta p_u\end{bmatrix}$$

- Fixed point nature is revealed by **eigenvalues** of $\mathcal{M}_J$, i.e. solutions of the characteristic polynomial $\det|\mathcal{M}_J - \lambda \mathbf{I}| = 0$

Fixed point for conservative systems

- For **conservative systems** of 1 degree of freedom, the second order characteristic polynomial for any fixed point has two possible solutions:
  - Two **complex eigenvalues** with opposite sign, corresponding to **elliptic** fixed points. Phase space flow is described by **ellipses**, with particles evolving clockwise or anti-clockwise

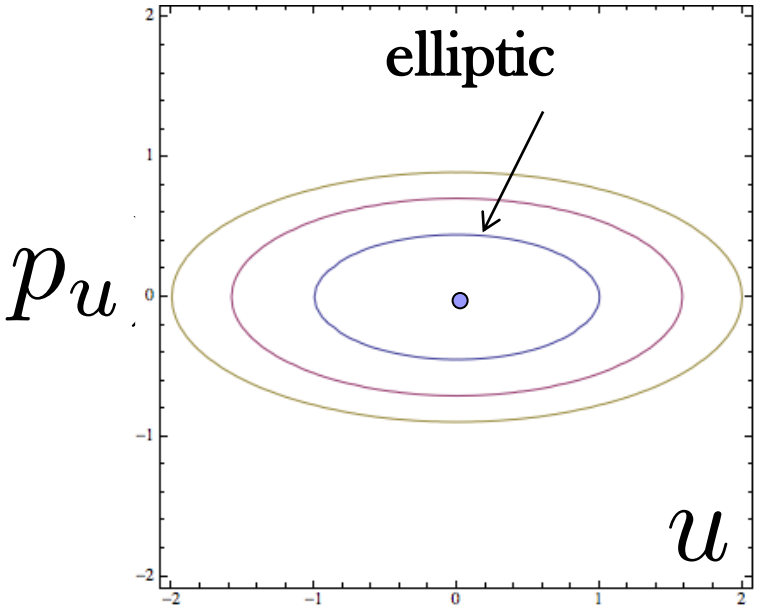

Fixed point for conservative systems

- For **conservative systems** of 1 degree of freedom, the second order characteristic polynomial for any fixed point has two possible solutions:
  - Two **complex eigenvalues** with opposite sign, corresponding to **elliptic** fixed points. Phase space flow is described by **ellipses**, with particles evolving clockwise or anti-clockwise
  - Two **real eigenvalues** with opposite sign, corresponding to **hyperbolic** (or saddle) fixed points. Flow described by two lines (or manifolds), incoming (stable) and outgoing (unstable)

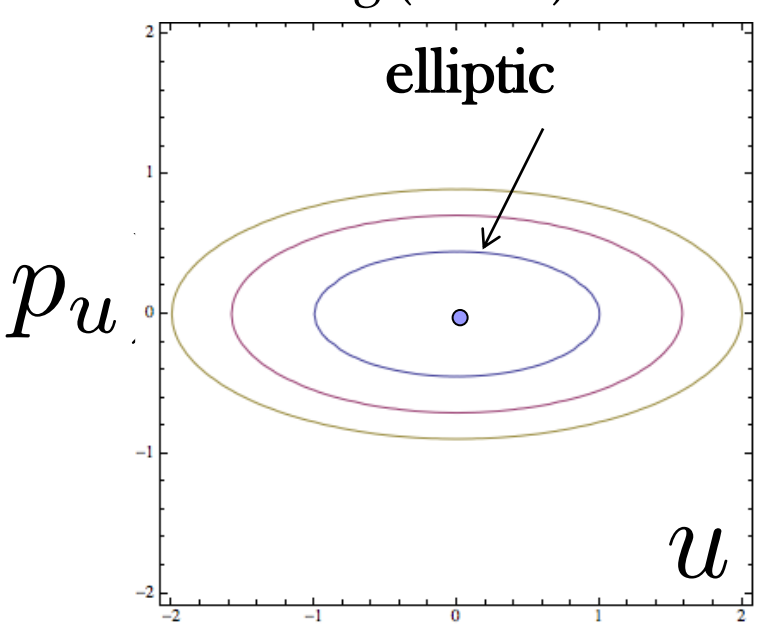

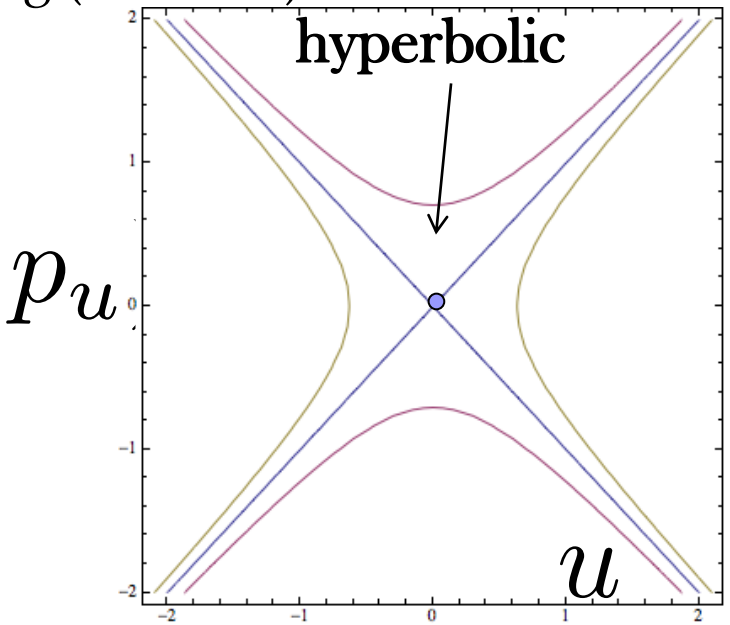

Pendulum fixed point analysis

- The "fixed" points for a pendulum can be found at

$$(\phi_n, p_\phi) = (\pm n\pi, 0)\ ,\ n = 0, 1, 2\ldots$$

- The Jacobian matrix is $\begin{bmatrix} 0 & 1 \\ -\frac{g}{L}\cos\phi_n & 0 \end{bmatrix}$
- The eigenvalues are $\lambda_{1,2} = \pm i\sqrt{\frac{g}{L}\cos\phi_n}$

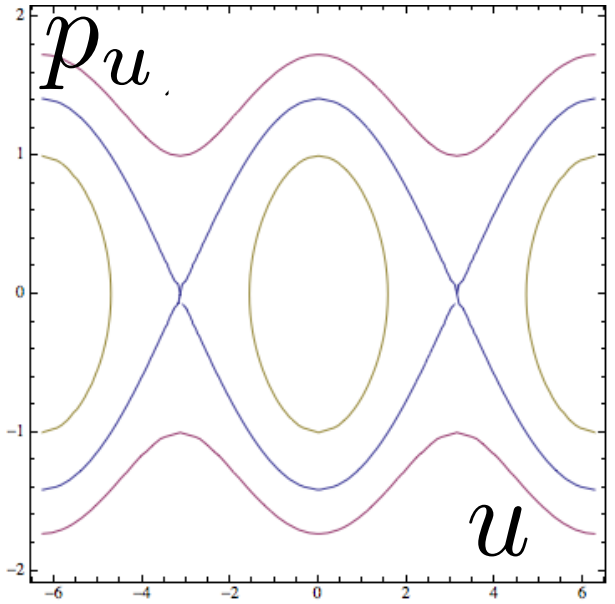

Pendulum fixed point analysis

- The "fixed" points for a pendulum can be found at

$$(\phi_n, p_\phi) = (\pm n\pi, 0)\ ,\ n = 0, 1, 2\ldots$$

- The Jacobian matrix is $\begin{bmatrix} 0 & 1 \\ -\frac{g}{L}\cos\phi_n & 0 \end{bmatrix}$
- The eigenvalues are $\lambda_{1,2} = \pm i\sqrt{\frac{g}{L}\cos\phi_n}$
- Two cases can be distinguished:
  - $\phi_n = 2n\pi$, for which $\lambda_{1,2} = \pm i\sqrt{\frac{g}{L}}$

    corresponding to **elliptic** fixed points

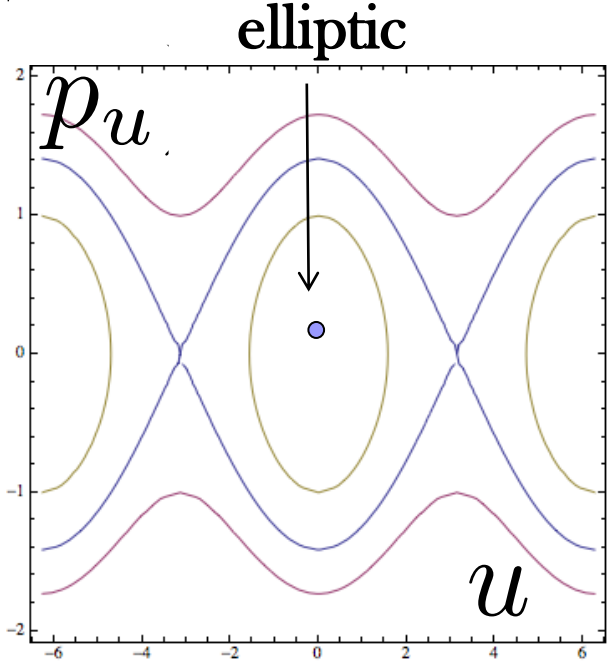

Pendulum fixed point analysis

- The "fixed" points for a pendulum can be found at

$$(\phi_n, p_\phi) = (\pm n\pi, 0)\ ,\ n = 0, 1, 2\ldots$$

- The Jacobian matrix is $\begin{bmatrix} 0 & 1 \\ -\frac{g}{L}\cos\phi_n & 0 \end{bmatrix}$
- The eigenvalues are $\lambda_{1,2} = \pm i\sqrt{\frac{g}{L}\cos\phi_n}$
- Two cases can be distinguished:
  - $\phi_n = 2n\pi$, for which $\lambda_{1,2} = \pm i\sqrt{\frac{g}{L}}$ corresponding to **elliptic** fixed points
  - $\phi_n = (2n+1)\pi$, for which $\lambda_{1,2} = \pm\sqrt{\frac{g}{L}}$ corresponding to **hyperbolic** fixed points
  - The **separatrix** are the stable and unstable manifolds through the hyperbolic points, separating bounded **librations** and unbounded **rotations**

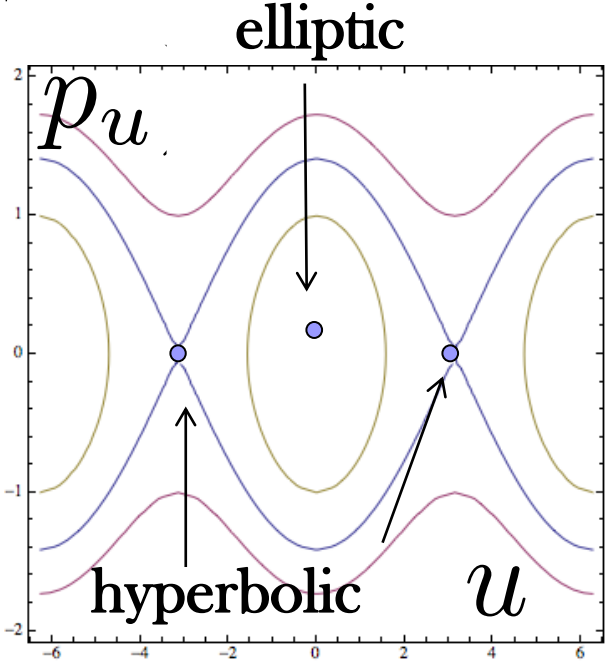

Phase space for time-dependent systems

- Consider now a simple harmonic oscillator where the **frequency** is **time-dependent**

$$H = \frac{1}{2}\left(p_u^2 + \omega_0^2(t)u^2\right)$$

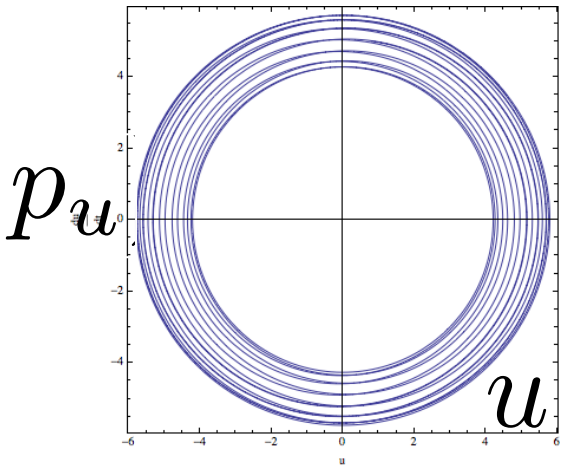

- Plotting the evolution in phase space, provides trajectories that **intersect** each other
- The phase space has **time** as **extra dimension**

Phase space for time-dependent systems

- Consider now a simple harmonic oscillator where the **frequency** is **time-dependent**

$$H = \frac{1}{2}\left(p_u^2 + \omega_0^2(t)u^2\right)$$

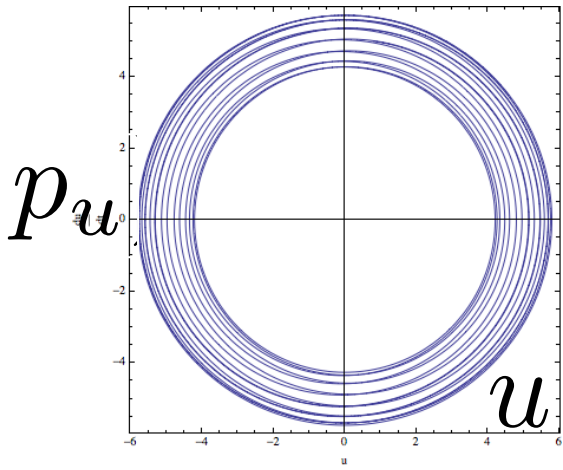

- Plotting the evolution in phase space, provides trajectories that **intersect** each other
- The phase space has **time** as **extra dimension**
- By **rescaling** the **time** to become $\tau = \omega_0 t$ and considering every integer interval of the **new** "**time**" variable, the **phase space** looks like the one of the **harmonic oscillator**

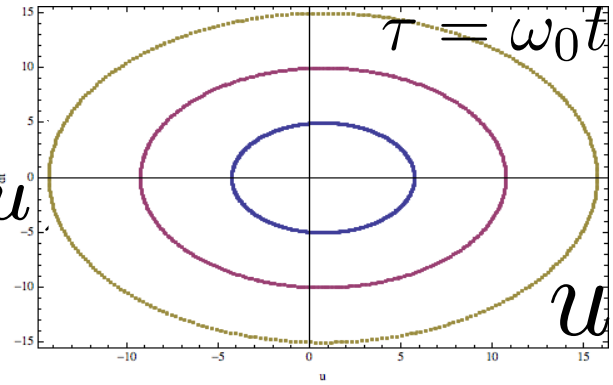

- This is the simplest version of a **Poincaré surface of section**, which is useful for studying geometrically phase space of multi-dimensional systems

Phase space for time-dependent systems

- Consider now a simple harmonic oscillator where the **frequency** is **time-dependent**

$$H = \frac{1}{2}\left(p_u^2 + \omega_0^2(t)u^2\right)$$

- Plotting the evolution in phase space, provides trajectories that **intersect** each other
- The phase space has **time** as **extra dimension**
- By **rescaling** the **time** to become $\tau = \omega_0 t$ and considering every integer interval of the **new** "**time**" variable, the **phase space** looks like the one of the **harmonic oscillator**
- This is the simplest version of a **Poincaré surface of section**, which is useful for studying geometrically phase space of multi-dimensional systems
- The **fixed point** in the surface of section is now a periodic orbit

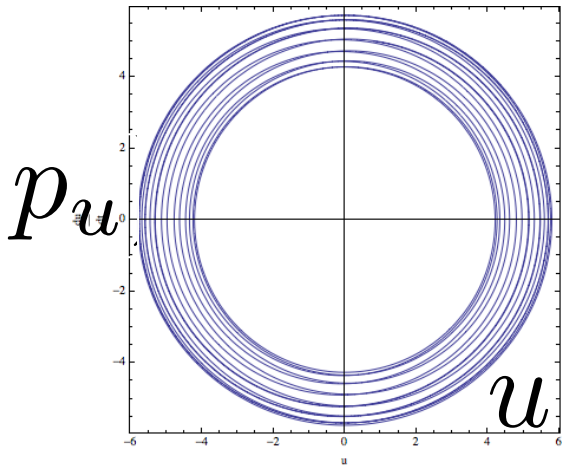

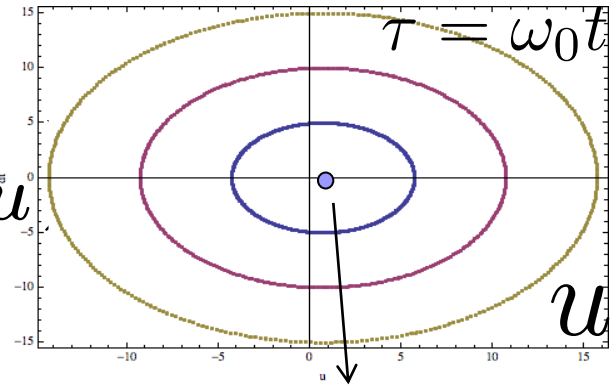

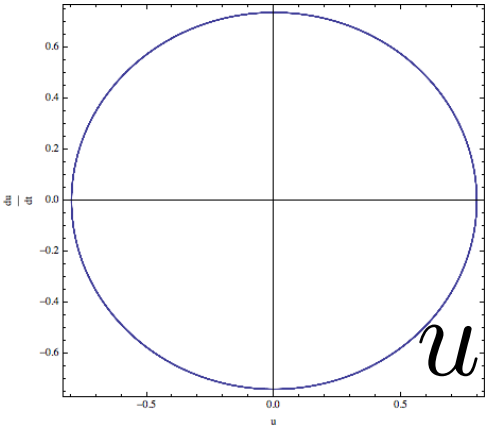

Poincaré map

Poincaré map

- **First recurrence** or **Poincaré map** (or surface of section) is defined by the intersection of trajectories of a dynamical system, with a fixed surface in phase space

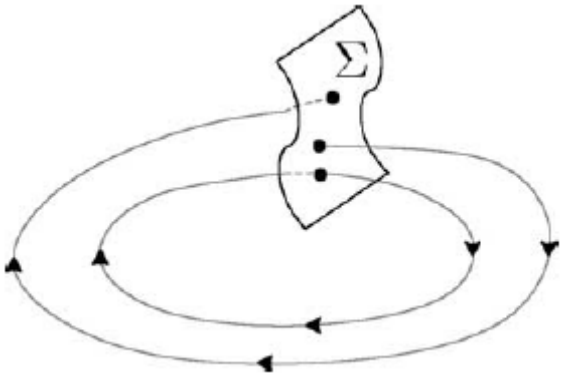

Poincaré map

- **First recurrence** or **Poincaré map** (or surface of section) is defined by the intersection of trajectories of a dynamical system, with a fixed surface in phase space

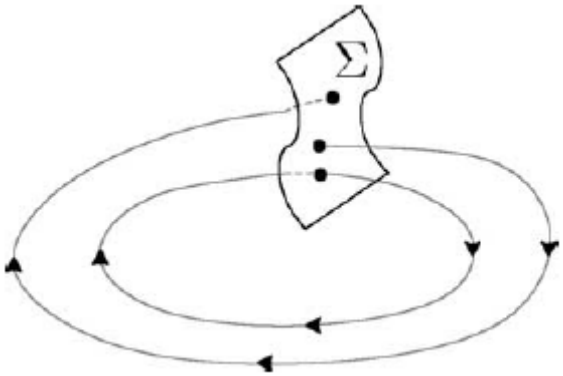

- For an **autonomous** Hamiltonian system $H(\mathbf{q}, \mathbf{p})$ (no **explicit** time dependence), it can be chosen to be any fixed surface in phase space, e.g. $q_i = 0$
- For a **non-autonomous** Hamiltonian system $H(\mathbf{q}, \mathbf{p}, t)$ (explicit time dependence), which is **periodic,** it can be chosen as the period $t = T_0$

Poincaré map

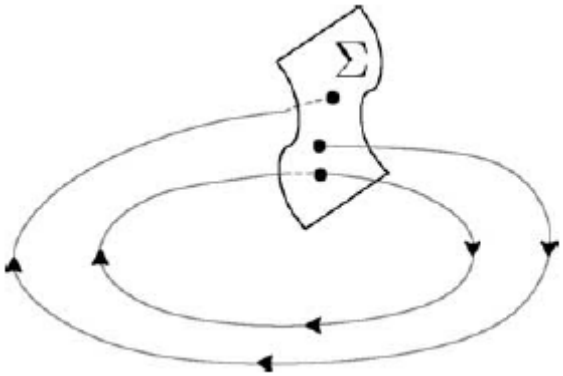

- **First recurrence** or **Poincaré map** (or surface of section) is defined by the intersection of trajectories of a dynamical system, with a fixed surface in phase space
- For an **autonomous** Hamiltonian system $H(\mathbf{q}, \mathbf{p})$ (no **explicit** time dependence), it can be chosen to be any fixed surface in phase space, e.g. $q_i = 0$
- For a **non-autonomous** Hamiltonian system $H(\mathbf{q}, \mathbf{p}, t)$ (explicit time dependence), which is **periodic,** it can be chosen as the period $t = T_0$
- In a system with n degrees of freedom (or $n+1$ including time), the phase space has $2n$ (or $2n+2$) dimensions
- By fixing the value of the Hamiltonian to H_0, the motion on a Poincaré map is reduced to $2n-2$ (or $2n$)

Poincaré map

- Particularly useful for a system with **2 degrees** of **freedom**, or **1 degree** of **freedom + time**, as the motion on Poincaré map is described by 2-dimensional curves
- For continuous system, numerical techniques exist to compute the surface exactly (e.g. M.Henon Physica D 5, 1982)

Poincaré map

- Particularly useful for a system with **2 degrees** of **freedom**, or **1 degree** of **freedom + time**, as the motion on Poincaré map is described by 2-dimensional curves
- For continuous system, numerical techniques exist to compute the surface exactly (e.g. M.Henon Physica D 5, 1982)
- Example from Astronomy: the logarithmic galactic potential

$$H_q(x, y, X, Y) = \frac{1}{2}(X^2 + Y^2) + \ln\left(x^2 + \frac{y}{q^2} + R_c^2\right)$$

$$(x, y, X, Y) \mapsto (\phi_x, \phi_y, J_x, J_y)$$

$y = 0$

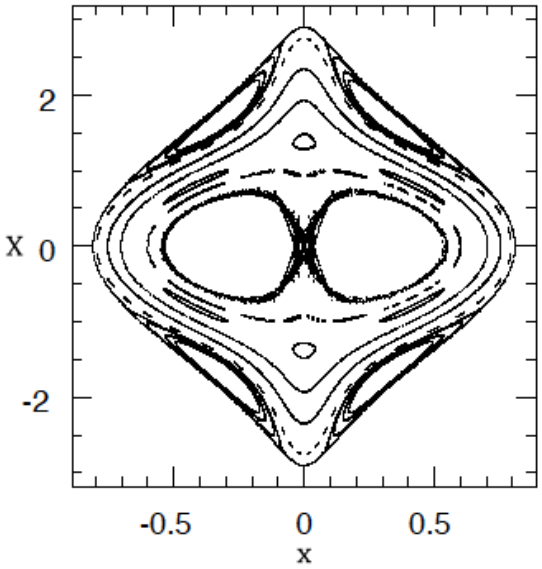

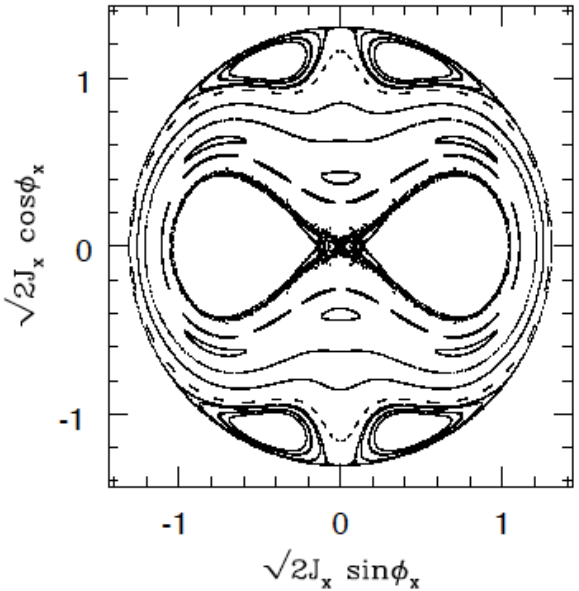

$\phi_y = 0$

Poincaré Section for a ring

- Record the particle coordinates at one location in a ring
- Unperturbed motion lies on a circle in normalized coordinates (simple rotation)

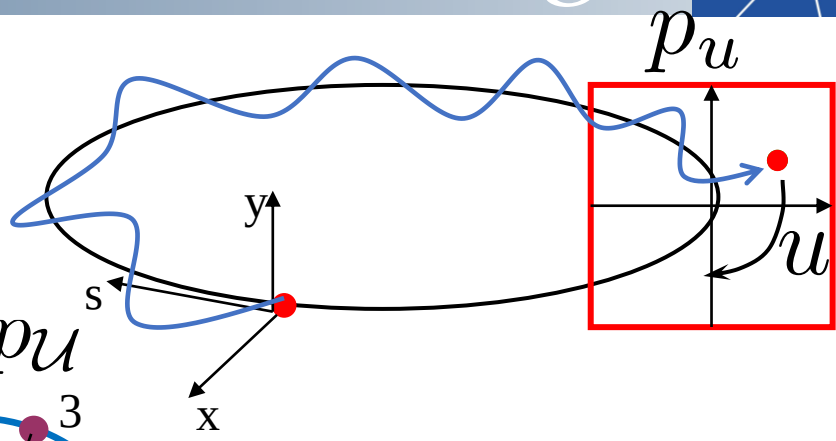

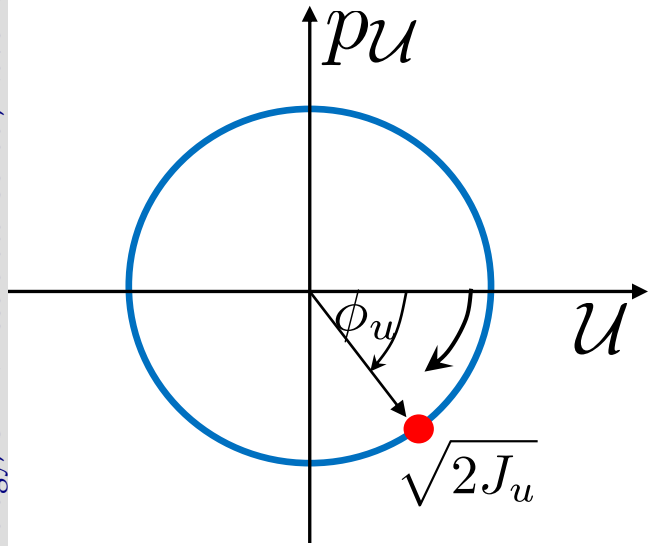

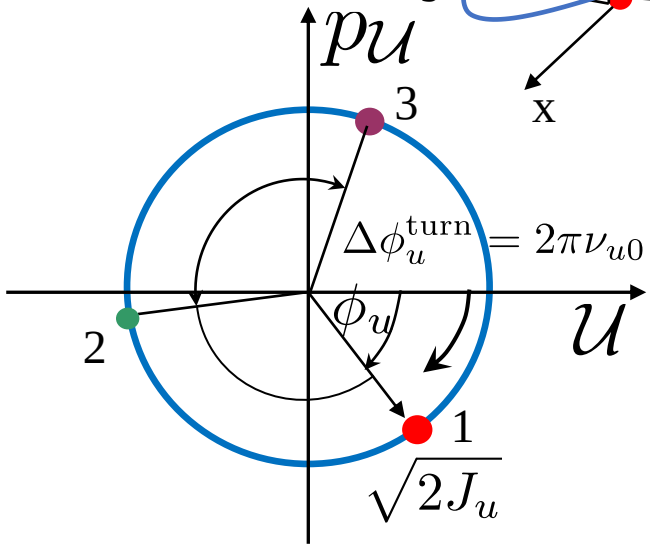

Poincaré Section for a ring

- Record the particle coordinates at one location in a ring
- Unperturbed motion lies on a circle in normalized coordinates (simple rotation)

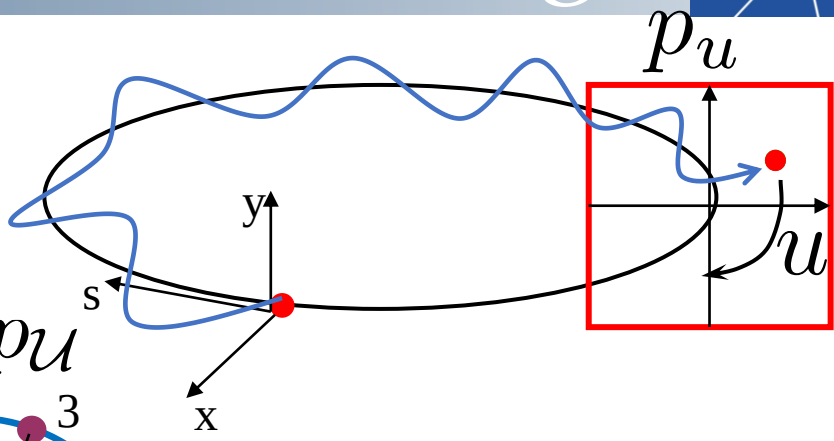

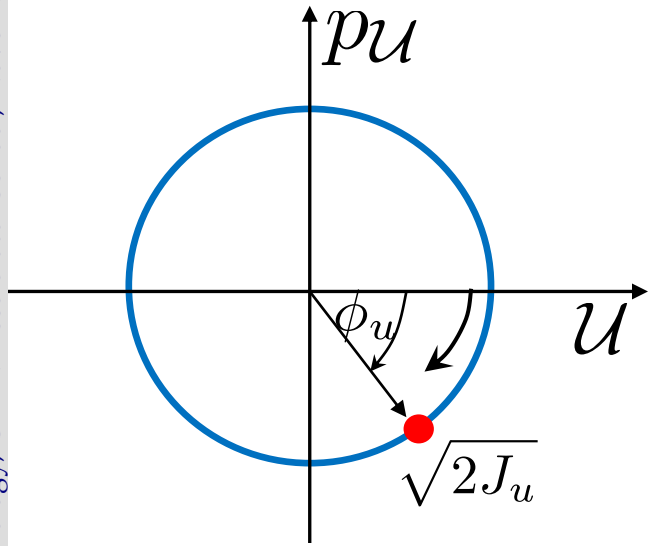

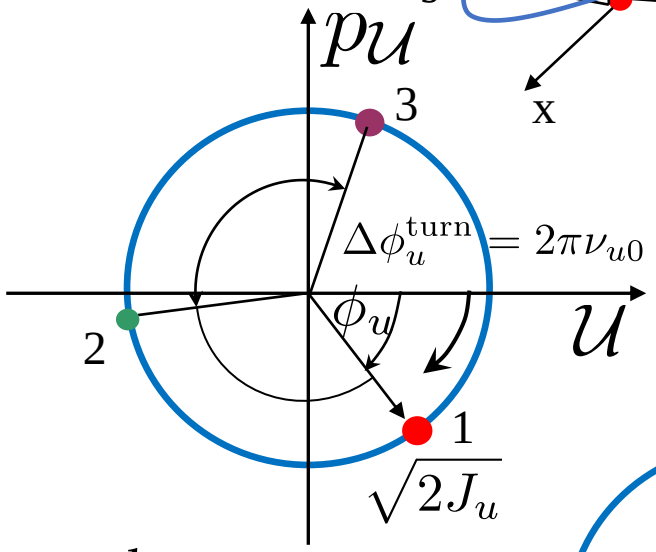

- Resonance condition corresponds to a periodic orbit or fixed points in phase space
- For a non-linear kick, the radius will change by $\delta(\sqrt{2J})$ and the particles stop lying on circles

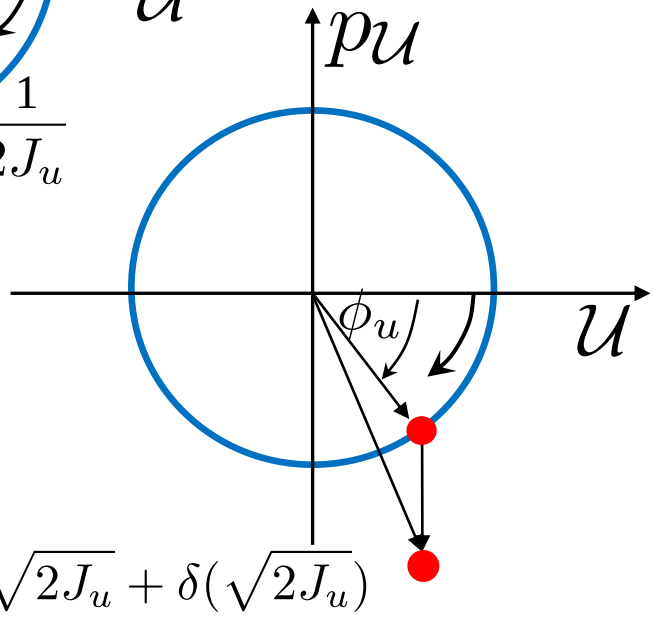

Example: Single Octupole

- Simple **map** with single octupole kick with integrated strength k_3 + rotation with phase advances (μ_x, μ_y)

```
def OctupoleMap(k3,x,px,y,py):
  x1  = x
  px1 = px - k3*(x**3-3*x*y**2)
  y1  = y
  py1 = py - k3*(-3*x**2*y+y**3)
  return x1,px1,y1,py1

def Rotation(mux,muy,x,px,y,py):
  x1  = cos(mux)*x+sin(mux)*px
  px1 =-sin(mux)*x+cos(mux)*px
  y1  = cos(muy)*y+sin(muy)*py
  py1 =-sin(muy)*y+cos(muy)*py
  return x1,px1,y1,py1
```

- Restrict motion in (x, p_x) plane i.e. $y_0 = p_{y0} = 0$
- Iterate for a number of "turns" (here 1000)

Example: Single Octupole

- Simple **map** with single octupole kick with integrated strength k_3 + rotation with phase advances (μ_x, μ_y)

```
def OctupoleMap(k3,x,px,y,py):
  x1  = x
  px1 = px - k3*(x**3-3*x*y**2)
  y1  = y
  py1 = py - k3*(-3*x**2*y+y**3)
  return x1,px1,y1,py1

def Rotation(mux,muy,x,px,y,py):
  x1  = cos(mux)*x+sin(mux)*px
  px1 =-sin(mux)*x+cos(mux)*px
  y1  = cos(muy)*y+sin(muy)*py
  py1 =-sin(muy)*y+cos(muy)*py
  return x1,px1,y1,py1
```

- Restrict motion in (x, p_x) plane i.e. $y_0 = p_{y0} = 0$
- Iterate for a number of "turns" (here 1000)

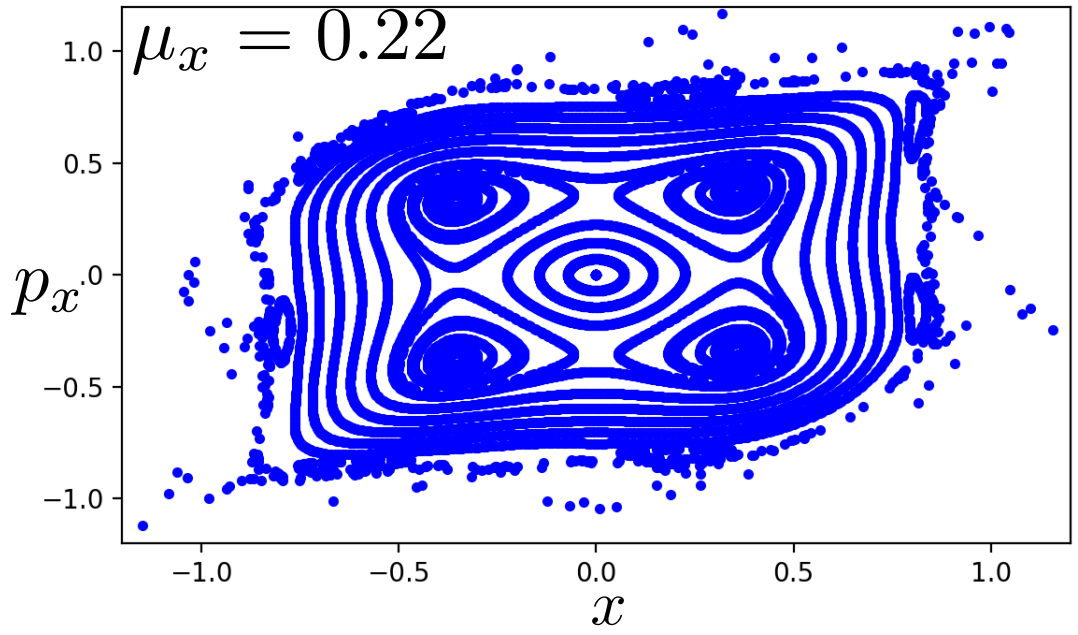

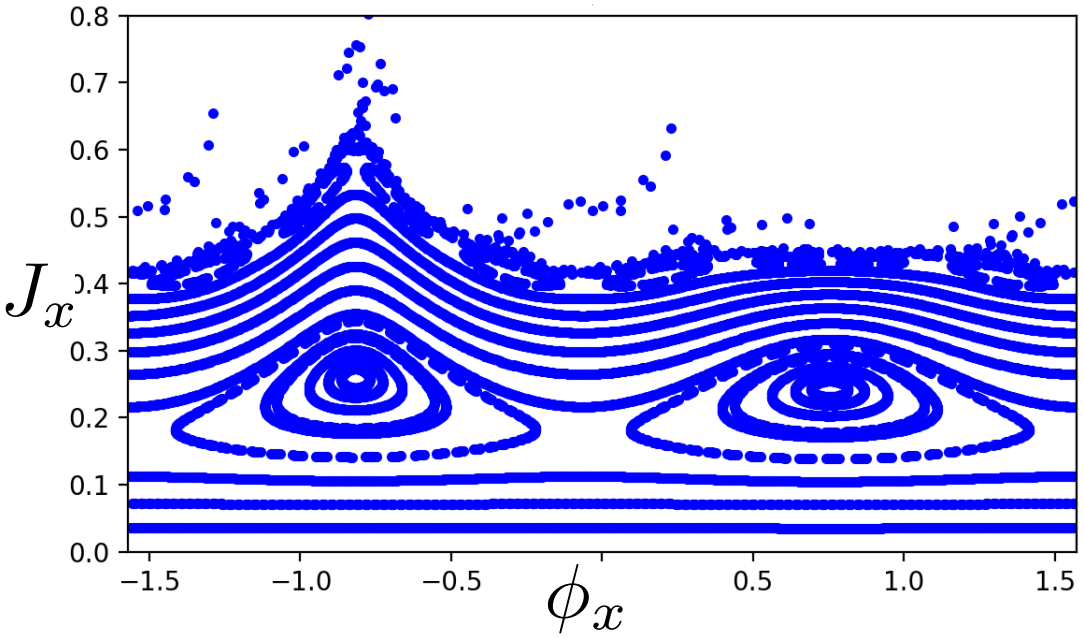

Example: Single Octupole

- Appearance of **invariant curves** (“distorted” circles), where “action” is an integral of motion
- **Resonant islands** with stable and separatrices with unstable fixed points
- **Chaotic motion**
- Electromagnetic fields coming from multi-pole expansions (polynomials) do not bound phase space and chaotic trajectories may eventually escape to infinity (**Dynamic Aperture**)
- For some fields like beam-beam and space-charge this is not true, i.e. chaotic motion leads to halo formation

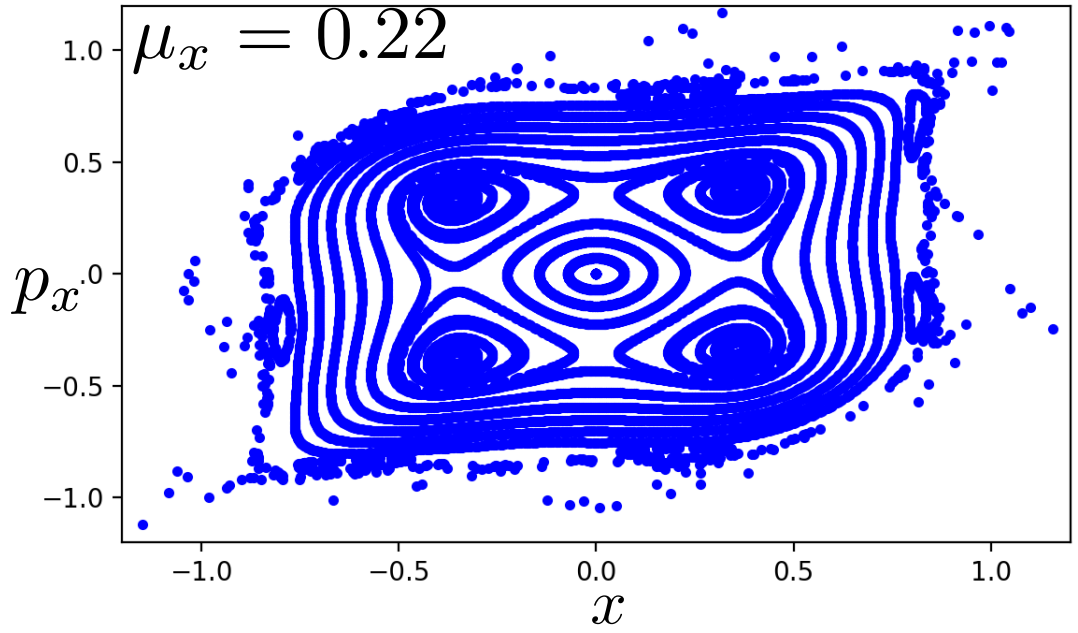

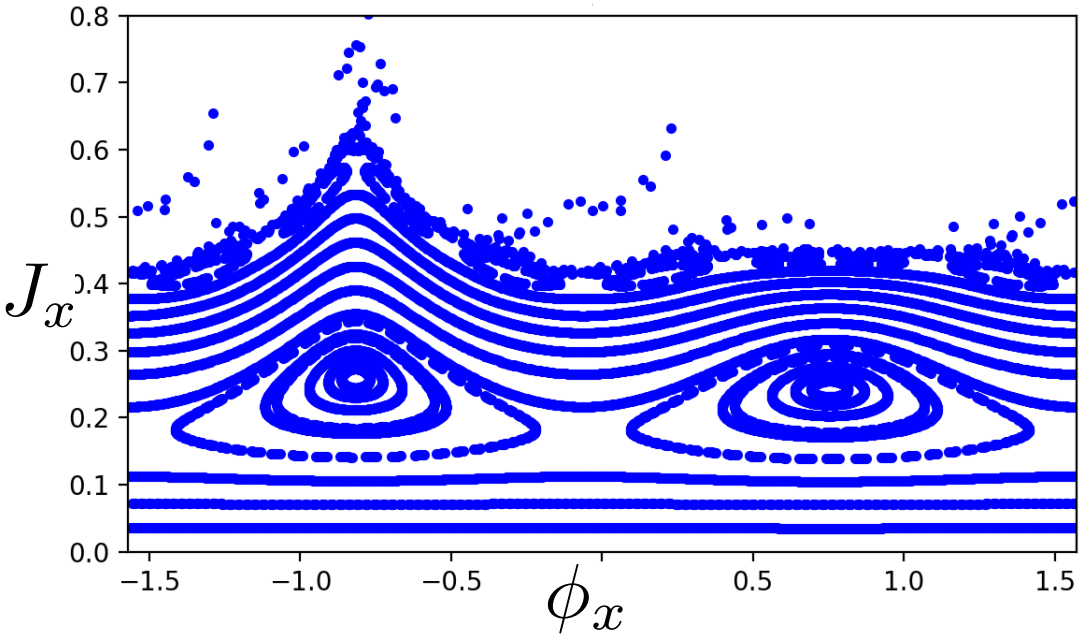

Motion close to a resonance

Secular perturbation theory

- The vicinity of a resonance $n_1\omega_1 + n_2\omega_2 = 0$, can be studied through **secular perturbation theory** (see appendix) or transforming the 1-turn map (see Etienne's lectures)
- A canonical transformation is applied such that the new variables are in a frame remaining **on top** of the **resonance**
- If one frequency is slow, one can average the motion and remain only with a **1 degree of freedom Hamiltonian** which looks like the one of the **pendulum**
- Thereby, one can find the location and nature of the fixed points measure the width of the resonance

Fixed points for general multi-pole

- For **any polynomial perturbation** of the form x^k the "resonant" Hamiltonian is written as

$$\hat{H}_2 = \delta J_2 + \alpha(J_2) + J_2^{k/2} A_{kp} \cos(k\psi_2)$$

- With the **distance** to the resonance defined as $\nu = \frac{p}{3} + \delta \ , \ \ \delta << 1$
- The non-linear shift of the tune is described by the term $\alpha(J_2)$
- The conditions for the fixed points are

$$\sin(k\psi_2) = 0 \ , \ \ \delta + \frac{\partial \alpha(J_2)}{\partial J_2} + \frac{k}{2} J_2^{k/2-1} A_{kp} \cos(k\psi_2) = 0$$

- There are **fixed points** for which $\cos(k\psi_{20}) = -1$ and the fixed points are **stable** (elliptic). They are surrounded by ellipses
- There are also **fixed points** for which $\cos(k\psi_{20}) = 1$ and the fixed points are **unstable** (hyperbolic). The trajectories are hyperbolas

Fixed points for 3rd order resonance

- The Hamiltonian for a sextupole close to a third order resonance is $\hat{H}_2 = \delta J_2 + J_2^{3/2} A_{3p} \cos(3\psi_2)$
- Note the absence of the non-linear tune-shift term (in this 1st order approximation!)
- By setting the Hamilton's equations equal to zero, three fixed points can be found at $\psi_{20} = \frac{\pi}{3}, \frac{3\pi}{3}, \frac{5\pi}{3}, \quad J_{20} = \left(\frac{2\delta}{3A_{3p}}\right)^2$
- For $\frac{\delta}{A_{3p}} > 0$ all three points are unstable
- Close to the elliptic one at $\psi_{20} = 0$ the motion in phase space is described by circles that they get more and more distorted to end up in the "triangular" **separatrix** uniting the unstable fixed points
- The tune separation from the resonance is $\delta = \frac{3A_{3p}}{2} J_{20}^{1/2}$

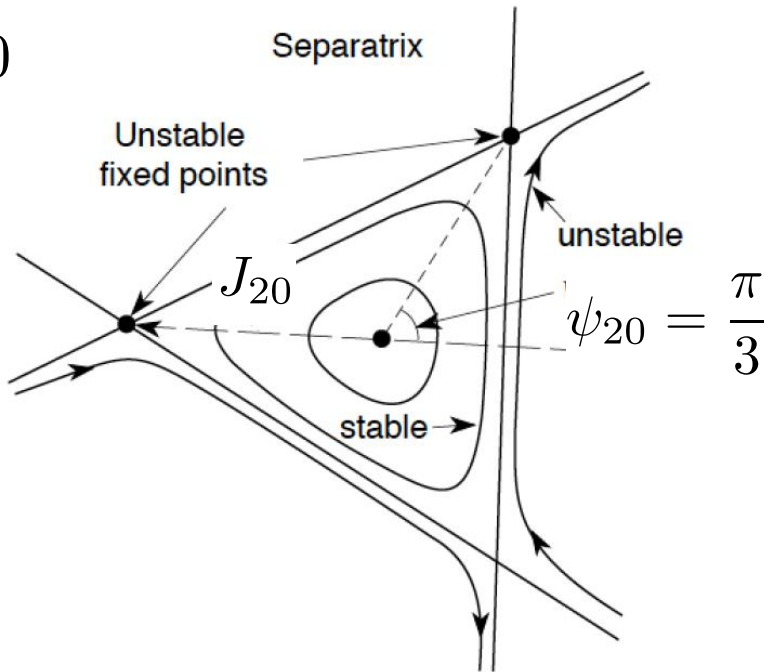

Example: Single Sextupole

- Simple **map** with single **sextupole kick** with integrated strength k_2 + rotation with phase advances (μ_x, μ_y)

```
def SextupoleMap(k2,x,px,y,py):
  x1  = x
  px1 = px - k2*(x**2-y**2)
  y1  = y
  py1 = py - k2*(-2*x*y)
  return x1,px1,y1,py1

def Rotation(mux,muy,x,px,y,py):
  x1  = cos(mux)*x+sin(mux)*px
  px1 =-sin(mux)*x+cos(mux)*px
  y1  = cos(muy)*y+sin(muy)*py
  py1 =-sin(muy)*y+cos(muy)*py
  return x1,px1,y1,py1
```

- Restrict motion in (x, p_x) plane i.e. $y_0 = p_{y0} = 0$
- Iterate for a number of "turns" (here 1000)

Example: Single Sextupole

- Simple **map** with single **sextupole kick** with integrated strength k_2 + rotation with phase advances (μ_x, μ_y)

```
def SextupoleMap(k2,x,px,y,py):
  x1  = x
  px1 = px - k2*(x**2-y**2)
  y1  = y
  py1 = py - k2*(-2*x*y)
  return x1,px1,y1,py1

def Rotation(mux,muy,x,px,y,py):
  x1  = cos(mux)*x+sin(mux)*px
  px1 =-sin(mux)*x+cos(mux)*px
  y1  = cos(muy)*y+sin(muy)*py
  py1 =-sin(muy)*y+cos(muy)*py
  return x1,px1,y1,py1
```

- Restrict motion in (x, p_x) plane i.e. $y_0 = p_{y0} = 0$
- Iterate for a number of "turns" (here 1000)

$$\mu_x = 0.38$$

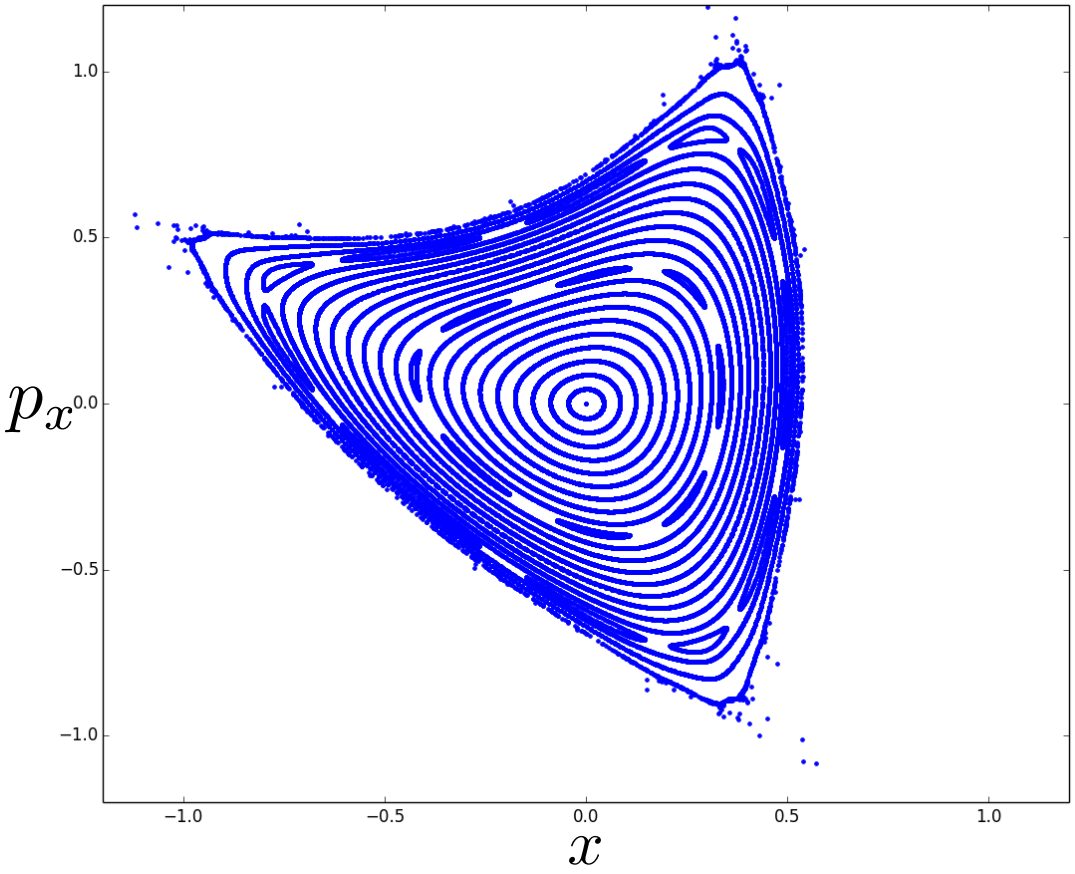

Example: Single Sextupole

- Appearance of 3rd order resonance for certain phase advance
- … but also 4th order resonance

$$\mu_x = 0.38$$

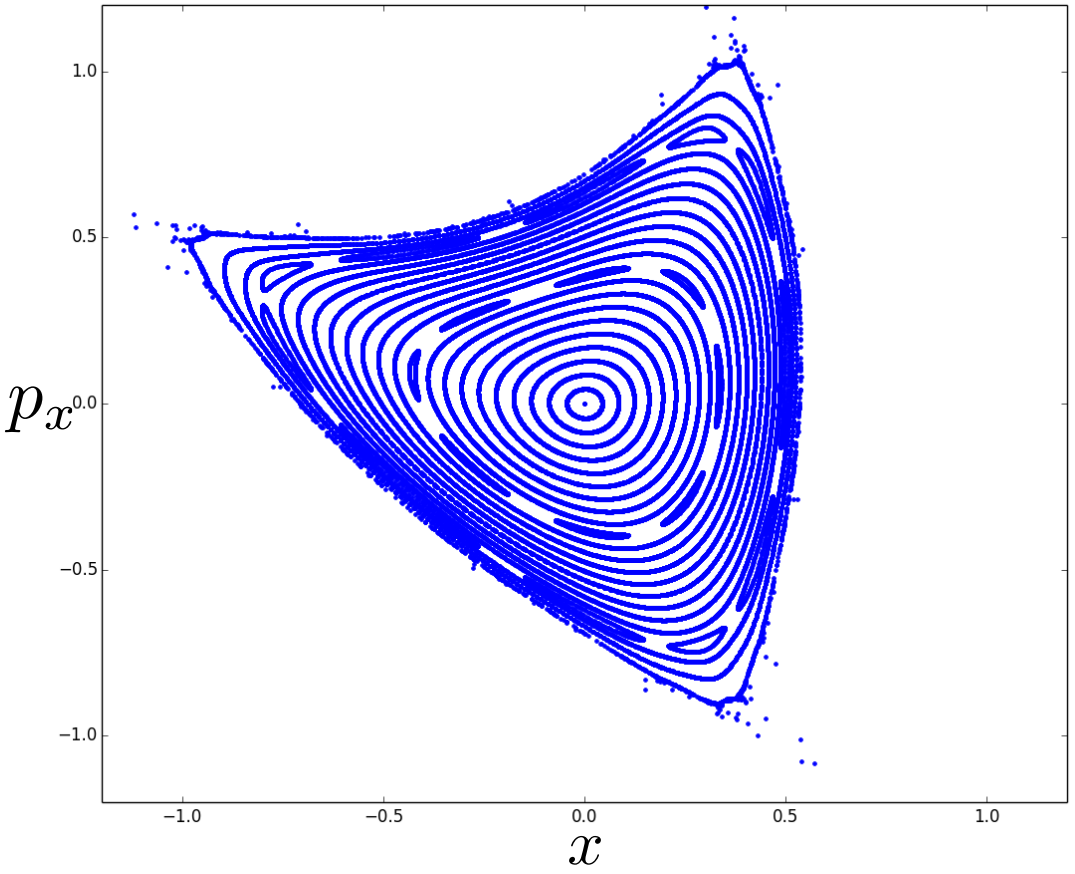

Example: Single Sextupole

- Appearance of 3rd order resonance for certain phase advance
- … but also 4th order resonance

$$\mu_x = 0.253$$

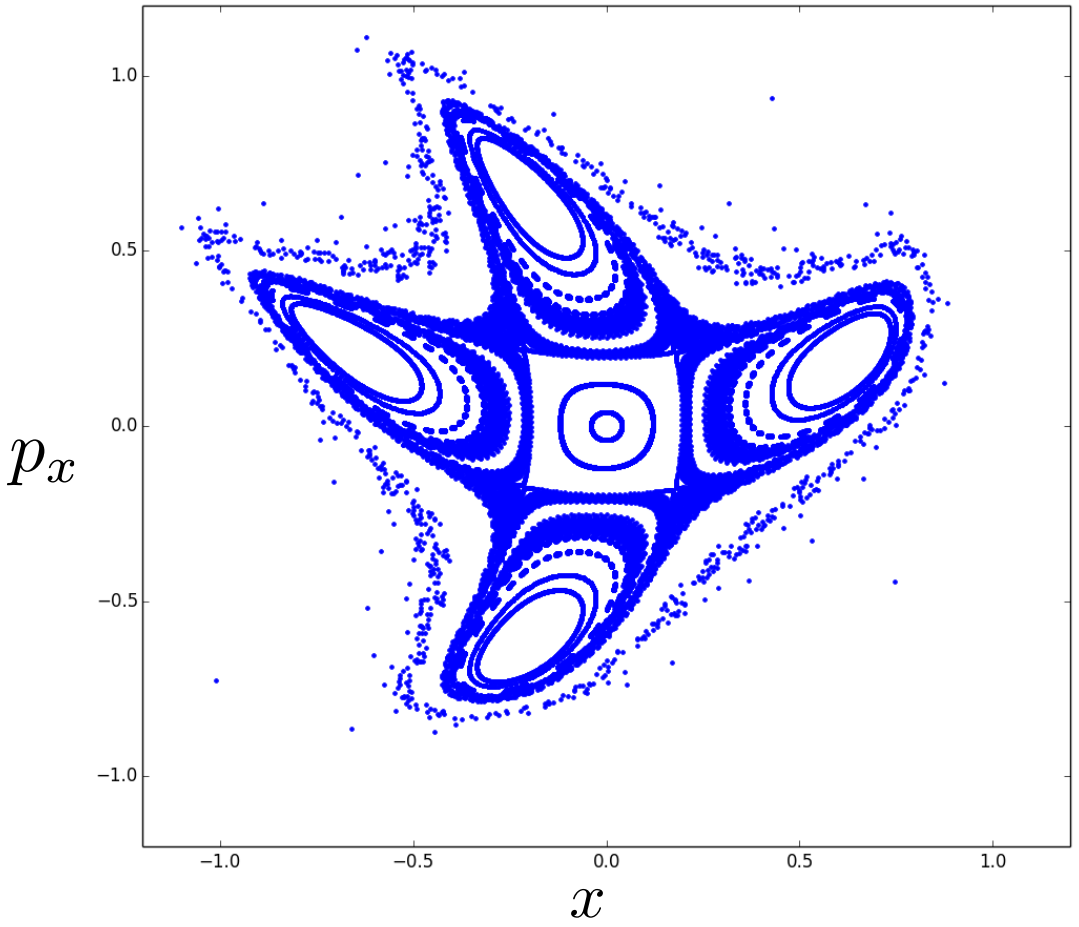

Example: Single Sextupole

- Appearance of 3rd order resonance for certain phase advance
- … but also 4th order resonance
- … and 5th order resonance

$$\mu_x = 0.21$$

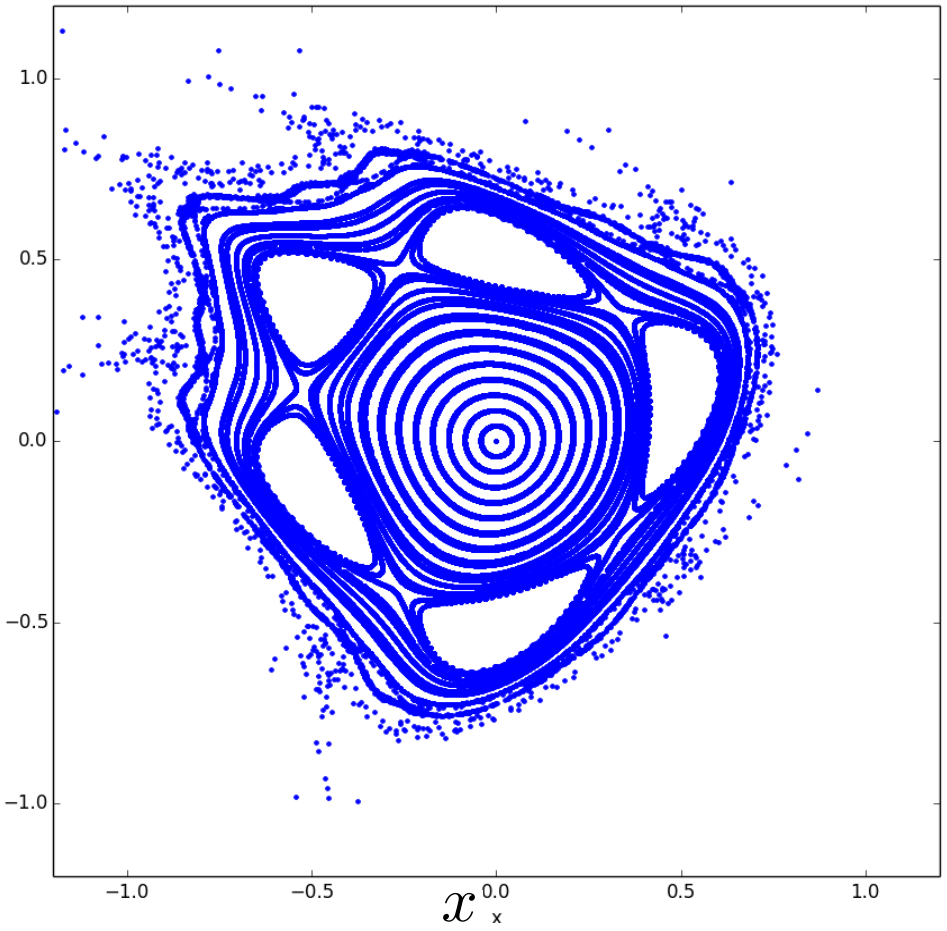

Example: Single Sextupole

- Appearance of 3rd order resonance for certain phase advance
- … but also 4th order resonance
- … and 5th order resonance
- … and 6th order and 7th order and several higher orders…

$$\mu_x = 0.18$$

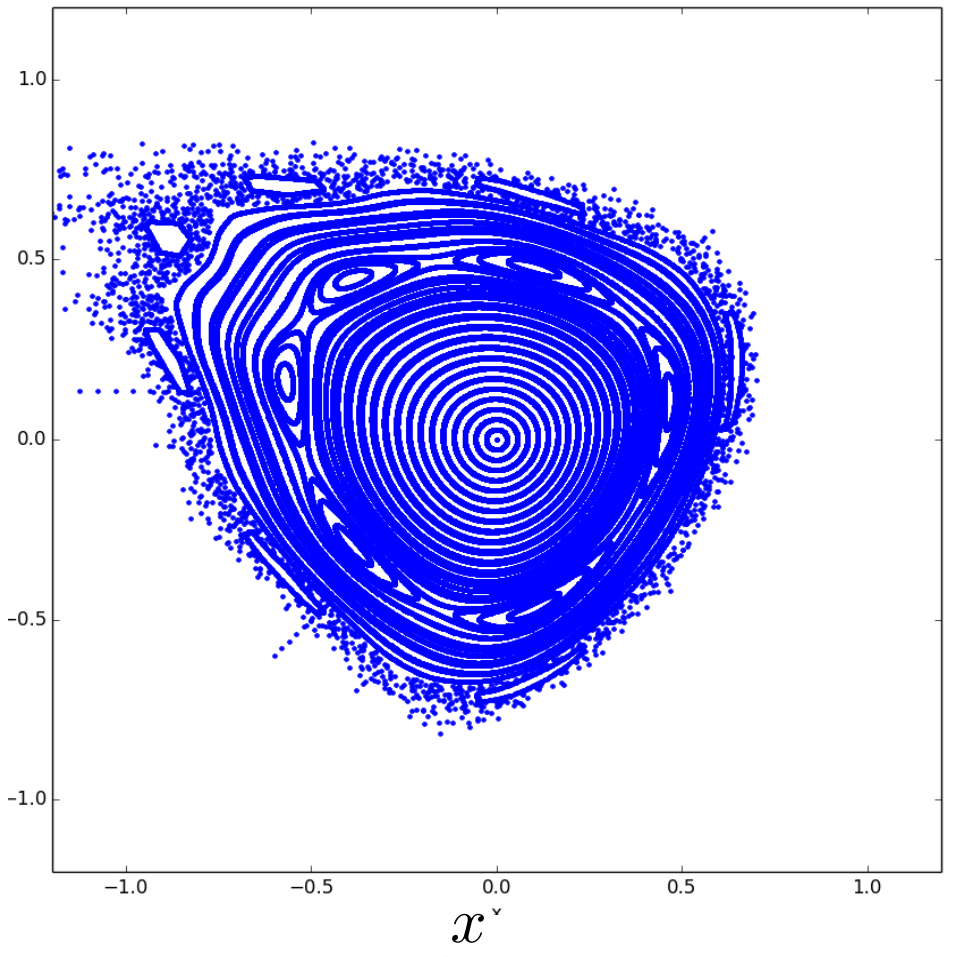

Fixed points for an octupole

- The resonant Hamiltonian close to the **4th order resonance** is written as

$$\hat{H}_2 = \delta J_2 + c J_2^2 + J_2^2 A_{4p} \cos(4\psi_2)$$

- The **fixed points** are found by taking the derivative over the two variables and setting them to zero, i.e.

$$\sin(4\psi_2) = 0 \ , \quad \delta + 2cJ_2 + 2J_2 A_{kp} \cos(4\psi_2) = 0$$

- The fixed points are at

$$\psi_{20} = \frac{\pi}{4}, \ \frac{\pi}{2}, \ \frac{3\pi}{4}, \ \pi, \ \frac{5\pi}{4}, \ \frac{3\pi}{2}, \ \frac{7\pi}{4}, \ 2\pi$$

- For **half** of them, there is a minimum in the potential as $\cos(4\psi_{20}) = -1$ and they are **elliptic** and **half** of them they are **hyperbolic** as $\cos(4\psi_{20}) = 1$

Topology of an octupole resonance

- **Regular motion** near the center, with curves getting more deformed towards a **rectangular shape**
- The **separatrix** passes through 4 unstable fixed points, but motion seems well contained
- **Four stable fixed points** exist and they are surrounded by stable motion (**islands of stability**)
- Question: Can the **central fixed point** become **hyperbolic** (answer in the appendix)

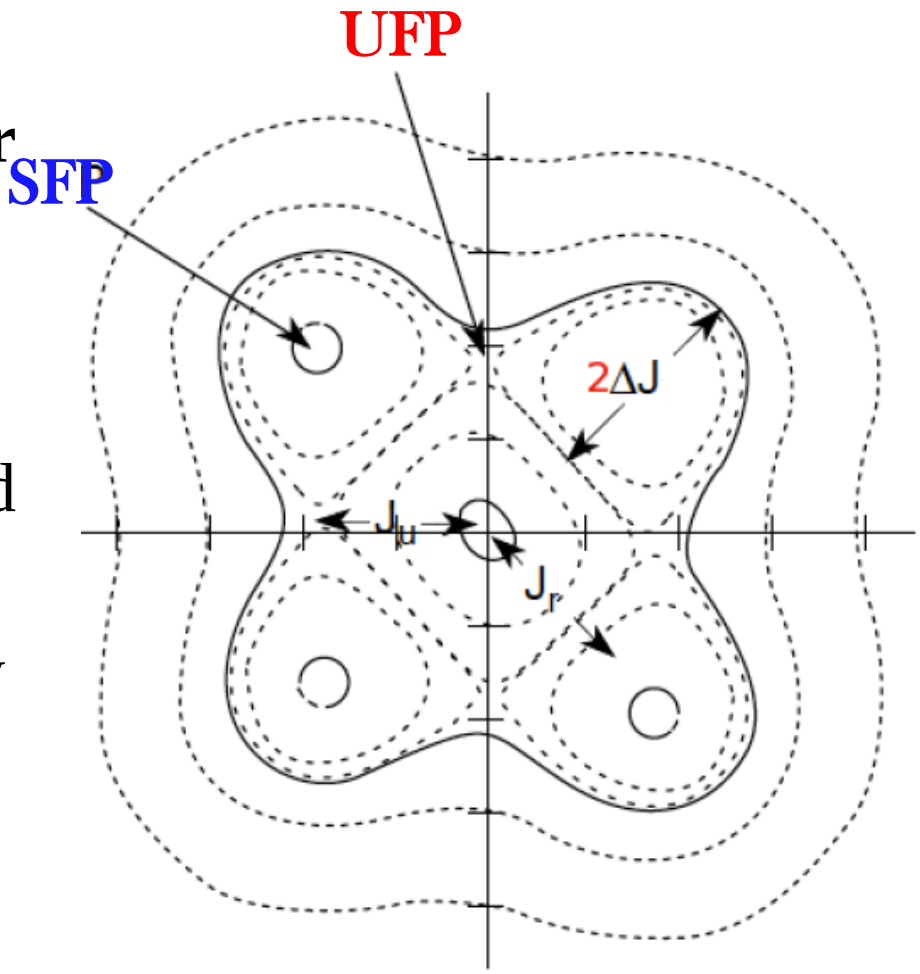

Octupole with hyperbolic central fixed point

- Now, if $c = 0$ the solution for the action is $J_{20} = 0$
- So there is **no minima** in the potential, i.e. the central fixed point is **hyperbolic**

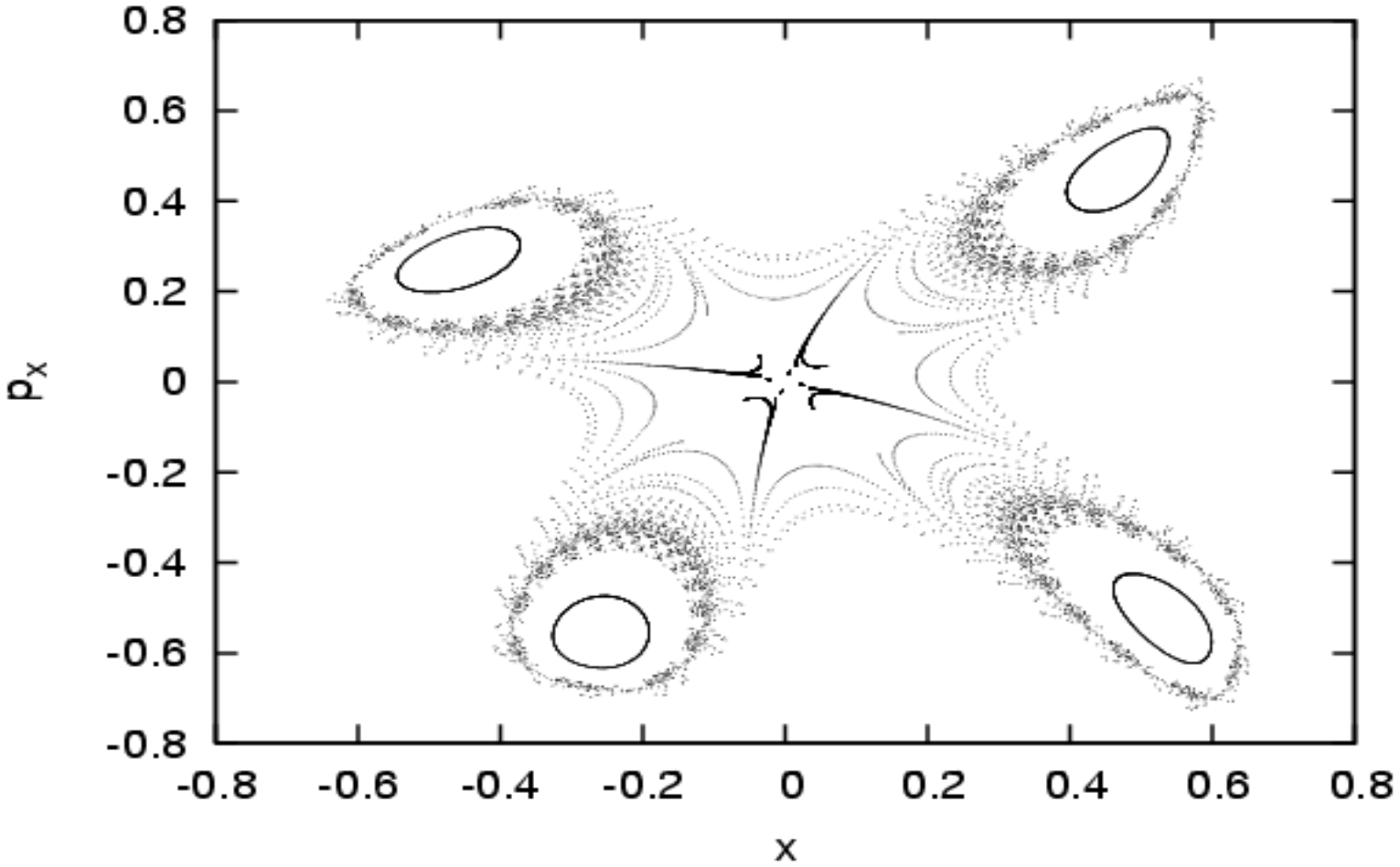

Single Octupole

- As for the sextupole, the octupole can excite any resonance
- Multi-pole magnets can excite **any resonance** order
- It depends on the **tunes**, **strength** of the **magnet** and particle **amplitudes**

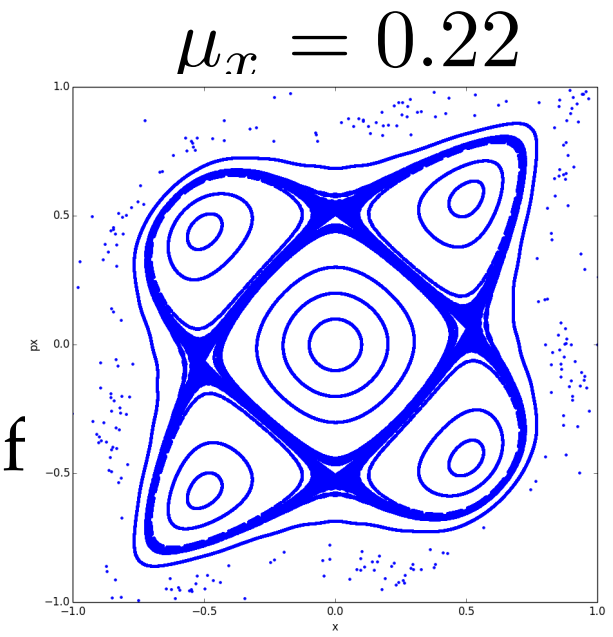

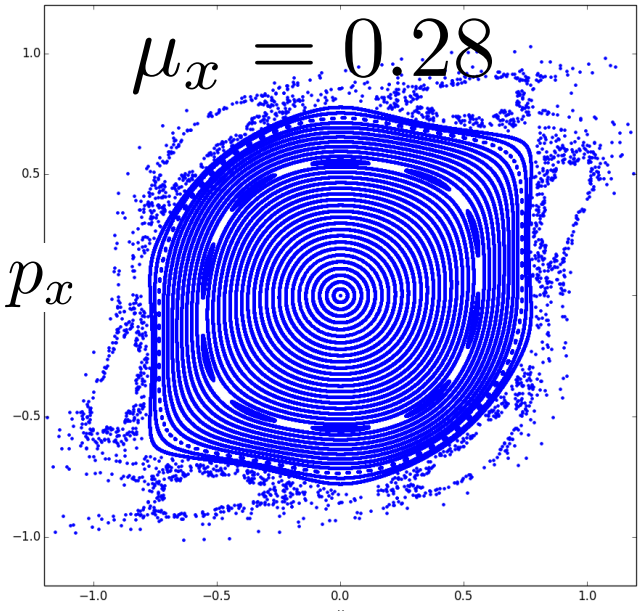

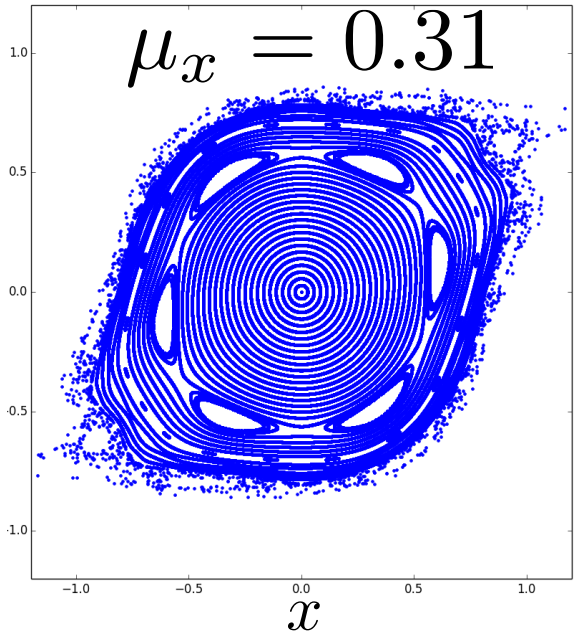

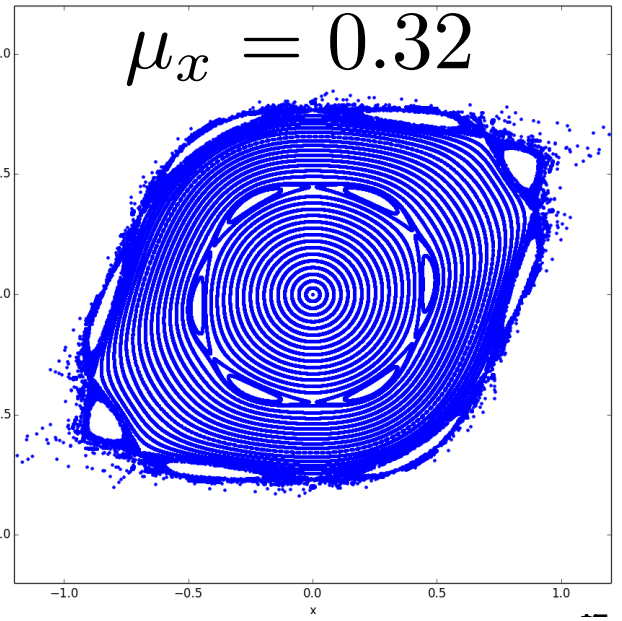

Single Octupole + Sextupole

- Adding a sextupole and an octupole increases the chaotic motion region, when close to the 4th order resonance

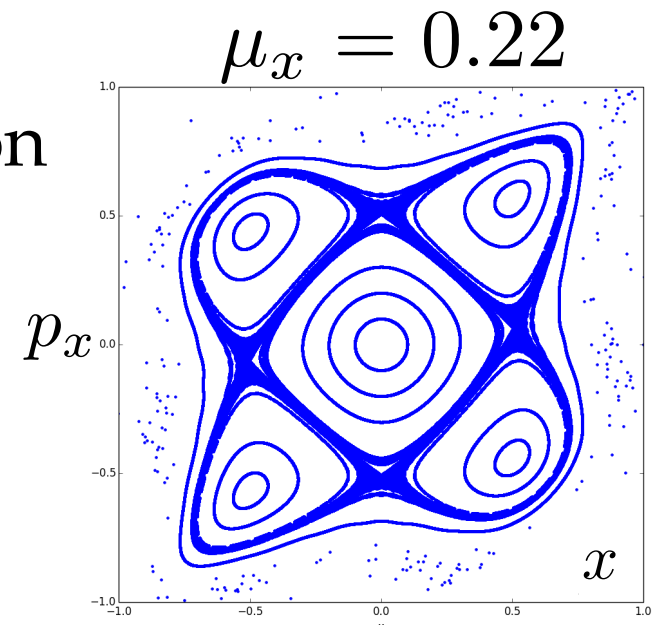

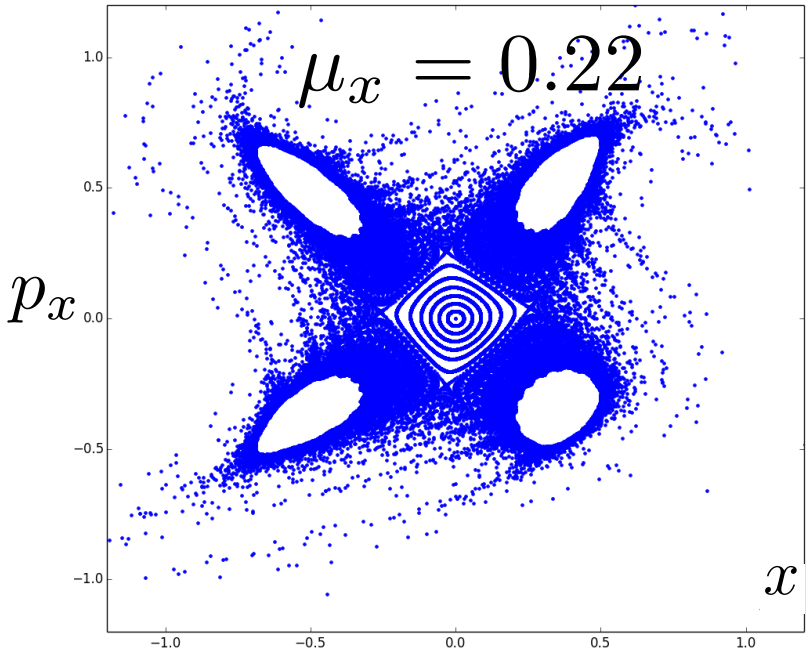

Single Octupole + Sextupole

- Adding a sextupole and an octupole increases the chaotic motion region, when close to the 4th order resonance
- But also allows the appearance of **3rd order resonance stable fixed points**

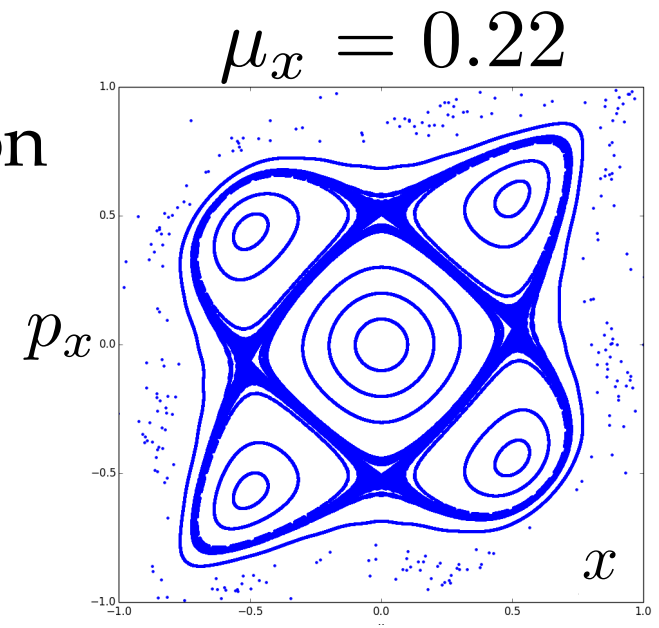

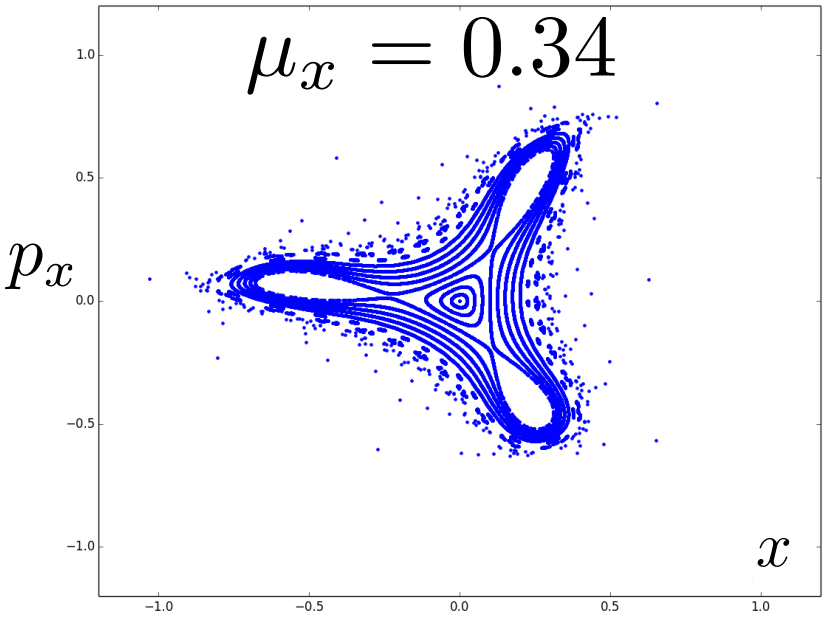

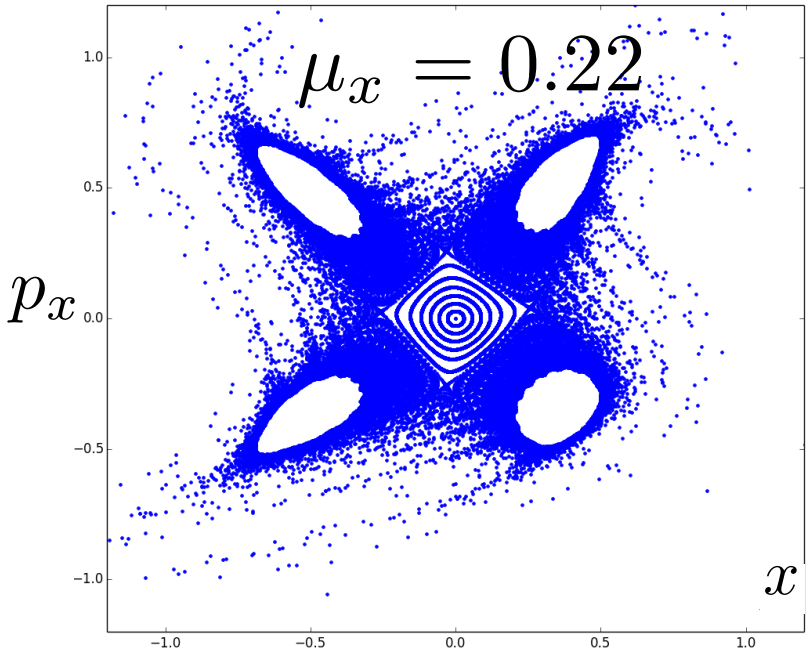

Onset of chaos

Path to chaos

- When **perturbation** becomes **higher**, motion around the **separatrix** becomes **chaotic** (producing **tongues** or **splitting** of the separatrix)
- **Unstable** fixed points are indeed the **source of chaos** when a perturbation is added

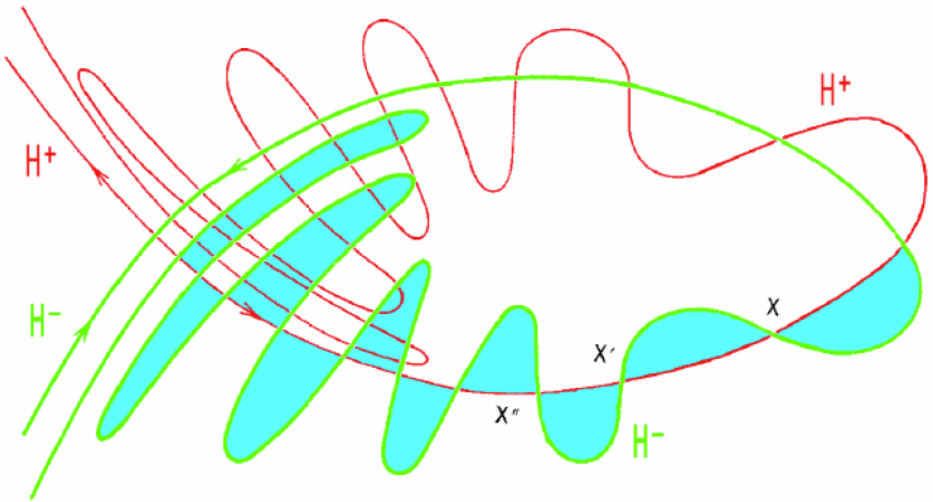

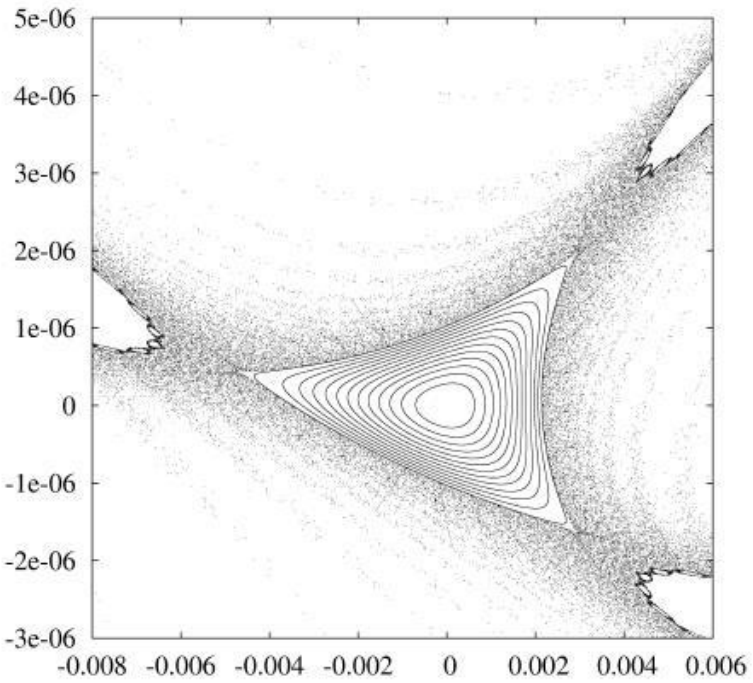

Chaotic motion

- **Poincare-Birkhoff** theorem states that under **perturbation** of a **resonance** only an **even number** of **fixed points** survives (**half stable** and the other **half unstable**)
- **Themselves** get **destroyed** when perturbation gets **higher**, etc. (**self-similar** fixed points)
- Resonance **islands grow** and **resonances** can **overlap** allowing diffusion of particles

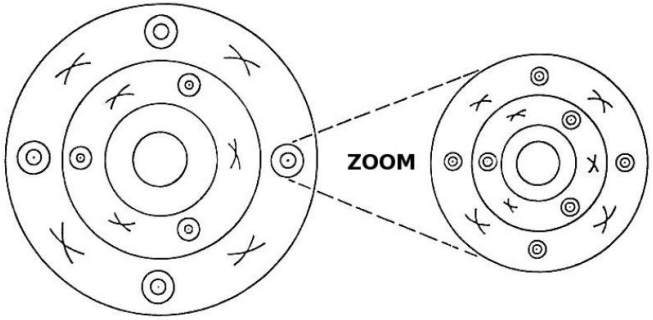

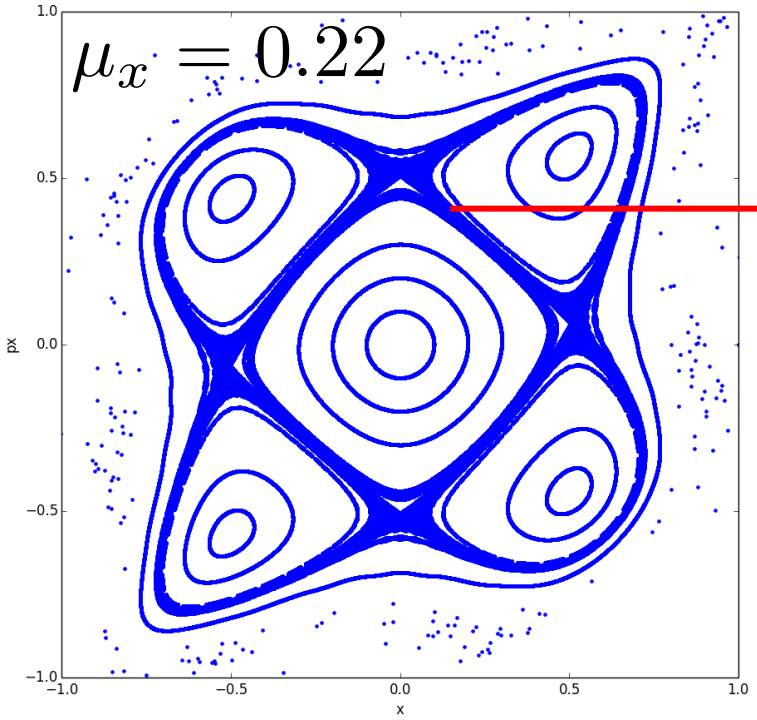

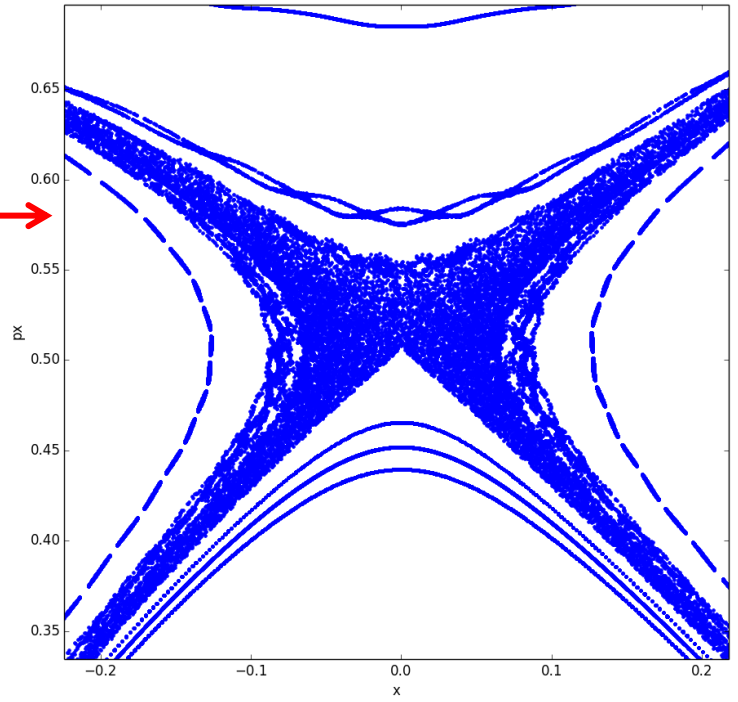

Resonance overlap criterion

- When perturbation grows, the resonance island width grows
- **Chirikov** (1960, 1979) proposed a **criterion** for the **overlap** of two **neighboring resonances** and the onset of orbit diffusion
- The **distance** between two resonances is $\delta \hat{J}_{1\ n,n'} = \dfrac{2\left(\frac{1}{n_1+n_2} - \frac{1}{n_1'+n_2'}\right)}{\left|\frac{\partial^2 \bar{H}_0(\hat{\mathbf{J}})}{\partial \hat{J}_1^{\,2}}\right|_{\hat{J}_1=\hat{J}_{10}}}$
- The **simple overlap criterion** is

$$\Delta \hat{J}_{n\ max} + \Delta \hat{J}_{n'\ max} \geq \delta \hat{J}_{n,n'}$$

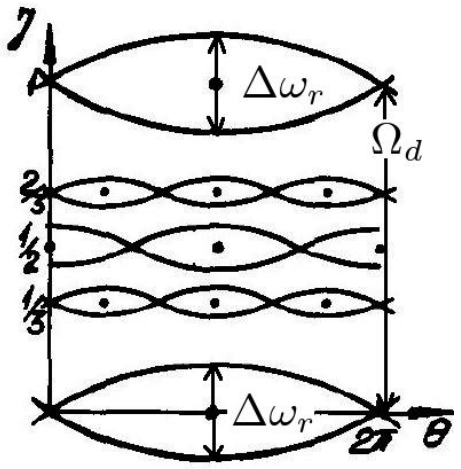

Resonance overlap criterion

- When perturbation grows, the resonance island width grows
- **Chirikov** (1960, 1979) proposed a **criterion** for the **overlap** of two **neighboring resonances** and the onset of orbit diffusion
- The **distance** between two resonances is $\delta\hat{J}_{1\ n,n'} = \dfrac{2\left(\frac{1}{n_1+n_2} - \frac{1}{n_1'+n_2'}\right)}{\left|\frac{\partial^2 \bar{H}_0(\hat{\mathbf{J}})}{\partial \hat{J}_1^{\,2}}\right|_{\hat{J}_1=\hat{J}_{10}}}$
- The **simple overlap criterion** is
  $\Delta\hat{J}_{n\ max} + \Delta\hat{J}_{n'\ max} \geq \delta\hat{J}_{n,n'}$
- Considering the **width** of **chaotic layer** and **secondary islands**, the "two thirds" rule apply $\Delta\hat{J}_{n\ max} + \Delta\hat{J}_{n'\ max} \geq \frac{2}{3}\delta\hat{J}_{n,n'}$
- Example: **Chirikov's standard map**

$$p_{n+1} = p_n + K\sin(\theta_n) \qquad \theta_{n+1} = \theta_n + p_{n+1}$$

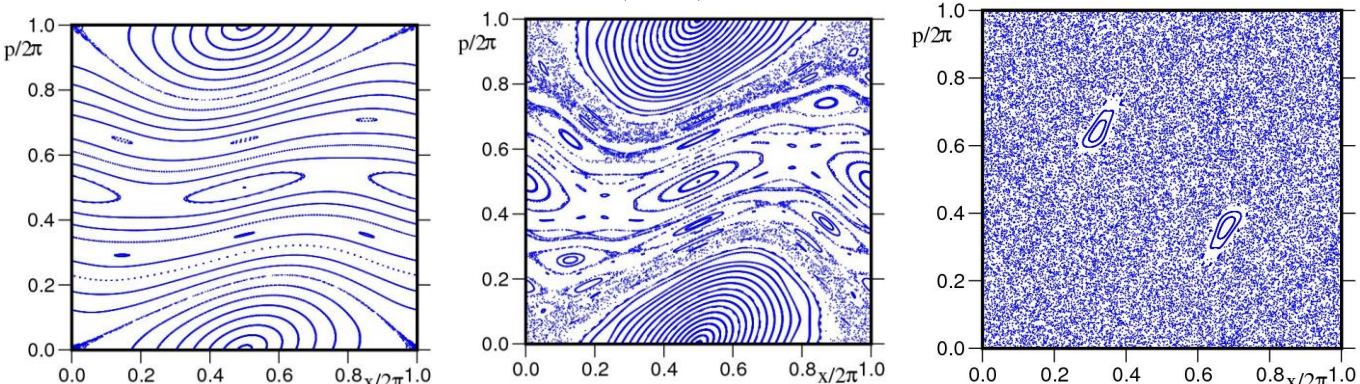

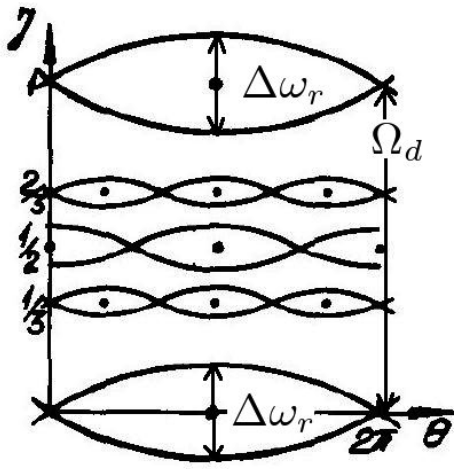

Resonance overlap criterion

- When perturbation grows, the resonance island width grows
- **Chirikov** (1960, 1979) proposed a **criterion** for the **overlap** of two **neighboring resonances** and the onset of orbit diffusion
- The **distance** between two resonances is $\delta \hat{J}_{1\ n,n'} = \dfrac{2\left(\frac{1}{n_1+n_2} - \frac{1}{n_1'+n_2'}\right)}{\left|\frac{\partial^2 \bar{H}_0(\hat{\mathbf{J}})}{\partial \hat{J}_1^{\,2}}\right|_{\hat{J}_1=\hat{J}_{10}}}$
- The **simple overlap criterion** is
  $\Delta \hat{J}_{n\ max} + \Delta \hat{J}_{n'\ max} \geq \delta \hat{J}_{n,n'}$
- Considering the **width** of **chaotic layer** and **secondary islands**, the "two thirds" rule apply $\Delta \hat{J}_{n\ max} + \Delta \hat{J}_{n'\ max} \geq \frac{2}{3}\delta \hat{J}_{n,n'}$
- The main limitation is the **geometrical nature** of the criterion (**difficulty** to be **extended** for **> 2 degrees of freedom**)

$$p_{n+1} = p_n + K\sin(\theta_n) \qquad \theta_{n+1} = \theta_n + p_{n+1}$$

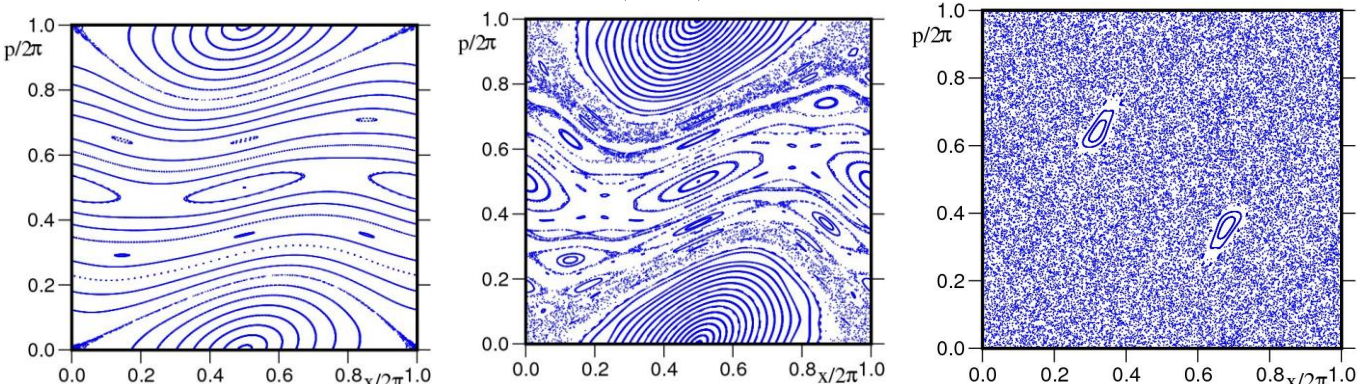

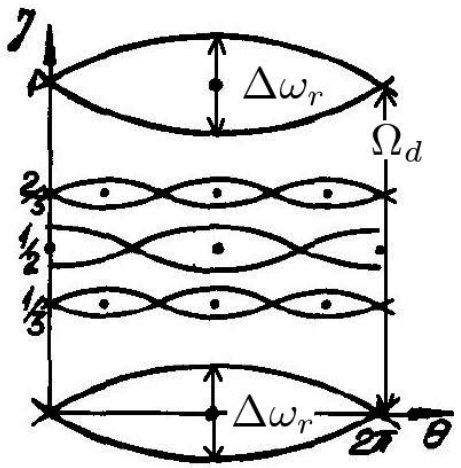

Increasing dimensions

- For $(y_0, p_{y0}) \neq (0,0)$, i.e. by adding another degree of freedom **chaotic motion** is **enhanced**

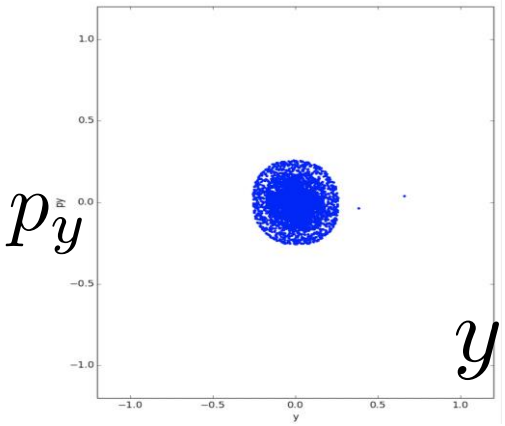

$$(\mu_x, \mu_y) = (0.22, 0.24)$$

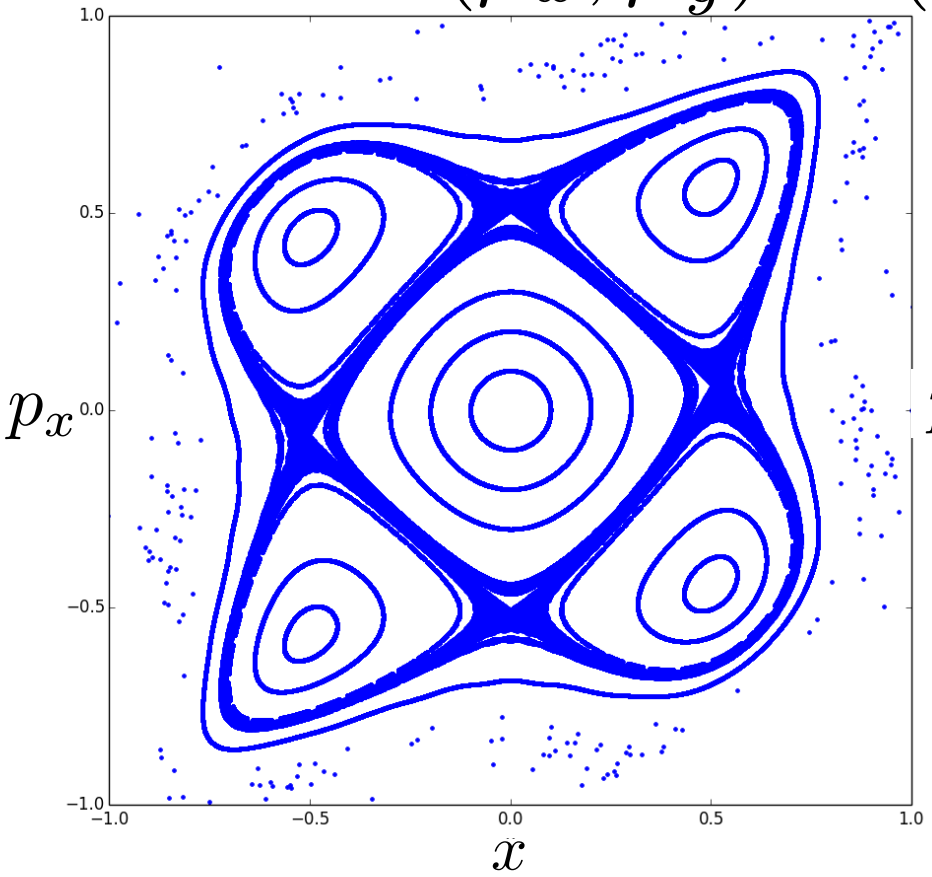

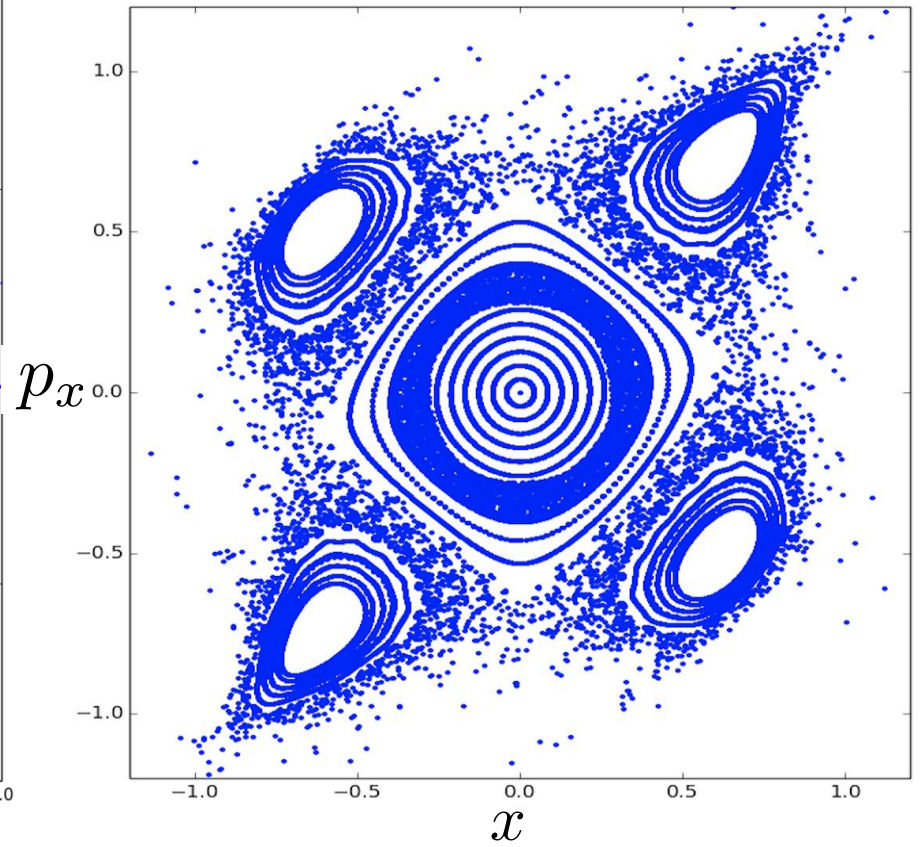

Increasing dimensions

- For $(y_0, p_{y0}) \neq (0,0)$, i.e. by adding another degree of freedom **chaotic motion** is **enhanced**
- At the same time, **analysis** of phase space on **surface of section** becomes **difficult** to interpret, as these are projections of 4D objects on a 2D plane

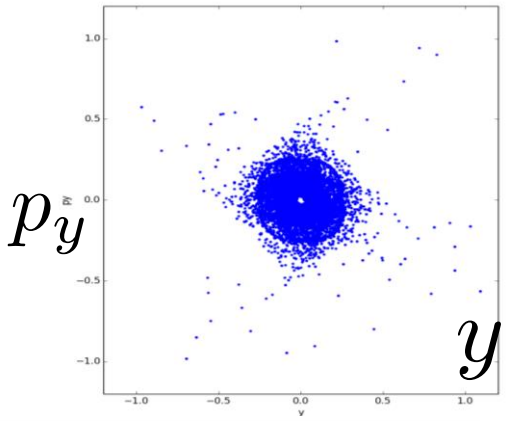

$$(\mu_x, \mu_y) = (0.22, 0.24)$$

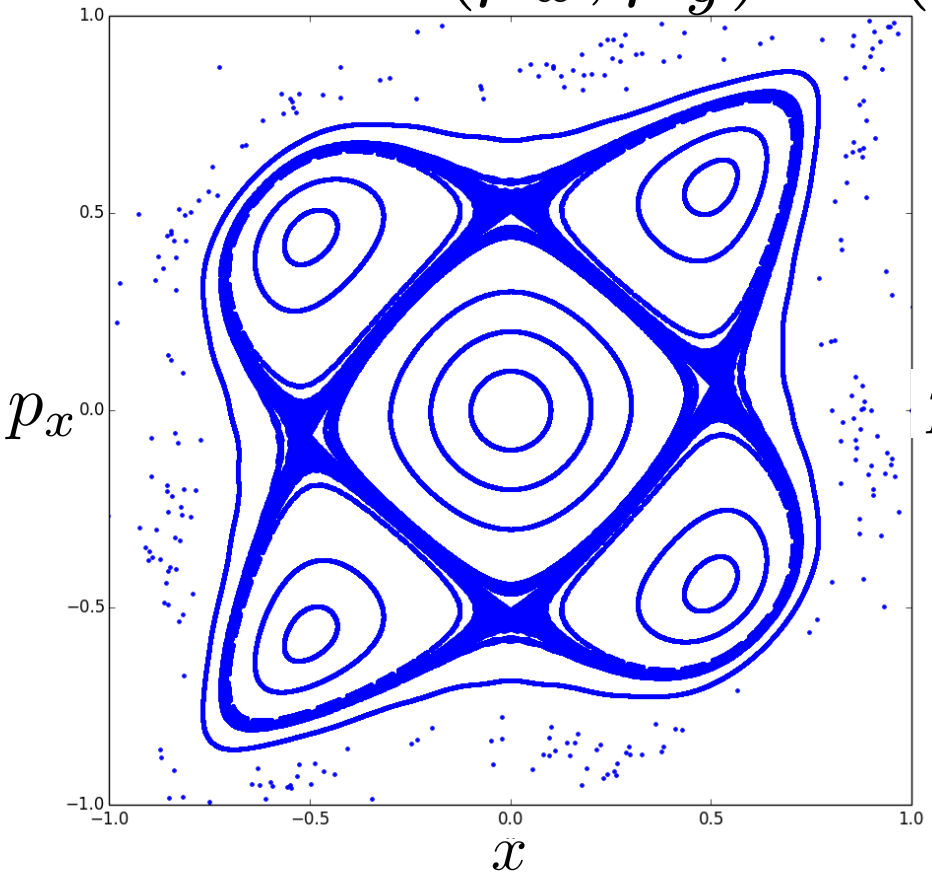

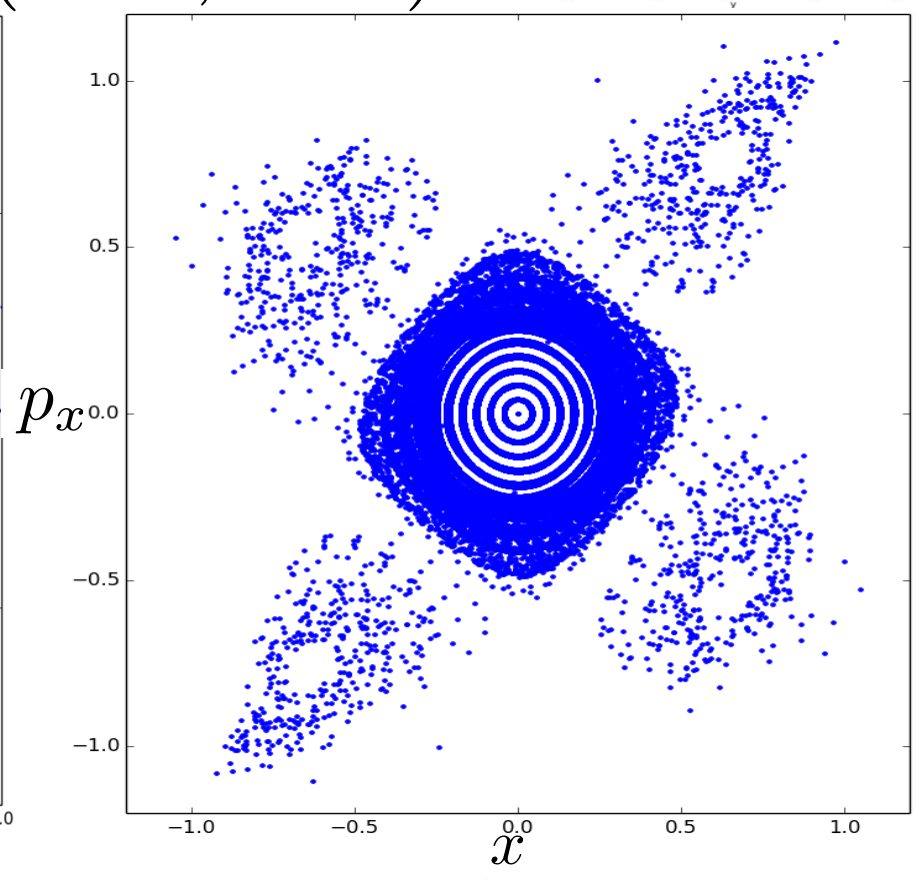

Chaos detection methods

- Computing/measuring **dynamic aperture** (DA) or particle survival

  A. Chao et al., PRL 61, 24, 2752, 1988;
  F. Willeke, PAC95, 24, 109, 1989.

- Computation of Lyapunov exponents

  F. Schmidt, F. Willeke and F. Zimmermann, PA, 35, 249, 1991;
  M. Giovannozi, W. Scandale and E. Todesco, PA 56, 195, 1997

- Variance of unperturbed action (a la Chirikov)

  B. Chirikov, J. Ford and F. Vivaldi, AIP CP-57, 323, 1979
  J. Tennyson, SSC-155, 1988;
  J. Irwin, SSC-233, 1989

- Fokker-Planck diffusion coefficient in actions

  T. Sen and J.A. Elisson, PRL 77, 1051, 1996
  YP and F. Zimmerman, PRSTAB, 5 (7), 074001

- **Frequency map analysis**

Dynamic aperture

Dynamic Aperture

- The most direct way to evaluate the non-linear dynamics performance of a ring is the computation of **Dynamic Aperture**
- Particle motion due to multi-pole errors is generally non-bounded, so chaotic particles can **escape to infinity**
- This is not true for all non-linearities (e.g. the beam-beam force)
- Need a **symplectic** tracking code to follow particle trajectories (a lot of initial conditions) for a **number of turns** (depending on the given problem) until the particles start getting lost. This **boundary** defines the **Dynamic aperture**
- As multi-pole errors may not be completely known, one has to track through **several machine models** built by **random distribution** of these errors
- One could start with **4D** (only transverse) tracking but certainly needs to simulate **5D** (constant energy deviation) and finally **6D** (synchrotron motion included)

Dynamic Aperture plots

- Dynamic aperture plots show the maximum initial values of stable trajectories in x-y coordinate space at a particular point in the lattice, for a range of energy errors.
  - The beam size can be shown on the same plot.
  - Generally, the goal is to allow some significant margin in the design - the measured dynamic aperture is often smaller than the predicted dynamic aperture.

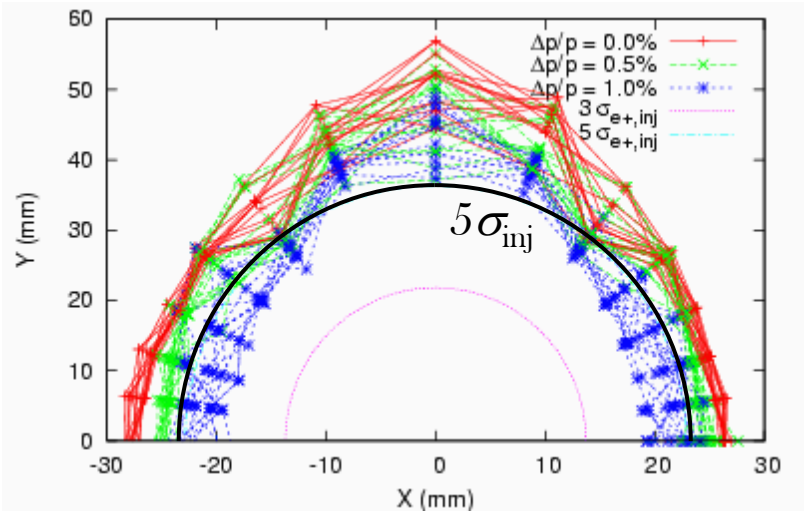

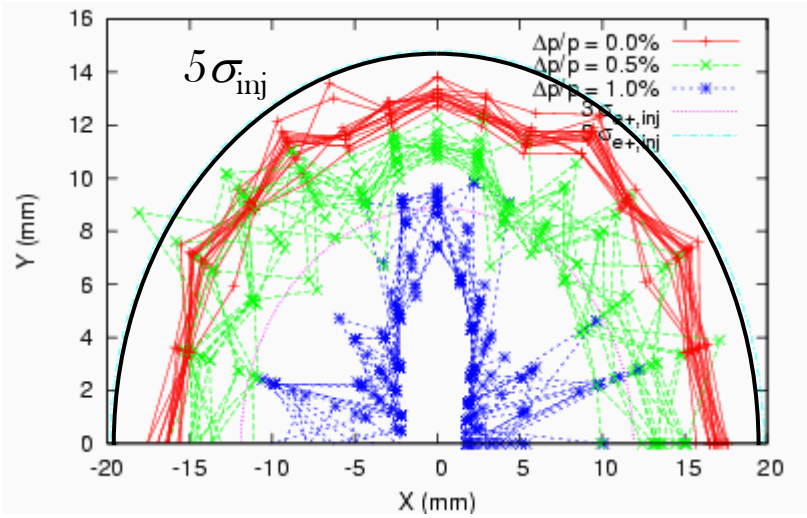

Dynamic aperture including damping

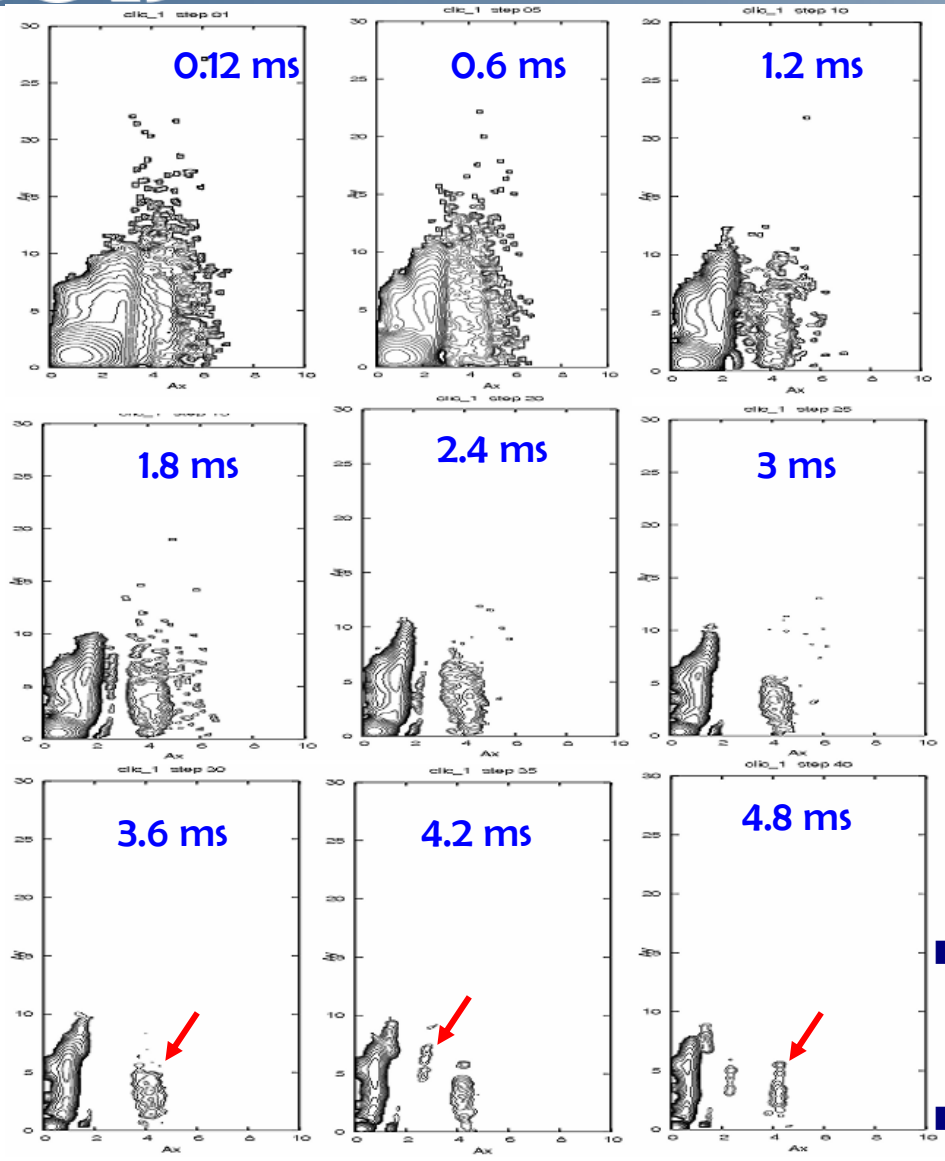

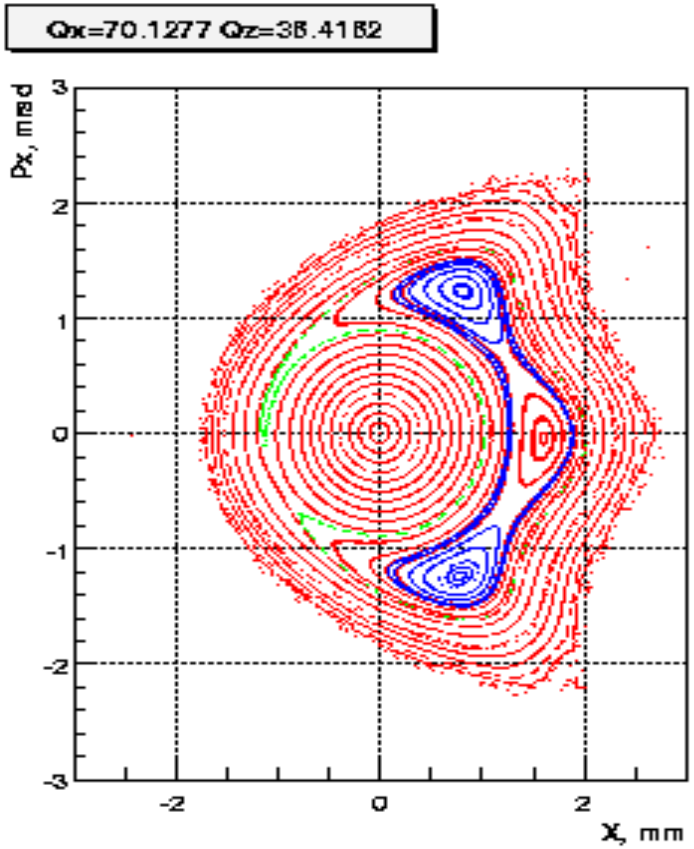

- Including radiation damping and excitation shows that 0.7% of the particles are lost during the damping
- Certain particles seem to damp away from the beam core, on resonance islands

DA scanning for the LHC

D.Pellegrini

- **Min. Dynamic Aperture (DA)** with **intensity** vs **crossing angle**, for **nominal optics** ($\beta^* = 40$ **cm**) and **BCMS** beam (**2.5 μm** emittance), 15 units of chromaticity
- For **1.1×10^{11} p**
  - At $\theta_c/2 = 185$ **μrad** (~**12 σ** separation), DA around **6 σ** **(good lifetime observed)**
  - At $\theta_c/2 = 140$ **μrad** (~**9 σ** separation), DA below **5 σ** **(reduced lifetime observed)**
  - **Improvement** for low octupoles, low chromaticity and WP optimisation (observed in **operation**)

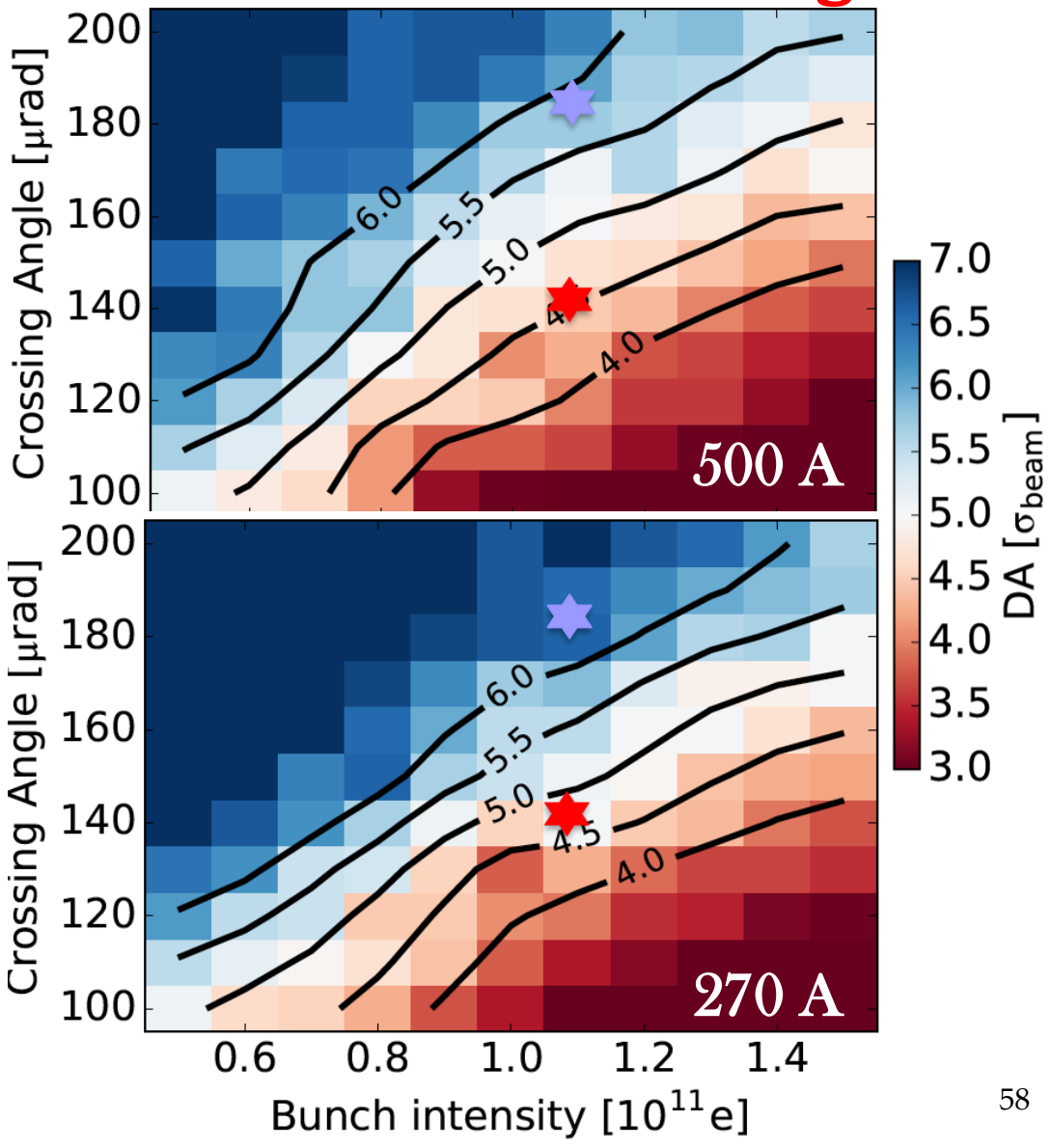

DA guiding machine performance

- B1 suffering from lower lifetime in the LHC
- DA simulations predicted the required adjustment
- Fine-tune scan performed and applied in operation, solving B1 lifetime problem

D. Pellegrini et al., 2016

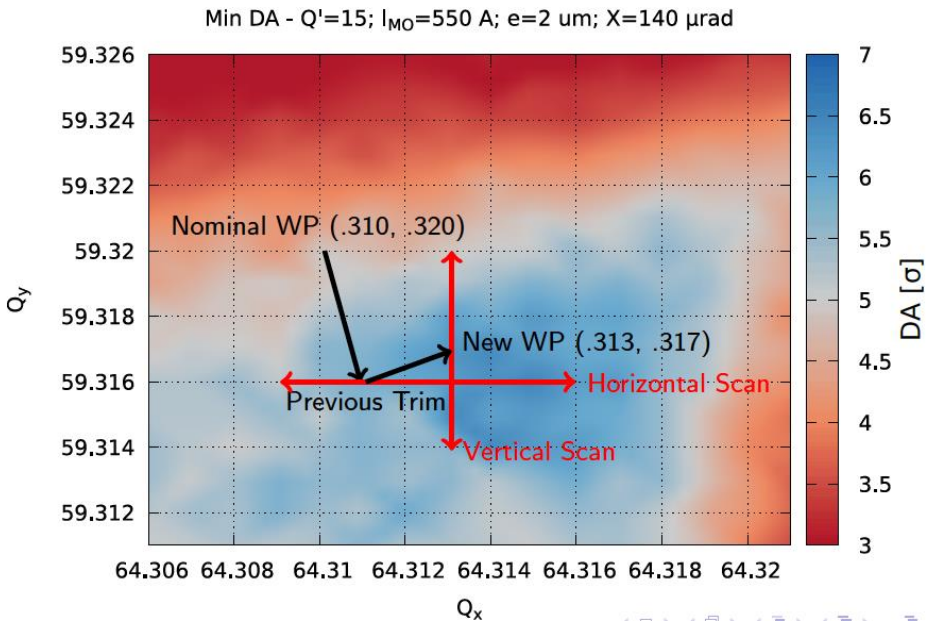

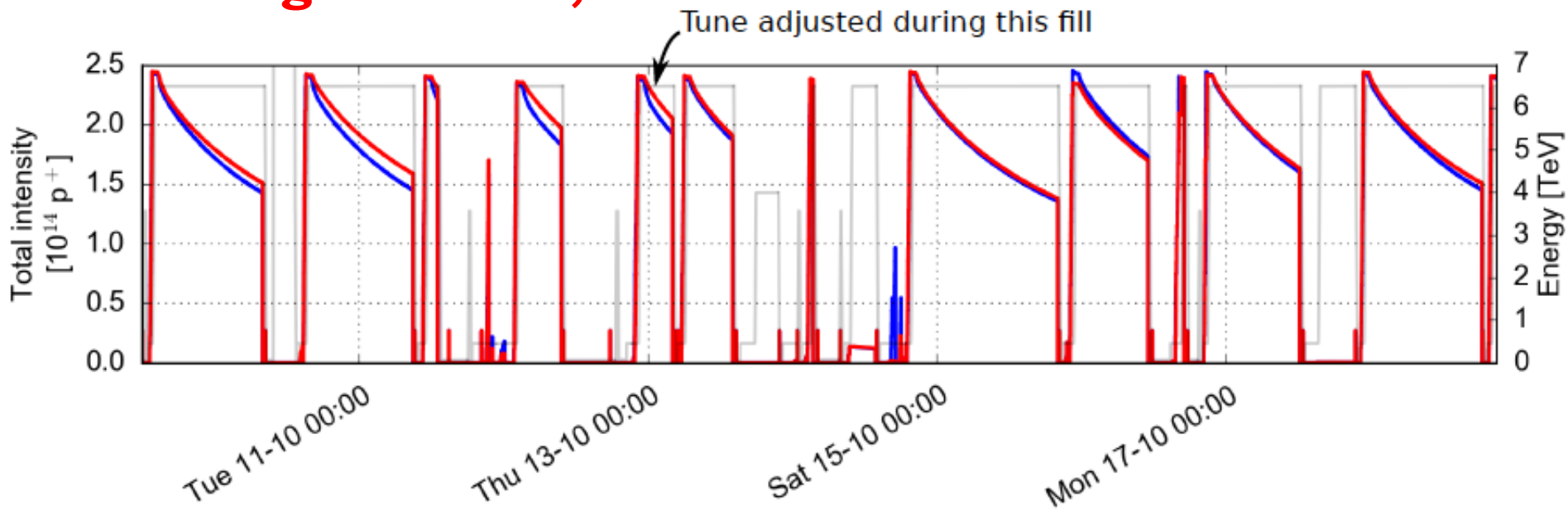

HL-LHC operational scenario

- Reduction of **crossing angle** at **constant luminosity**, reduces **pileup density** (by elongating the luminous region) and **triplet irradiation**

YP, N. Karastathis and D. Pellegrini et al., 2018

Relaxed DA

Aggressive DA

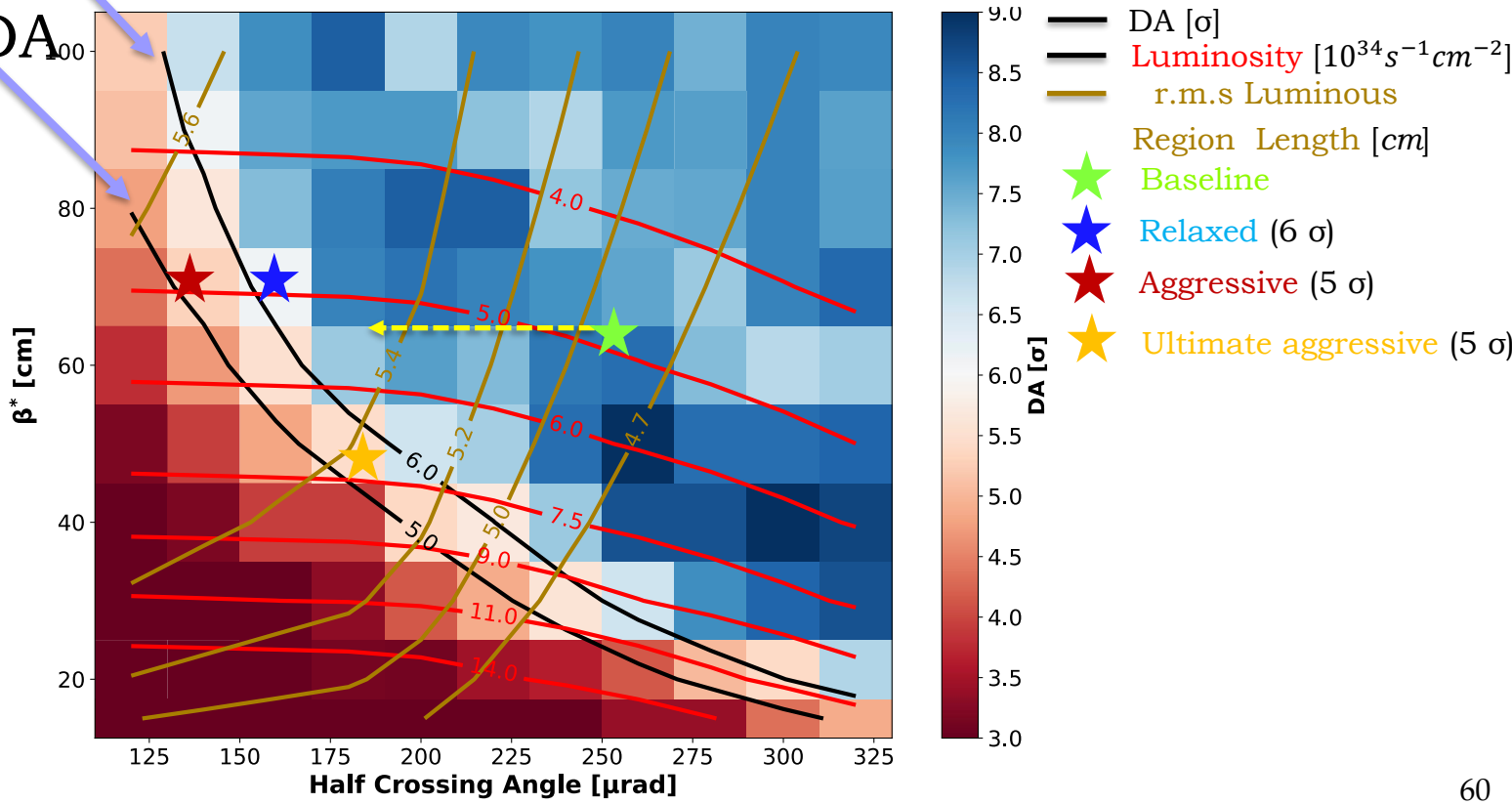

Genetic Algorithms for lattice optimisation

- MOGA – **Multi Objective Genetic Algorithms** are being recently used to optimise linear but also non-linear dynamics of electron low emittance storage rings
- Use **knobs** quadrupole strengths, chromaticity sextupoles and correctors with some constraints
- Target ultra-low horizontal emittance, increased lifetime and high dynamic aperture

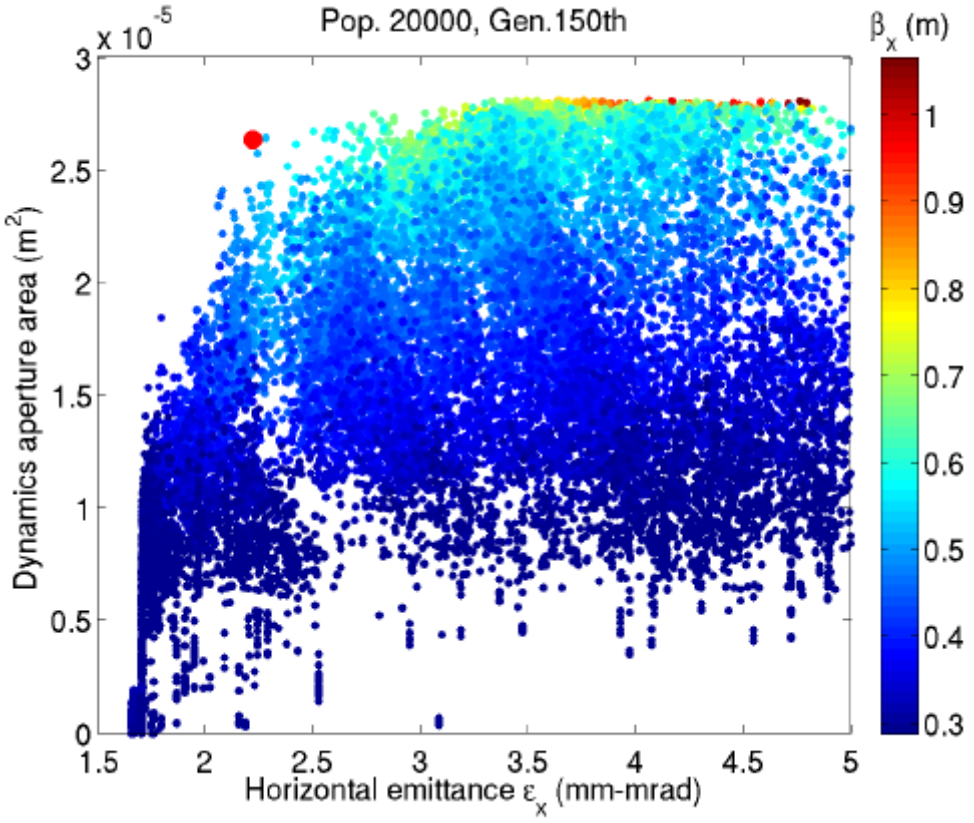

Measuring Dynamic Aperture

- During LHC design phase, DA target was 2x higher than collimator position, due to statistical fluctuation, finite mesh, linear imperfections, short tracking time, multi-pole time dependence, ripple and a 20% safety margin
- Better knowledge of the model led to good agreement between measurements and simulations for actual LHC
- Necessity to build an accurate magnetic model (from beam based measurements)

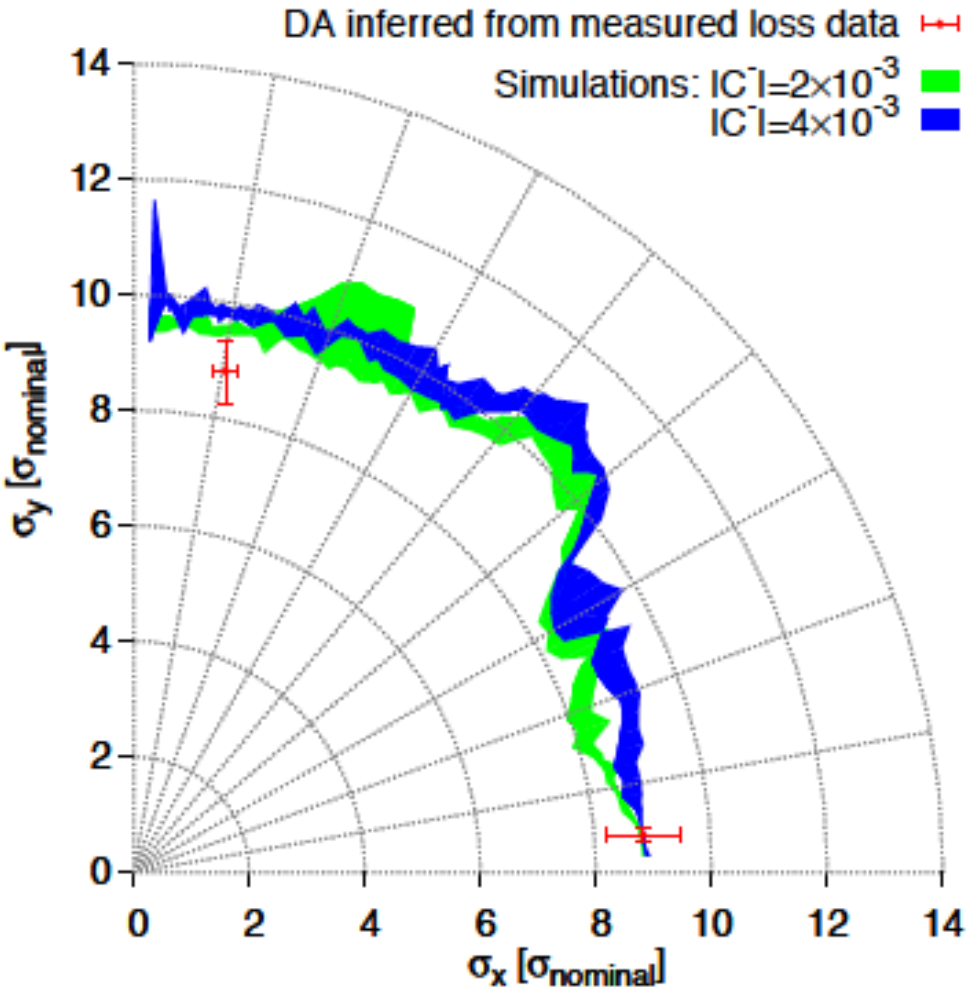

E.Mclean, PhD thesis, 2014

Lyapunov exponent

Lyapunov exponent

- Chaotic motion implies **sensitivity** to **initial condition**
- Two infinitesimally close **chaotic trajectories** in phase space with initial difference $\delta\mathbf{Z}_0$ will end-up diverging with rate
$$|\delta\mathbf{Z}(t)| \approx e^{\lambda t}|\delta\mathbf{Z}_0|$$
with λ the maximum **Lyapunov exponent**
- There is as many exponents as the phase space dimensions (Lyapunov spectrum)
- The largest one is the **Maximal Lyapunov exponent** (MLE) is defined as
$$\lambda = \lim_{t\to\infty}\lim_{\delta\mathbf{Z}_0\to 0}\frac{1}{t}\ln\frac{|\delta\mathbf{Z}(t)|}{|\delta\mathbf{Z}_0|}$$

Lyapunov exponent: chaotic orbit

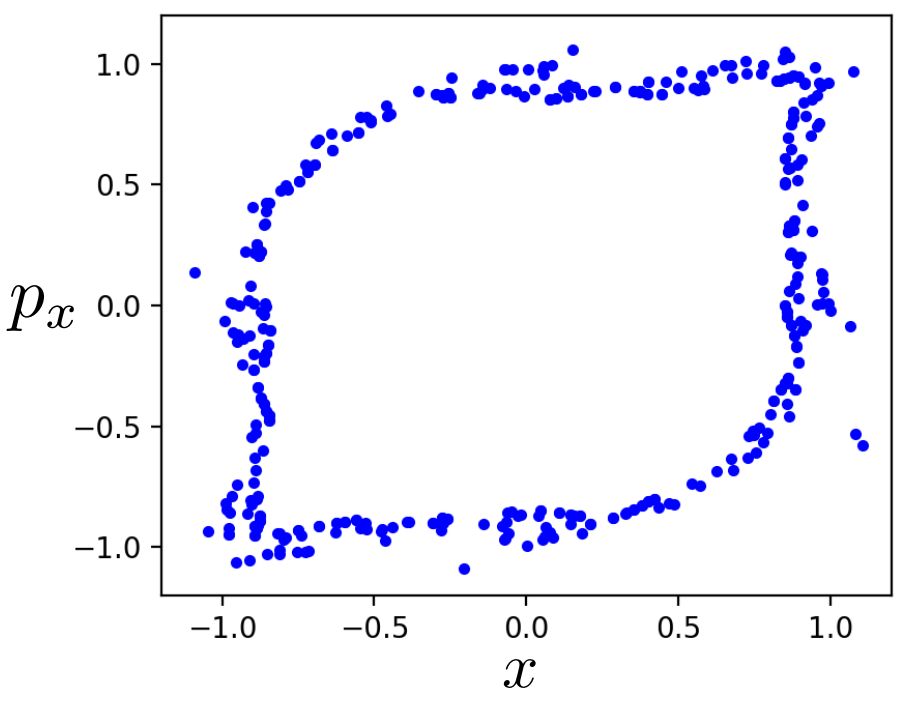

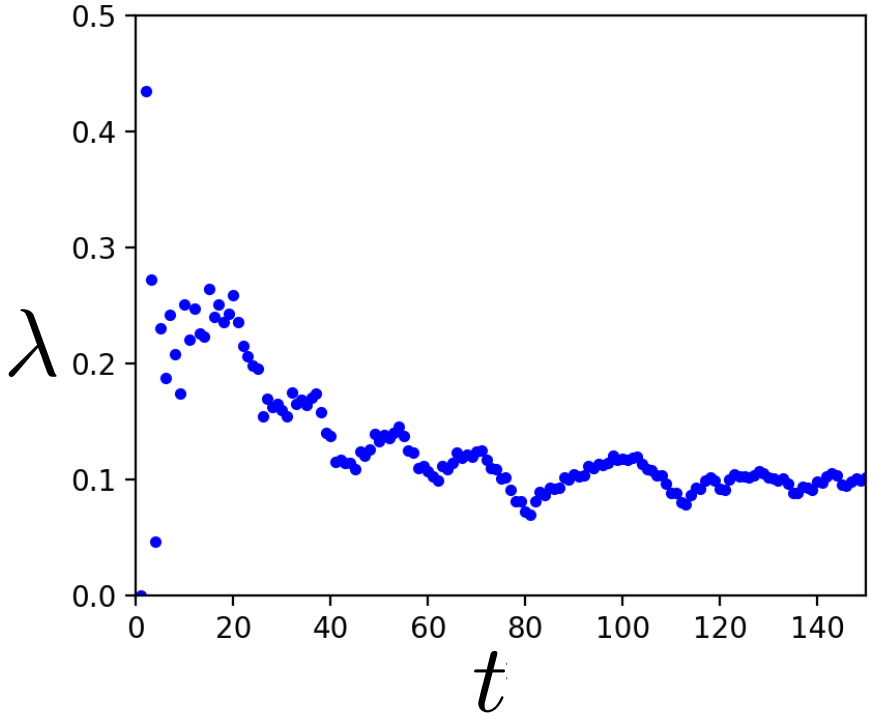

- Maximum Lyapounov exponent converges towards a **positive value** for a chaotic orbit

$$\lambda = \lim_{t\to\infty} \lim_{\delta\mathbf{Z}_0\to 0} \frac{1}{t} \ln \frac{|\delta\mathbf{Z}(t)|}{|\delta\mathbf{Z}_0|}$$

Lyapunov exponent: regular orbit

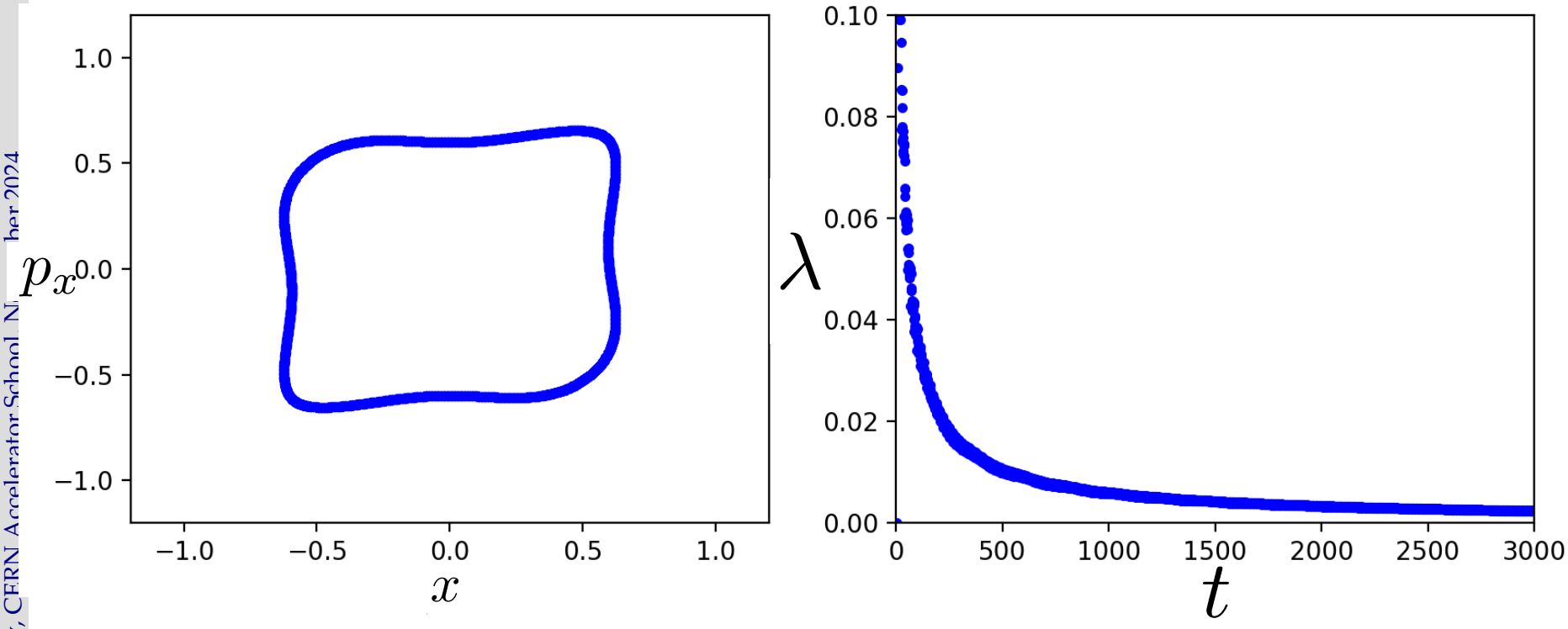

- Maximum Lyapounov exponent converges towards **zero** for a chaotic orbit

$$\lambda = \lim_{t\to\infty} \lim_{\delta\mathbf{Z}_0\to 0} \frac{1}{t} \ln \frac{|\delta\mathbf{Z}(t)|}{|\delta\mathbf{Z}_0|}$$

Lyapunov exponent: regular orbit

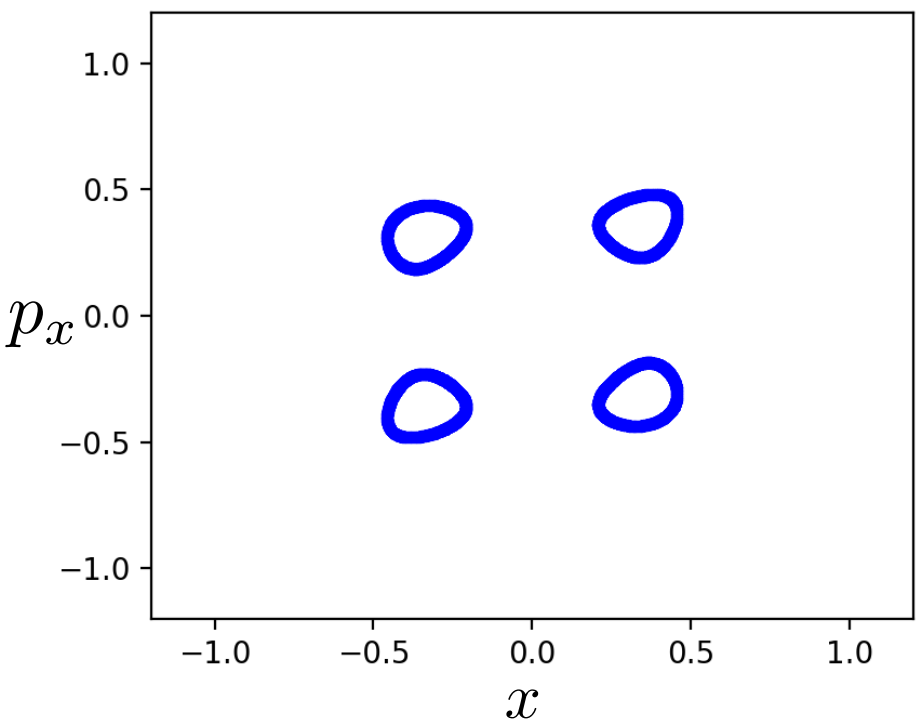

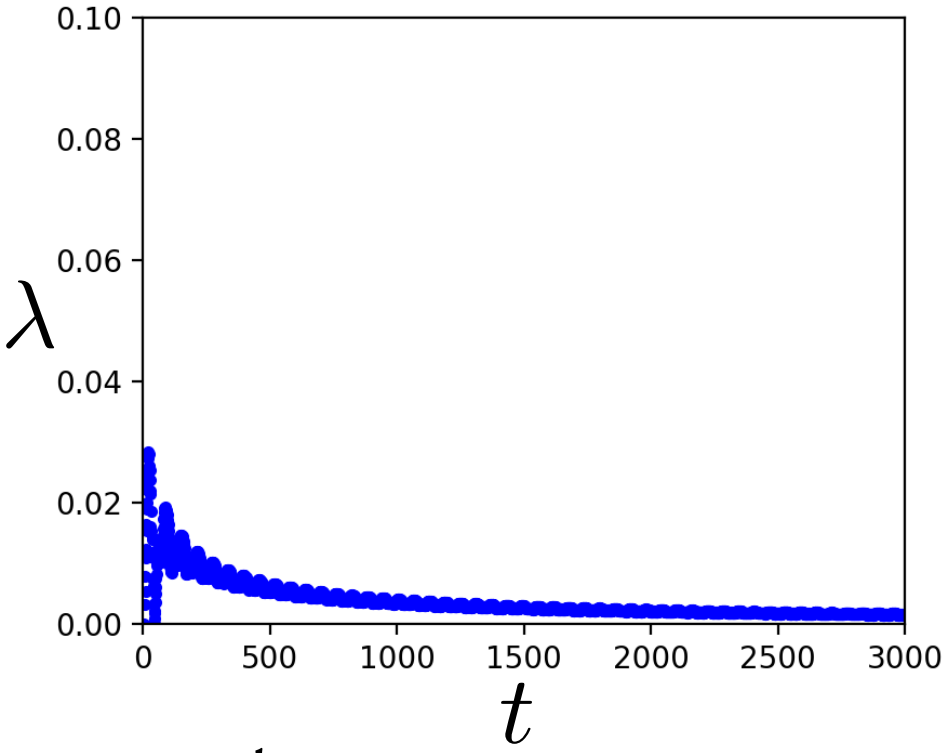

- Maximum Lyapounov exponent converges more slowly towards **zero** for a resonant orbit

$$\lambda = \lim_{t\to\infty} \lim_{\delta\mathbf{Z}_0\to 0} \frac{1}{t} \ln \frac{|\delta\mathbf{Z}(t)|}{|\delta\mathbf{Z}_0|}$$

Lyapunov exponent: regular orbit

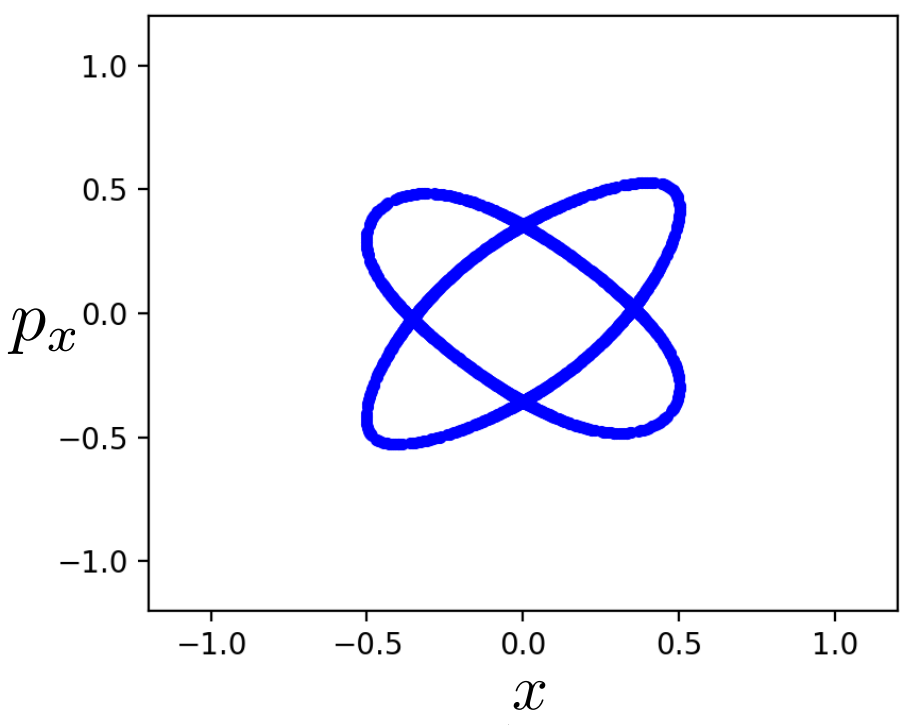

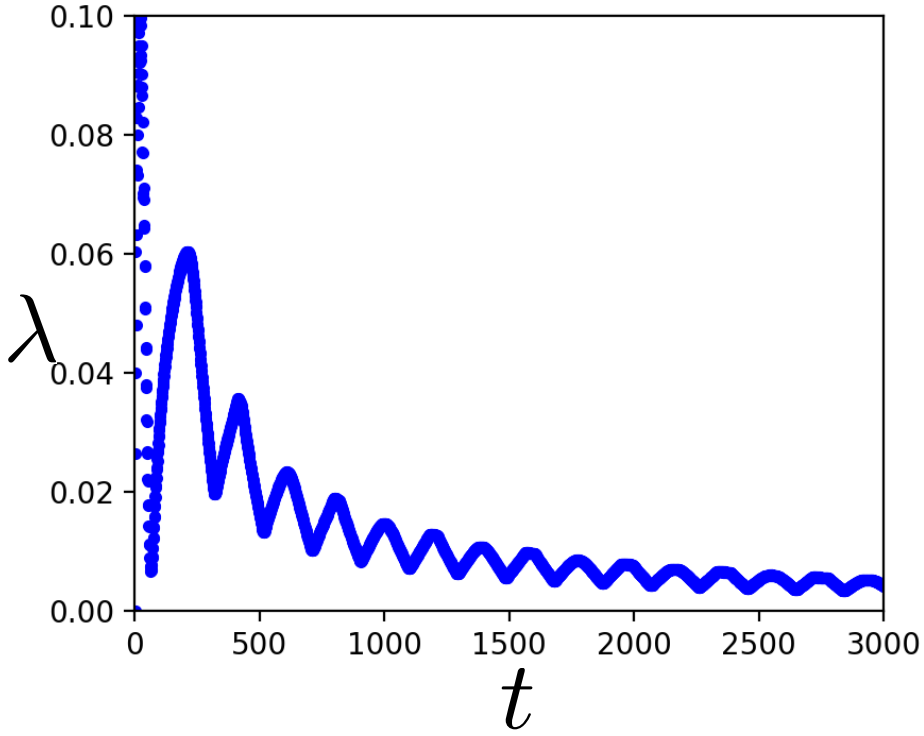

- Maximum Lyapounov exponent converges more slowly towards **zero** for a resonant orbit, in particular close to the separatrix

$$\lambda = \lim_{t\to\infty} \lim_{\delta\mathbf{Z}_0\to 0} \frac{1}{t} \ln \frac{|\delta\mathbf{Z}(t)|}{|\delta\mathbf{Z}_0|}$$

Frequency Map Analysis

Frequency map analysis

- Frequency Map Analysis (FMA) is a numerical method which springs from the studies of J. Laskar (Paris Observatory) putting in evidence the chaotic motion in the Solar Systems
- FMA was successively applied to several dynamical systems
  - Stability of Earth Obliquity and climate stabilization (Laskar, Robutel, 1993)
  - 4D maps (Laskar 1993)
  - Galactic Dynamics (Y.P and Laskar, 1996 and 1998)
  - Accelerator beam dynamics: lepton and hadron rings (Dumas, Laskar, 1993, Laskar, Robin, 1996, Y.P, 1999, Nadolski and Laskar 2001)

Motion on torus

- Consider an integrable Hamiltonian system of the usual form

$$H(\boldsymbol{J}, \boldsymbol{\varphi}, \theta) = H_0(\mathbf{J})$$

- Hamilton's equations give

$$\dot{\phi}_j = \frac{\partial H_0(\mathbf{J})}{\partial J_j} = \omega_j(\mathbf{J}) \Rightarrow \phi_j = \omega_j(\mathbf{J})t + \phi_{j0}$$

$$\dot{J}_j = -\frac{\partial H_0(\mathbf{J})}{\partial \phi_j} = 0 \Rightarrow J_j = \text{const.}$$

- The actions define the surface of an invariant torus
- In complex coordinates the motion is described by

$$\zeta_j(t) = J_j(0)e^{i\omega_j t} = z_{j0}e^{i\omega_j t}$$

- For a **non-degenerate** system $\det\left|\frac{\partial \omega(J)}{\partial J}\right| = \det\left|\frac{\partial^2 H_0(J)}{\partial J^2}\right| \neq 0$ there is a one-to-one correspondence between the actions and the frequency, a frequency map can be defined parameterizing the tori in the frequency space

$$F: \quad (\mathbf{J}) \longrightarrow (\omega)$$

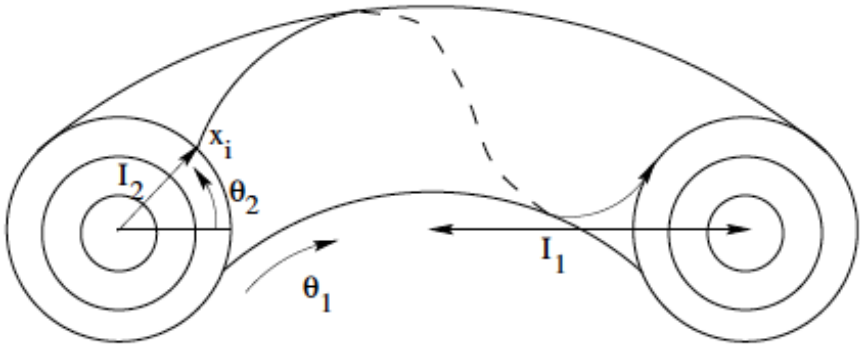

Quasi-periodic motion

- If a transformation is made to some new variables

$$\zeta_j = J_j e^{i\phi_j t} = z_j + \epsilon G_j(\mathbf{z}) = z_j + \epsilon \sum_{\mathbf{m}} c_{\mathbf{m}} z_1^{m_1} z_2^{m_2} \dots z_n^{m_n}$$

- The system is still integrable but the tori are distorted
- The motion is then described by

$$\zeta_j(t) = z_{j0} e^{i\omega_j t} + \sum_{\mathbf{m}} a_{\mathbf{m}} e^{i\,(\mathbf{m}\cdot\omega)\,t}$$

i.e. a quasi-periodic function of time, with

$$a_{\mathbf{m}} = \epsilon\, c_{\mathbf{m}} z_{10}^{m_1} z_{20}^{m_2} \dots z_{n0}^{m_n} \text{ and } \mathbf{m}\cdot\omega = m_1\omega_1 + m_2\omega_2 + \dots + m_n\omega_n$$

- For a non-integrable Hamiltonian, $H(\mathbf{J},\theta) = H_0(\mathbf{J}) + \epsilon H'(\mathbf{J},\theta)$ and especially if the perturbation is small, most tori persist (**KAM** theory)
- In that case, the motion is still quasi-periodic and a frequency map can be built
- The **regularity** (or not) of the map reveals stable (or chaotic) motion

Building the frequency map

- When a quasi-periodic function $f(t) = q(t) + ip(t)$ in the complex domain is given numerically, it is possible to recover a quasi-periodic approximation

$$f'(t) = \sum_{k=1}^{N} a'_k e^{i\omega'_k t}$$

in a very precise way over a finite time span $[-T, T]$ several orders of magnitude more precisely than simple Fourier techniques

- This approximation is provided by the Numerical Analysis of Fundamental Frequencies – **NAFF** algorithm
- The frequencies ω'_k and complex amplitudes a'_k are computed through an iterative scheme.

The NAFF algorithm

- The first frequency ω_1' is found by the location of the maximum of

$$\phi(\sigma) = \langle f(t), e^{i\sigma t} \rangle = \frac{1}{2T} \int_{-T}^{T} f(t) e^{-i\sigma t} \chi(t) dt$$

where $\chi(t)$ is a weight function

- In most of the cases the Hanning window filter is used $\chi_1(t) = 1 + \cos(\pi t/T)$
- Once the first term $e^{i\omega_1' t}$ is found, its complex amplitude a_1' is obtained and the process is restarted on the remaining part of the function

$$f_1(t) = f(t) - a_1' e^{i\omega_1' t}$$

- The procedure is continued for the number of desired terms, or until a required precision is reached

Frequency determination

- The accuracy of a simple FFT even for a simple sinusoidal signal is not better than $|\nu - \nu_T| = \frac{1}{T}$
- Calculating the Fourier integral explicitly

$$\phi(\omega) = < f(t),\ e^{j\omega t} > = \frac{1}{T}\int_0^T f(t)\, e^{-i\omega t}\, dt$$

shows that the maximum lies in between the main peaks of the FFT

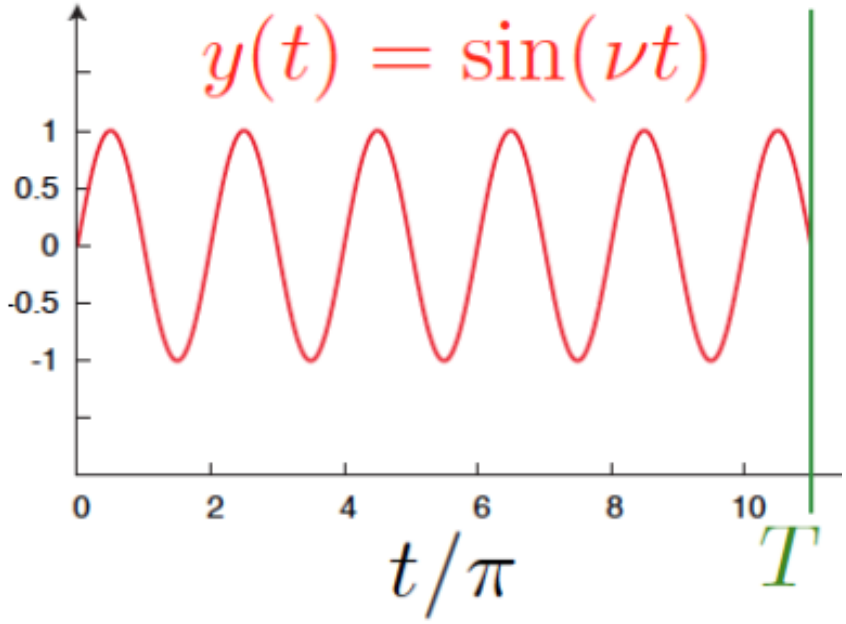

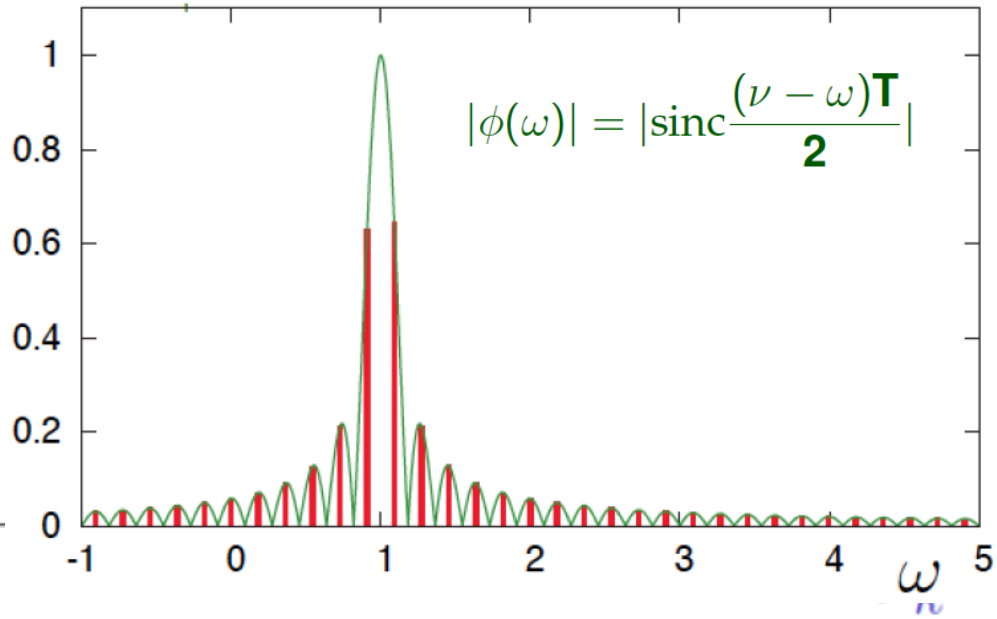

Frequency determination

- A more complicated signal with two frequencies $f(t) = a_1 e^{i\omega_1 t} + a_2 e^{i\omega_2 t}$ shifts slightly the maximum with respect to its real location

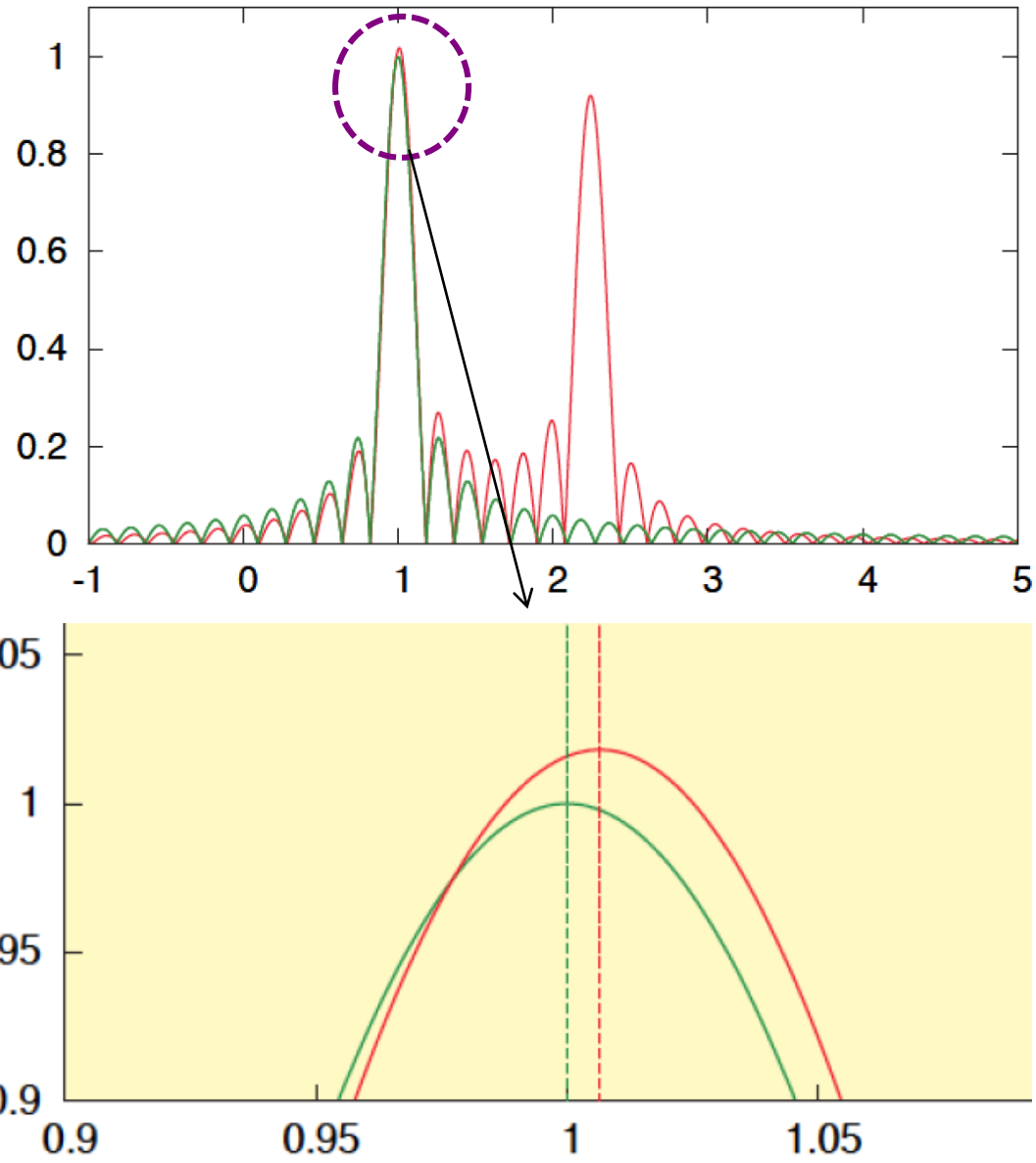

Window function

- A window function like the Hanning filter $\chi_1(t) = 1 + \cos(\pi t/T)$ kills side-lobs and allows a very accurate determination of the frequency

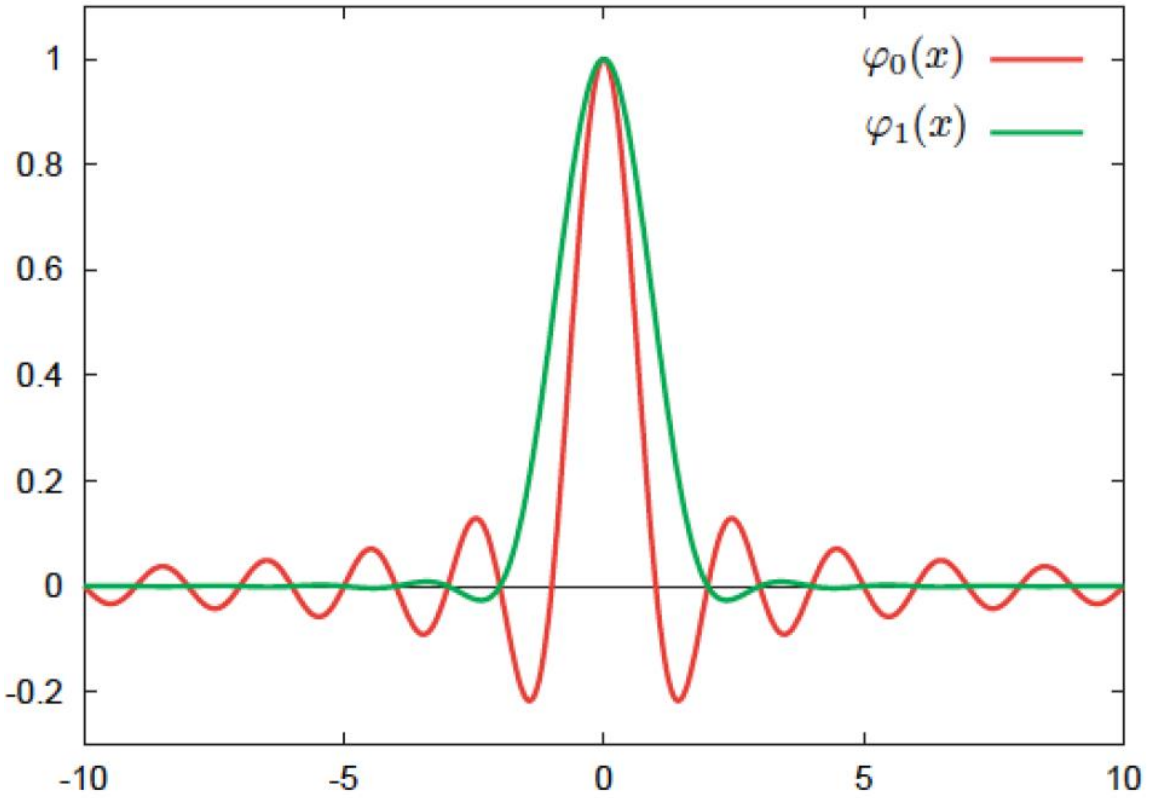

Precision of NAFF

- For a general window function of order p

$$\chi_p(t) = \frac{2^p (p!)^2}{(2p)!}(1+\cos \pi t)^p$$

Laskar (1996) proved a theorem stating that the solution provided by the NAFF algorithm converges asymptotically towards the real KAM quasi-periodic solution with precision

$$\nu_1 - \nu_1^T \propto \frac{1}{T^{2p+2}}$$

- In particular, for no filter (i.e. $p = 0$) the precision is $\frac{1}{T^2}$, whereas for the Hanning filter ($p = 1$), the precision is of the order of $\frac{1}{T^4}$

Aspects of the frequency map

- In the vicinity of a resonance the system behaves like a **pendulum**
- Passing through the **elliptic point** for a fixed angle, a **fixed frequency** (or rotation number) is observed
- Passing through the **hyperbolic point**, a **frequency jump** is observed

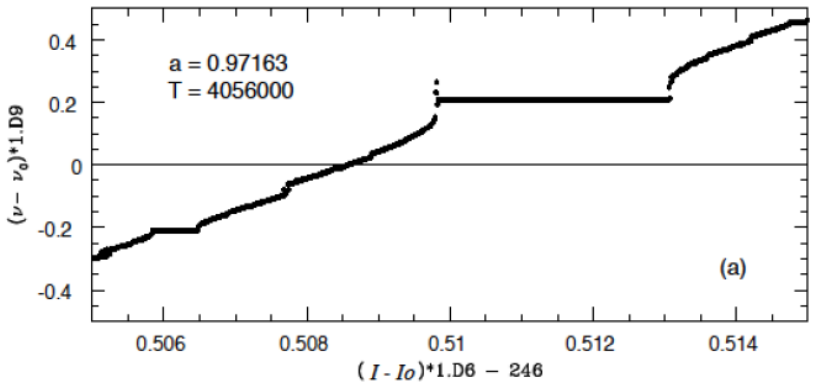

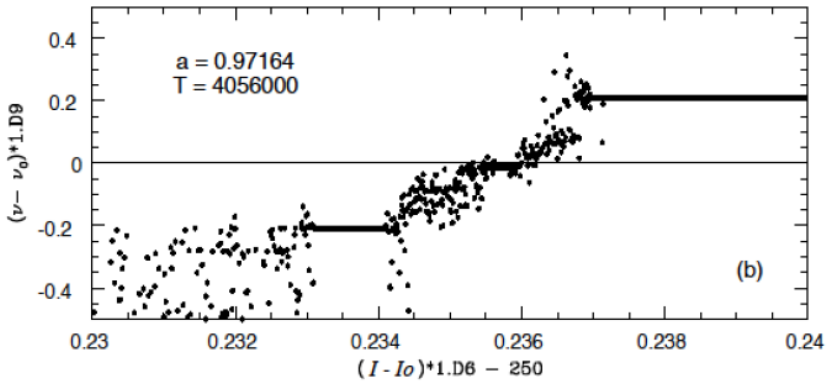

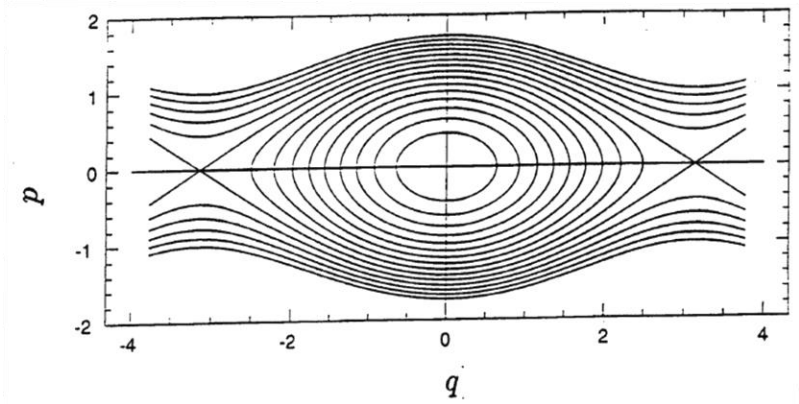

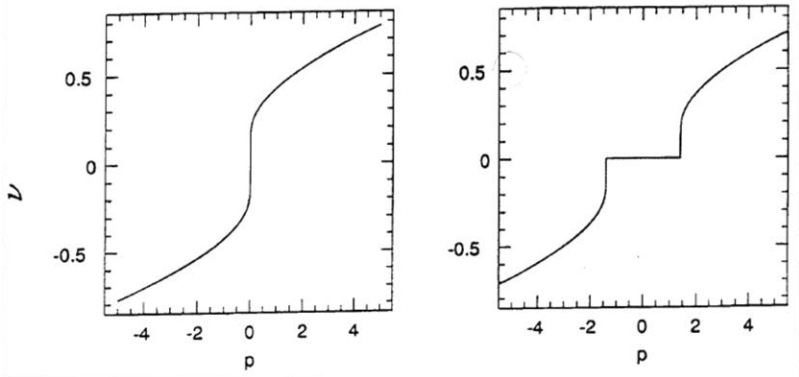

Example: Frequency map for BBLR

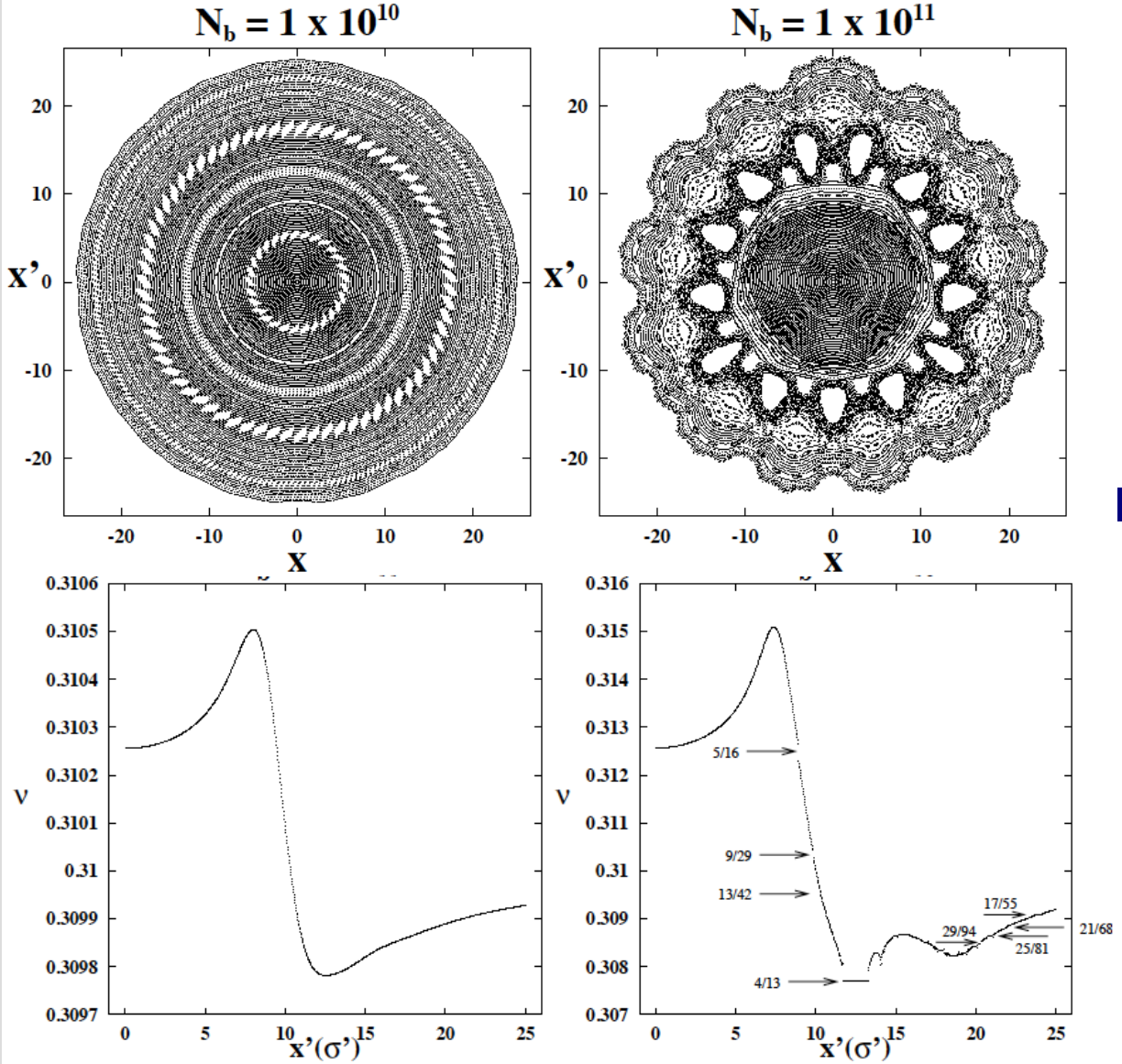

- Simple Beam-beam long range (BBLR) kick and a rotation

$$\begin{pmatrix} x \\ x' \end{pmatrix}_1 = \begin{pmatrix} \cos\mu & \beta^* \sin\mu \\ -\sin\mu/\beta^* & \cos\mu \end{pmatrix} \begin{pmatrix} x + f(x') \\ x' \end{pmatrix}_0 \qquad f(x') = K \left[\frac{1}{x' + \theta_c} \left(1 - e^{-\frac{(x'+\theta_c)^2}{2\sigma_x'^2}} \right) - \frac{1}{\theta_c} \left(1 - e^{-\frac{\theta_c^2}{2\sigma_x'^2}} \right) \right]$$

Example: Frequency map for BBLR

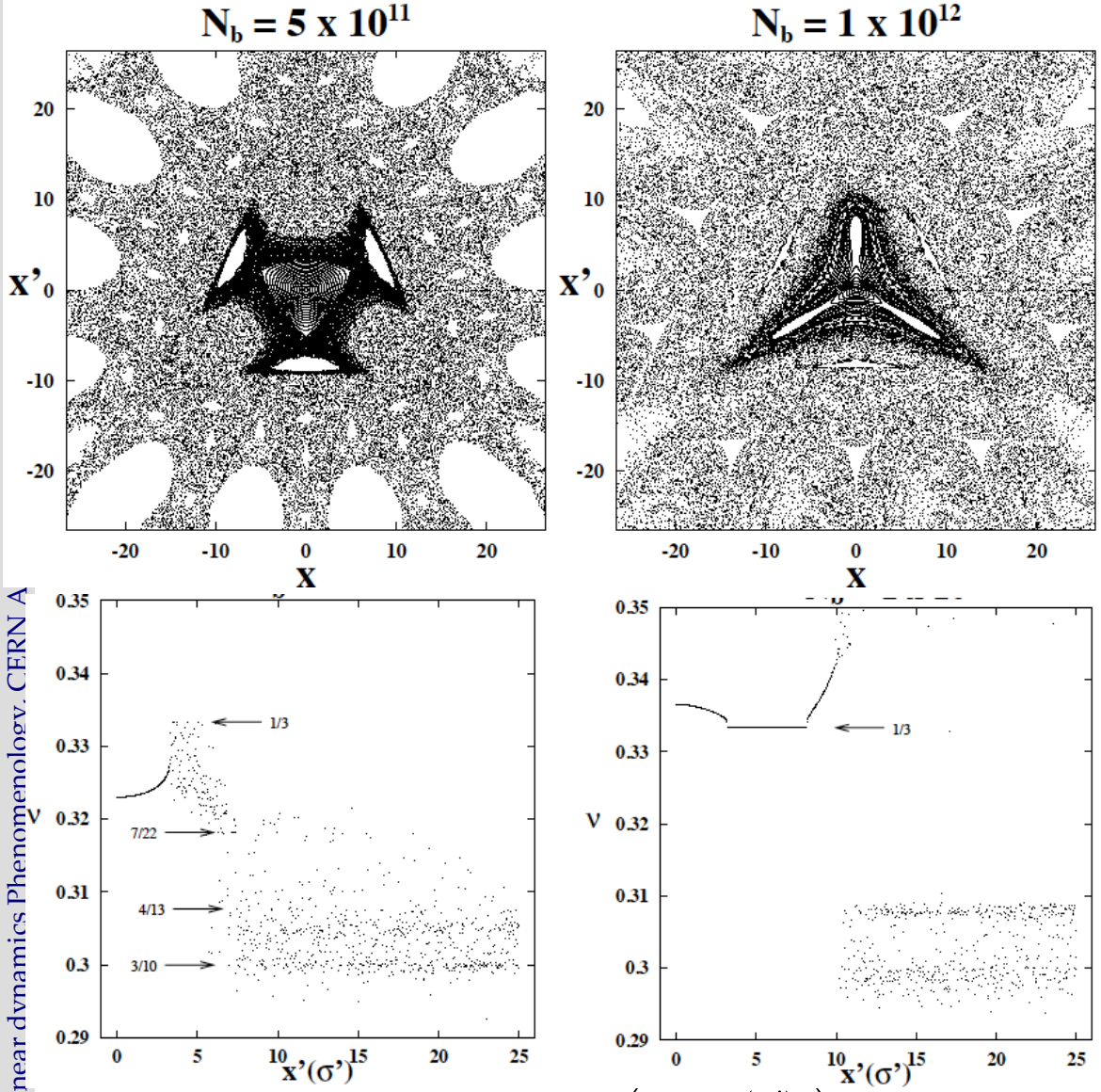

- Simple Beam-beam long range (BBLR) kick and a rotation

$$\begin{pmatrix} x \\ x' \end{pmatrix}_1 = \begin{pmatrix} \cos\mu & \beta^* \sin\mu \\ -\sin\mu/\beta^* & \cos\mu \end{pmatrix} \begin{pmatrix} x + f(x') \\ x' \end{pmatrix}_0 \quad f(x') = K\left[\frac{1}{x'+\theta_c}\left(1 - e^{-\frac{(x'+\theta_c)^2}{2\sigma_x'^2}}\right) - \frac{1}{\theta_c}\left(1 - e^{-\frac{\theta_c^2}{2\sigma_x'^2}}\right)\right]$$

Diffusion in frequency space

- For a **2 degrees of freedom** Hamiltonian system, the **frequency space** is a **line**, the tori are dots on this lines, and the **chaotic zones** are **confined** by the existing KAM tori
- For a system with 3 or more degrees of freedom, KAM tori are still represented by dots but do not prevent chaotic trajectories to diffuse
- This topological possibility of particles diffusing is called **Arnold diffusion**
- This diffusion is supposed to be extremely small in their vicinity, as tori act as effective barriers (**Nechoroshev theory**)

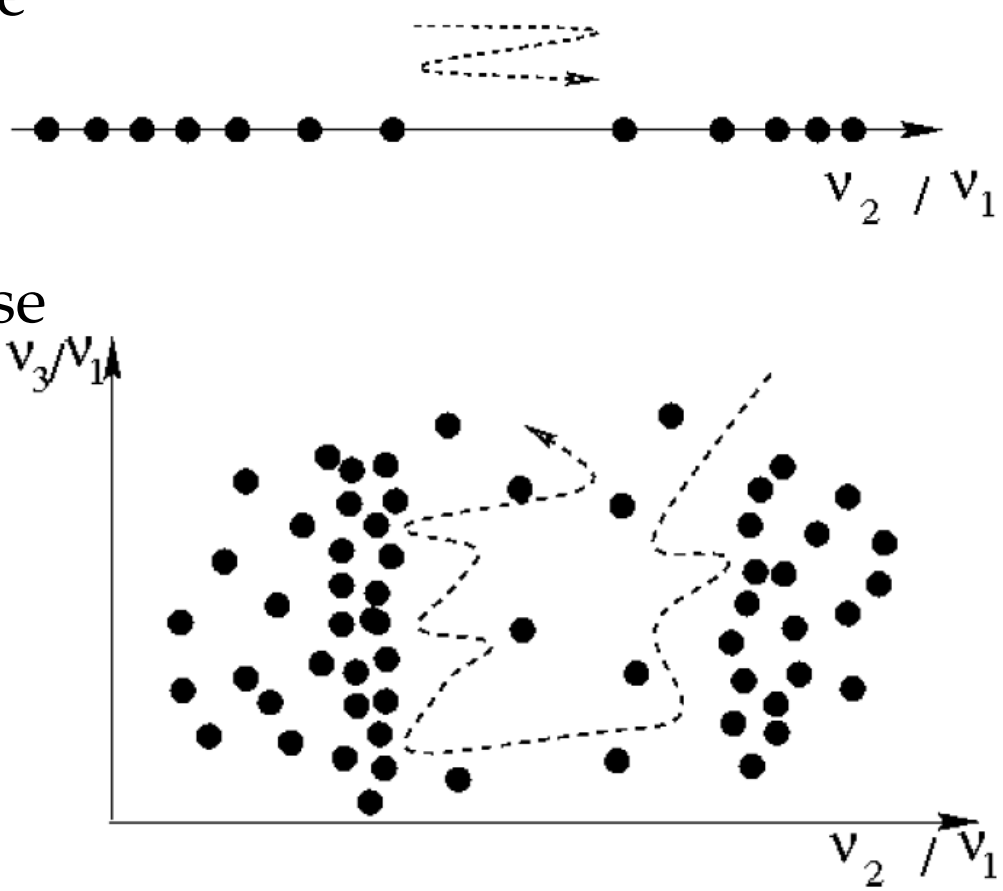

Building the frequency map

- Choose coordinates (x_i, y_i) with p_x and p_y=0
- Numerically integrate the phase trajectories through the lattice for sufficient number of turns
- Compute through NAFF Q_x and Q_y after sufficient number of turns
- Plot them in the tune diagram

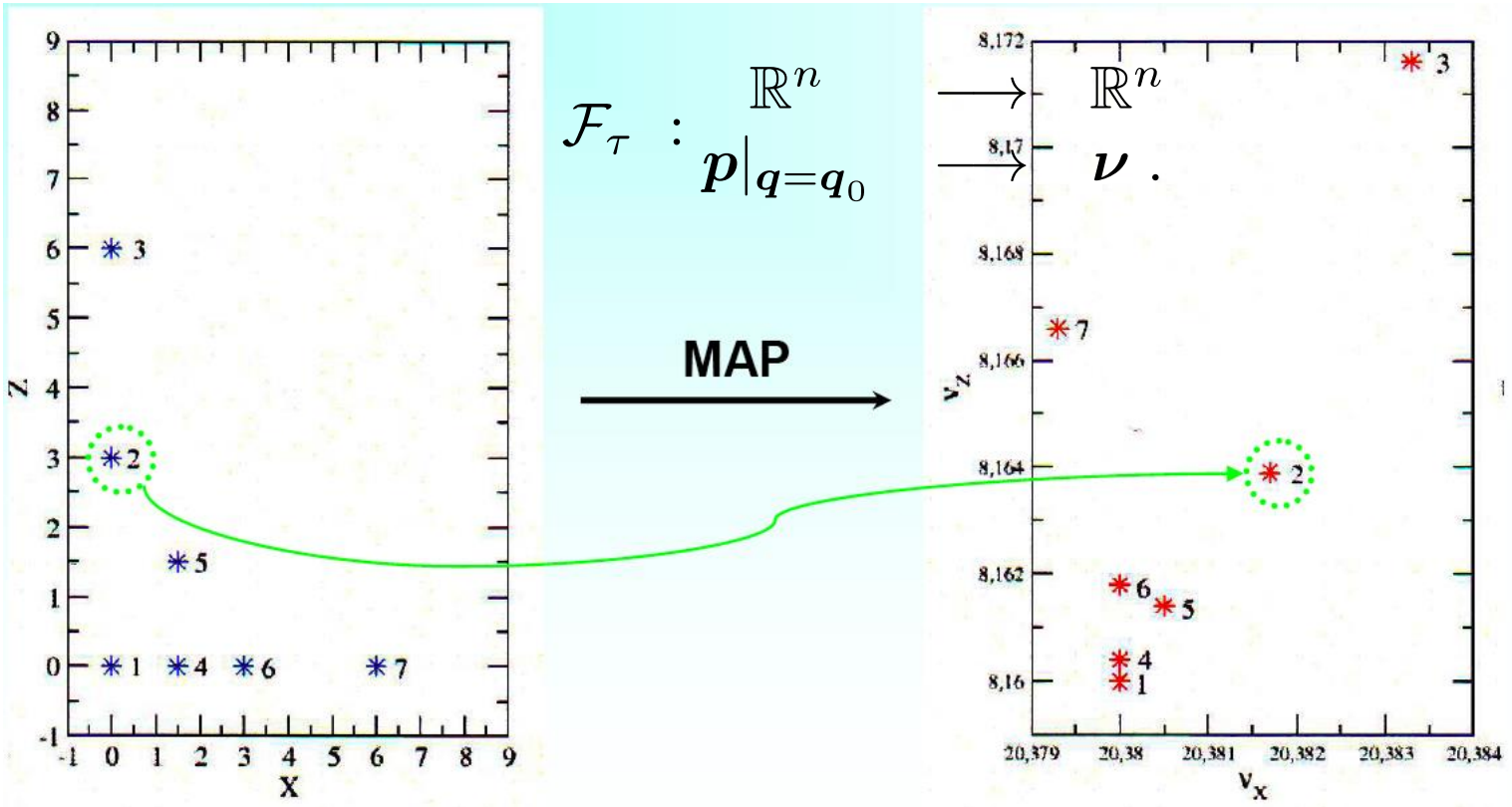

Example: Frequency maps for the LHC

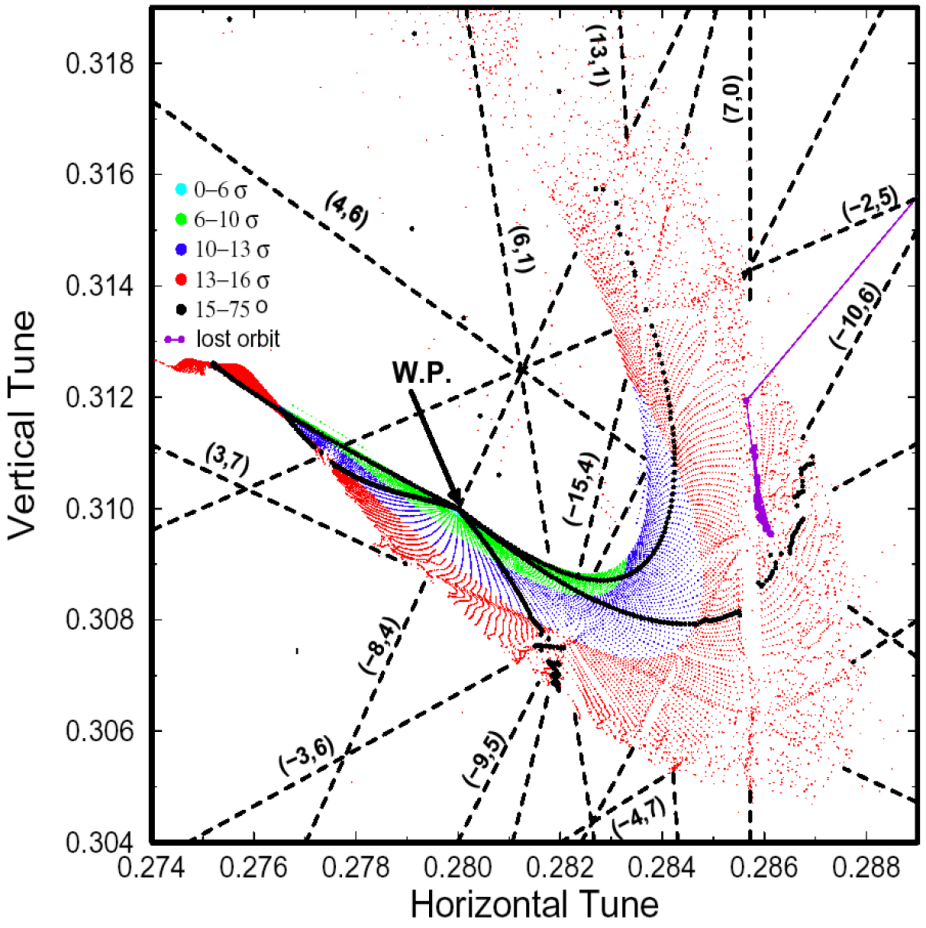

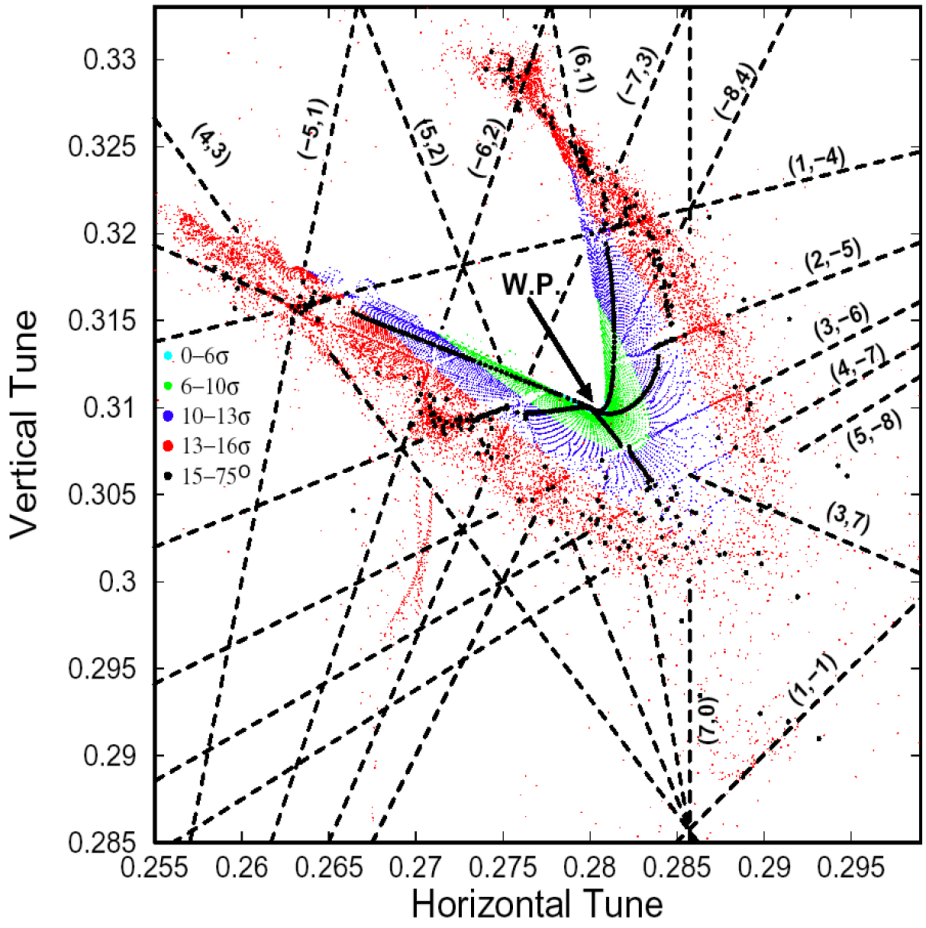

- Frequency maps for the target error table (left) and an increased random skew octupole error in the super-conducting dipoles (right)

Diffusion Maps

- Calculate frequencies for two equal and successive time spans and compute frequency diffusion vector:

$$\boldsymbol{D}\big|_{t=\tau} = \boldsymbol{\nu}\big|_{t\in(0,\tau/2]} - \boldsymbol{\nu}\big|_{t\in(\tau/2,\tau]}$$

- Plot the initial condition space color-coded with the norm of the diffusion vector
- Compute a diffusion quality factor by averaging all diffusion coefficients normalized with the initial conditions radius

$$D_{QF} = \left\langle \frac{|\boldsymbol{D}|}{(I_{x0}^2 + I_{y0}^2)^{1/2}} \right\rangle_R$$

Example: Diffusion maps for the LHC

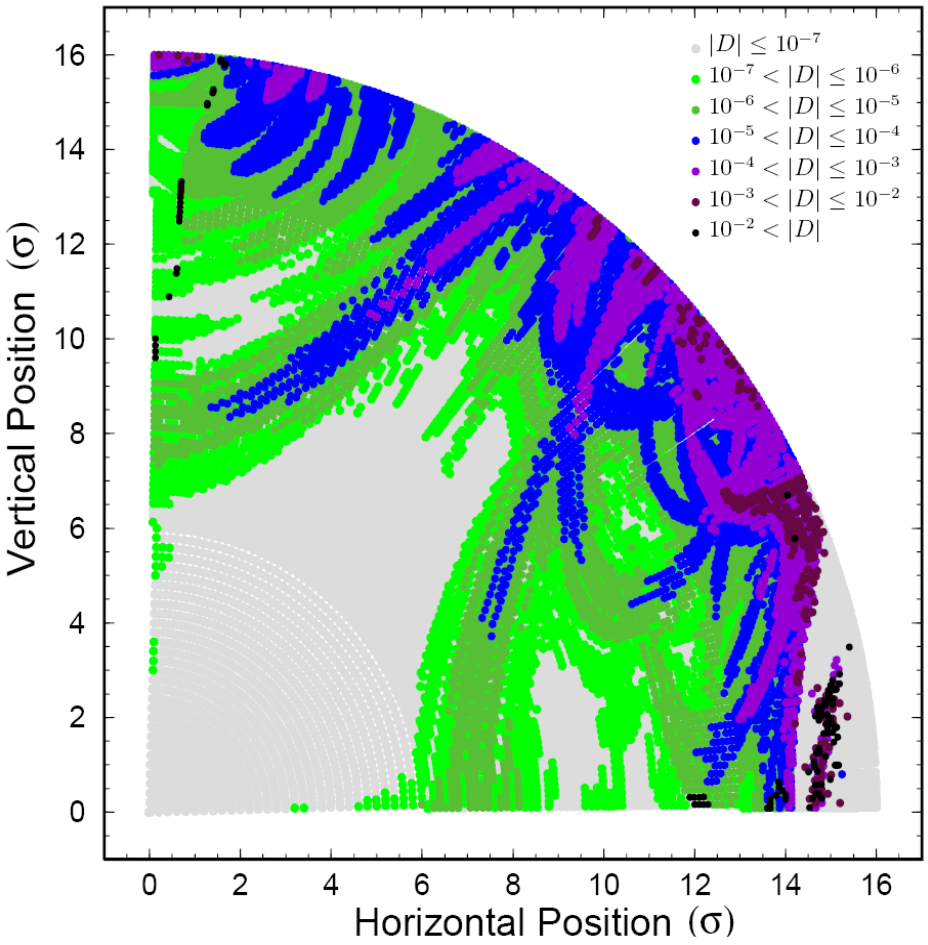

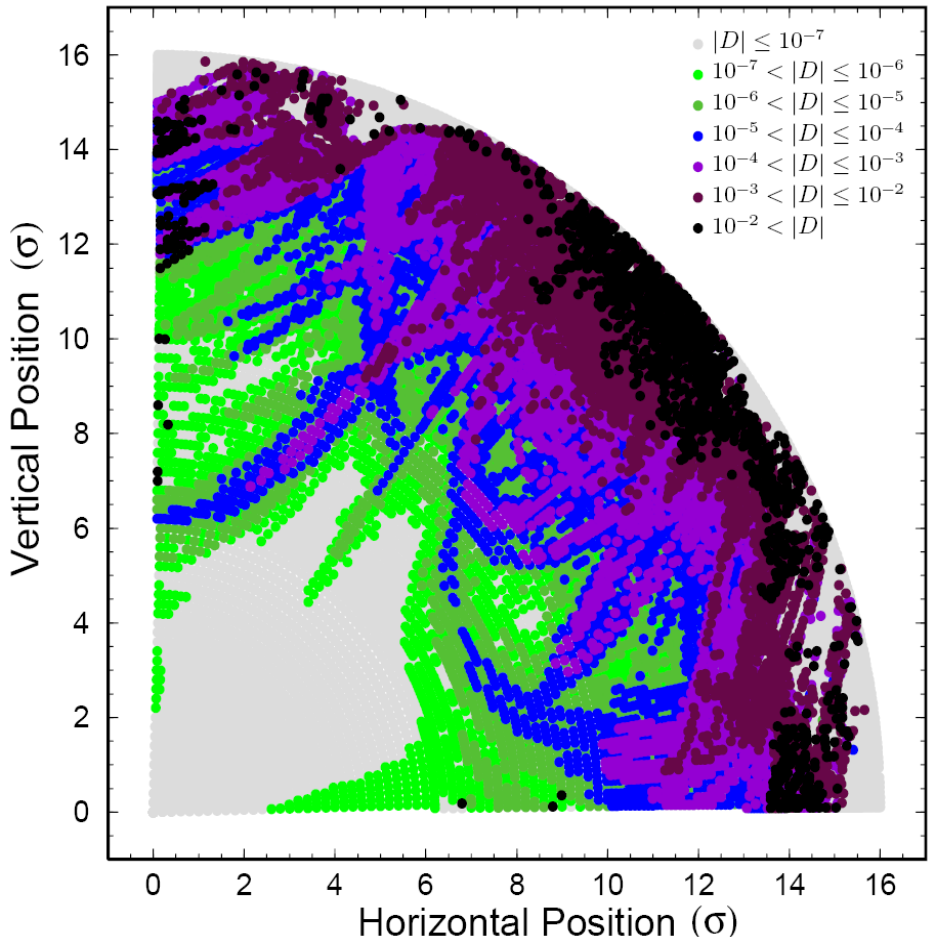

Diffusion maps for the target error table (left) and an increased random skew octupole error in the super-conducting dipoles (right)

Example: Frequency Map for the ESRF

- All dynamics represented in these two plots
- Regular motion represented by blue colors (close to zero amplitude particles or working point)

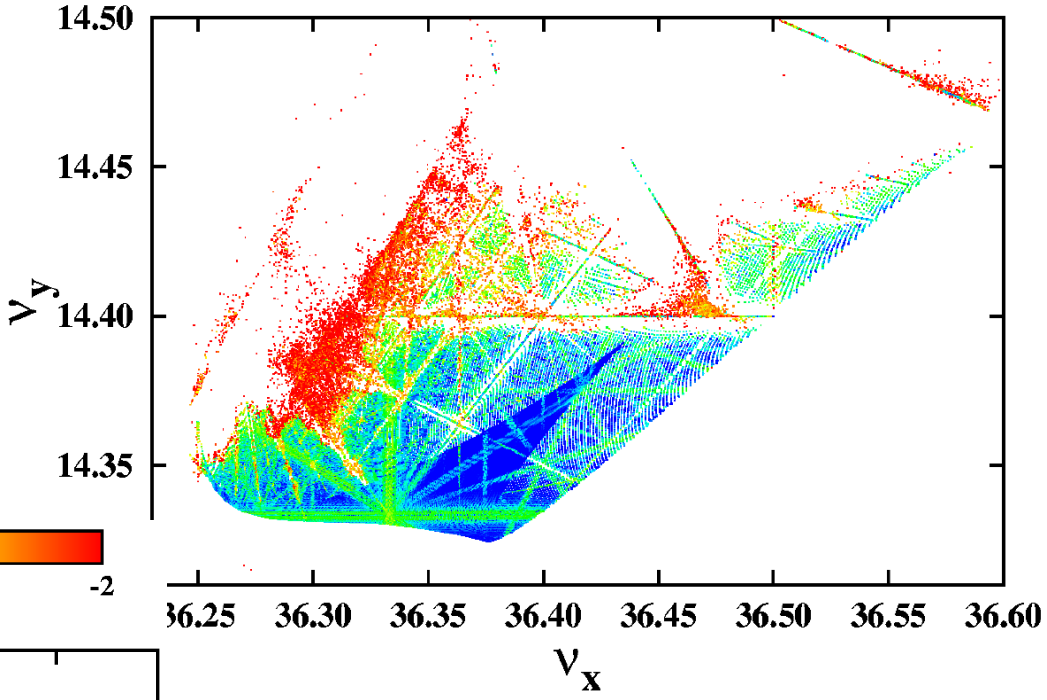

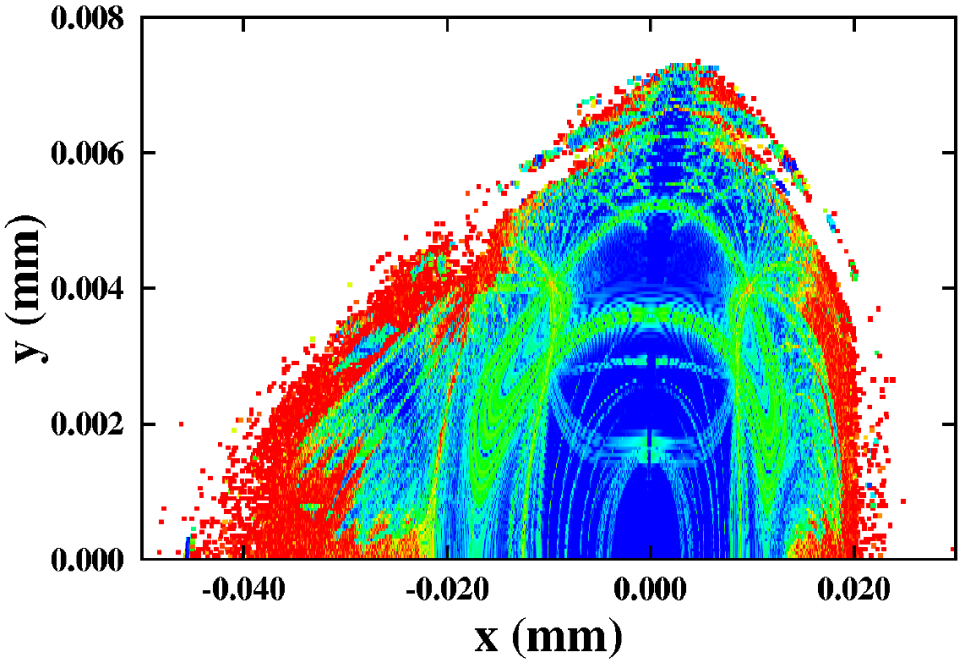

- Resonances appear as distorted lines in frequency space (or curves in initial condition space
- Chaotic motion is represented by red scattered particles and defines dynamic aperture of the machine

Numerical Applications

Correction schemes efficiency

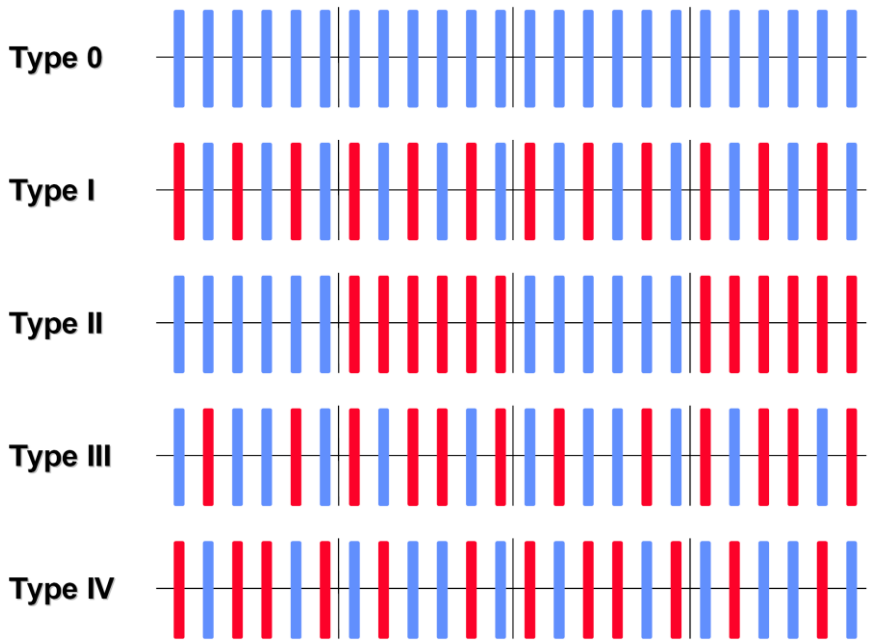

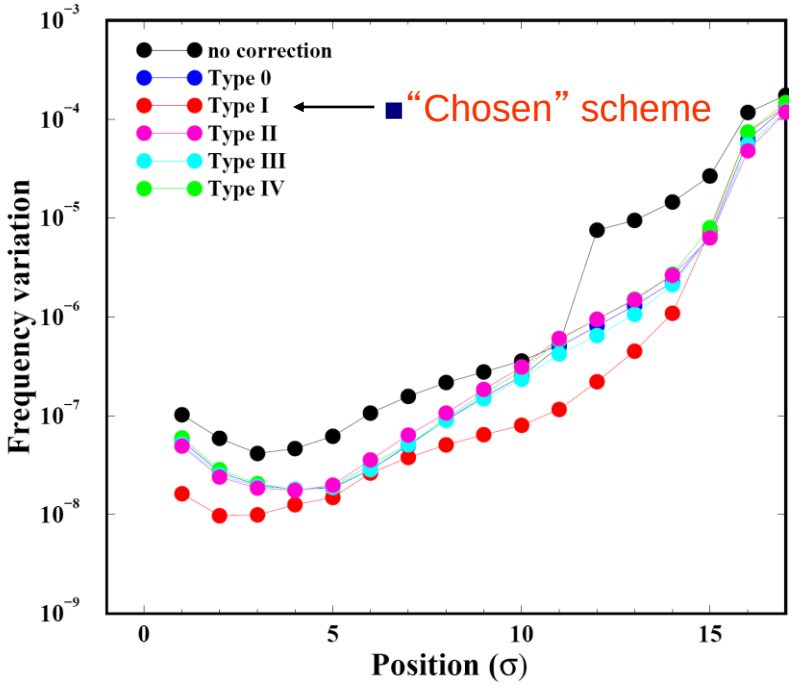

- Comparison of correction schemes for b_4 and b_5 errors in the LHC dipoles
- Frequency maps, resonance analysis, tune diffusion estimates, survival plots and short term tracking, proved that only half of the correctors are needed

Magnet fringe fields

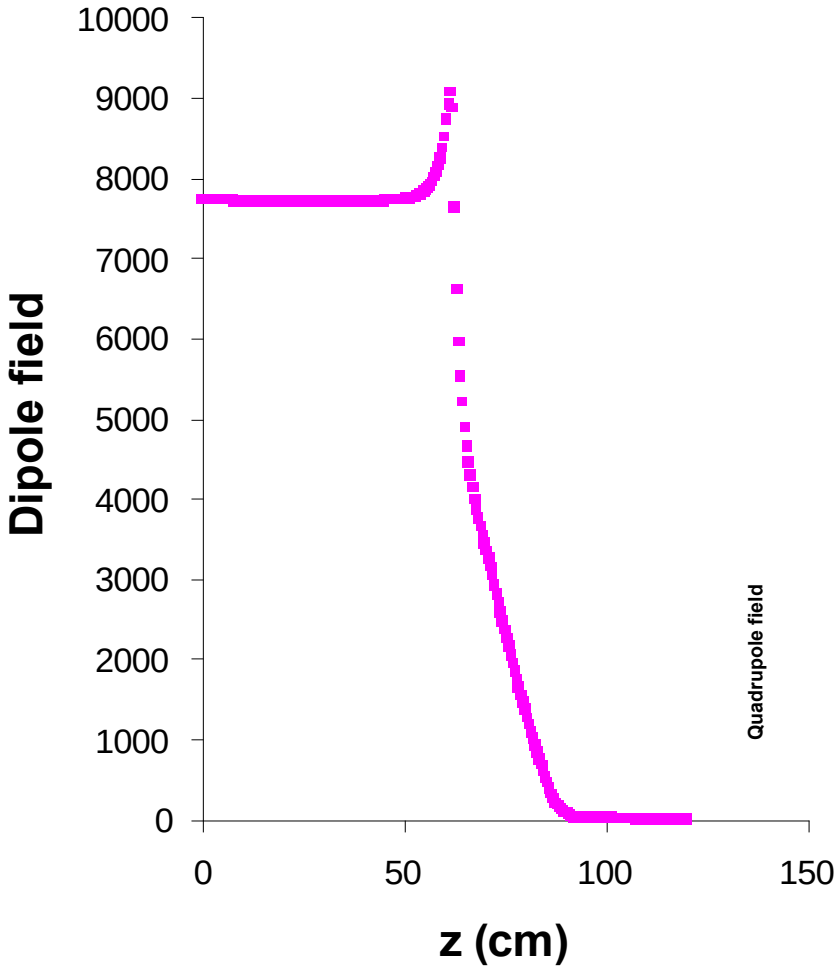

- Up to now we considered only transverse fields
- Magnet fringe field is the longitudinal dependence of the field at the magnet edges
- Important when magnet aspect ratios and/or emittances are big

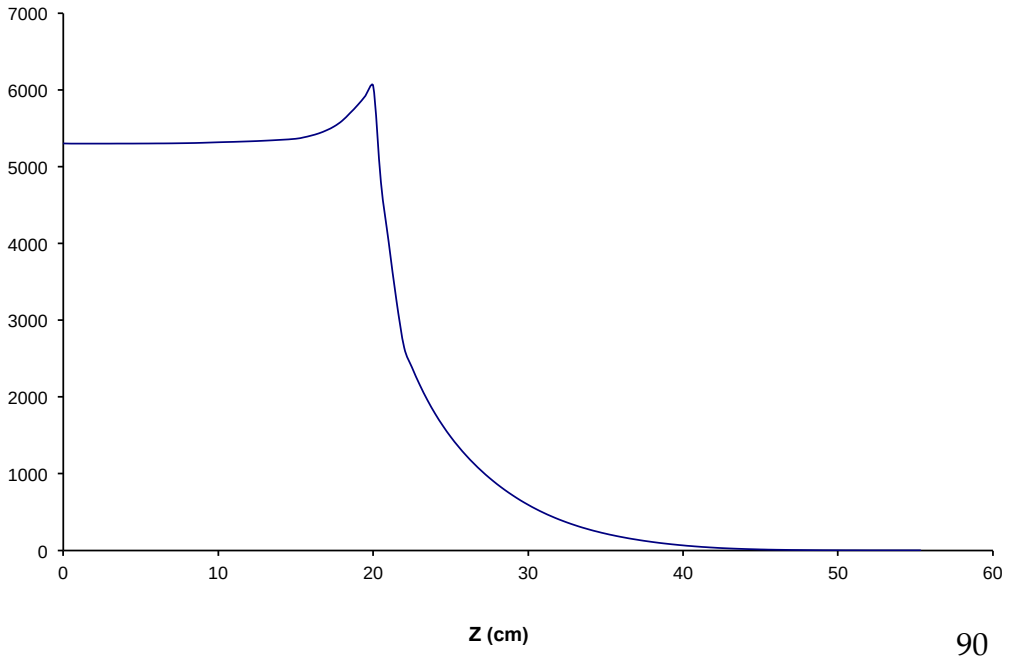

Quadrupole fringe field

General field expansion for a quadrupole magnet:

$$B_x = \sum_{m,n=0}^{\infty} \sum_{l=0}^{m} \frac{(-1)^m x^{2n} y^{2m+1}}{(2n)!(2m+1)!} \binom{m}{l} b_{2n+2m+1-2l}^{[2l]}$$

$$B_y = \sum_{m,n=0}^{\infty} \sum_{l=0}^{m} \frac{(-1)^m x^{2n+1} y^{2m}}{(2n+1)!(2m)!} \binom{m}{l} b_{2n+2m+1-2l}^{[2l]} \quad .$$

$$B_z = \sum_{m,n=0}^{\infty} \sum_{l=0}^{m} \frac{(-1)^m x^{2n+1} y^{2m+1}}{(2n+1)!(2m+1)!} \binom{m}{l} b_{2n+2m+1-2l}^{[2l+1]}$$

and to leading order

$$\begin{aligned} B_x &= y\left[b_1 - \frac{1}{12}(3x^2+y^2)b_1^{[2]}\right] + O(5) \\ B_y &= x\left[b_1 - \frac{1}{12}(3y^2+x^2)b_1^{[2]}\right] + O(5) \\ B_z &= xyb_1^{[1]} + O(4) \end{aligned}$$

The quadrupole fringe to leading order has an octupole-like effect

Magnet fringe fields

- From the hard-edge Hamiltonian

$$H_f = \frac{\pm Q}{12B\rho(1+\frac{\delta p}{p})}(y^3p_y - x^3p_x + 3x^2yp_y - 3y^2xp_x),$$

the first order shift of the frequencies with amplitude can be computed analytically

$$\begin{pmatrix}\delta\nu_x\\ \delta\nu_y\end{pmatrix} = \begin{pmatrix}a_{hh} & a_{hv}\\ a_{hv} & a_{vv}\end{pmatrix}\begin{pmatrix}2J_x\\ 2J_y\end{pmatrix},$$

with the "anharmonicity" coefficients (torsion)

$$a_{hh} = \frac{-1}{16\pi B\rho}\sum_i \pm Q_i\beta_{xi}\alpha_{xi}$$
$$a_{hv} = \frac{1}{16\pi B\rho}\sum_i \pm Q_i(\beta_{xi}\alpha_{yi} - \beta_{yi}\alpha_{xi})$$
$$a_{vv} = \frac{1}{16\pi B\rho}\sum_i \pm Q_i\beta_{yi}\alpha_{yi}$$

Tune footprint for the SNS based on hard-edge (red) and realistic (blue) quadrupole fringe-field

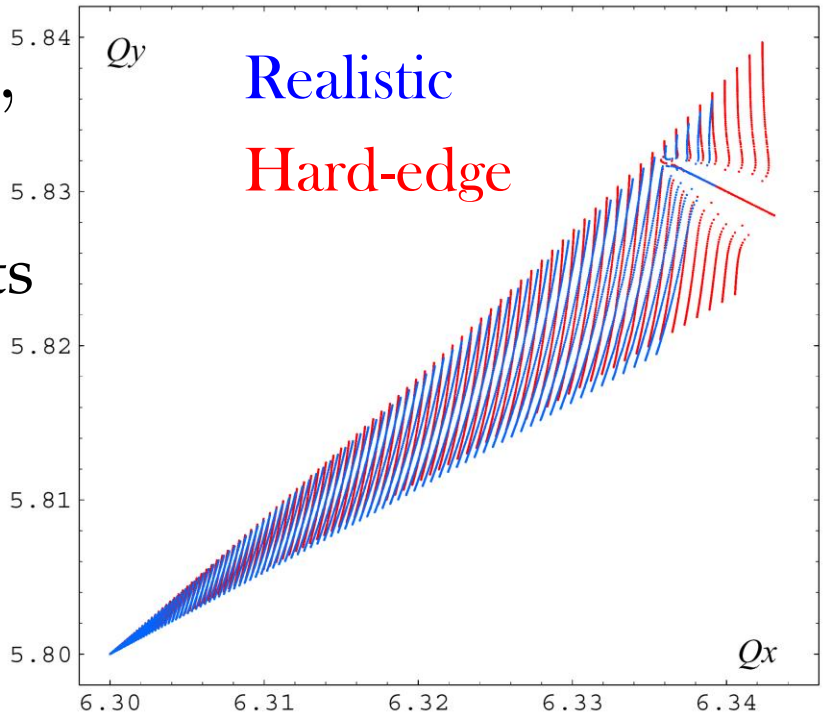

Off-momentum frequency maps

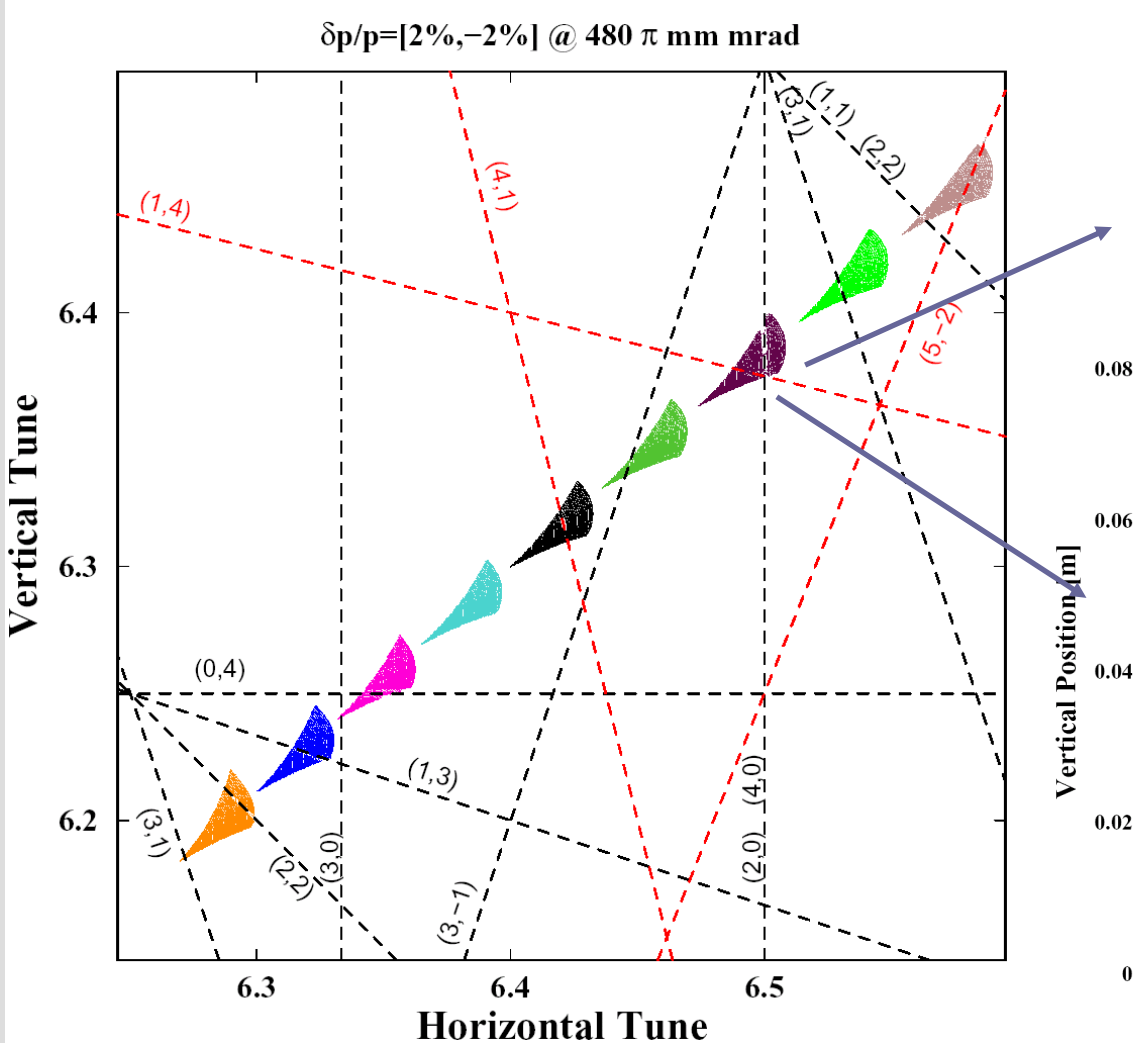

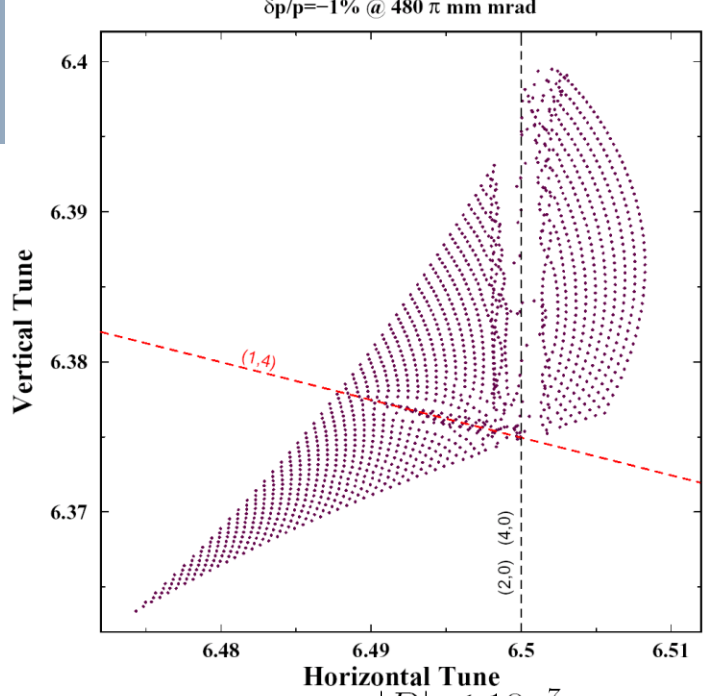

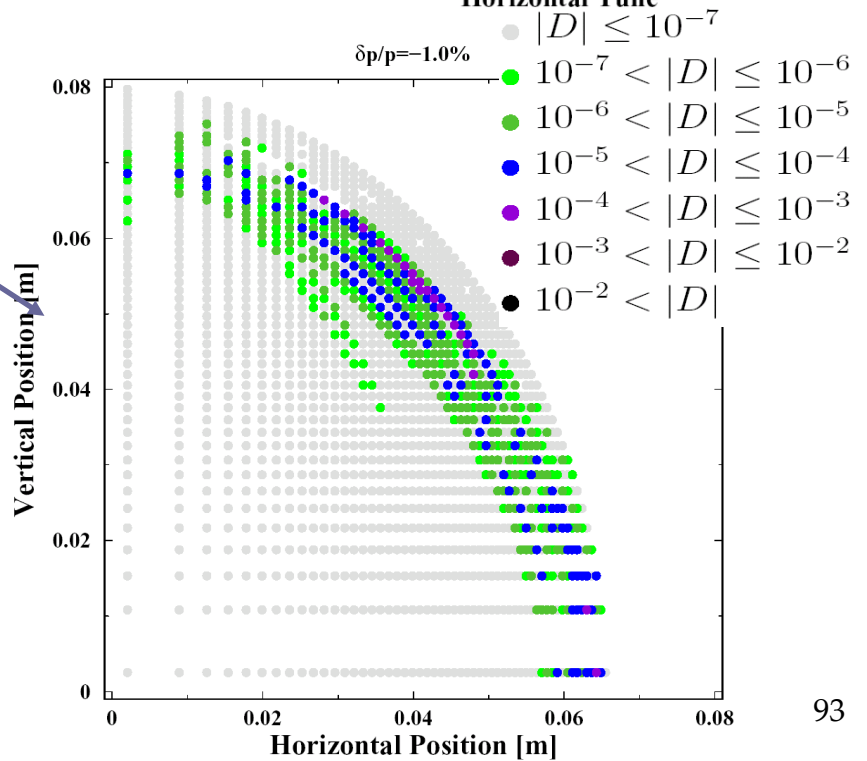

Choice of the SNS ring working point

Tune Diffusion quality factor

$$D_{QF} = \left\langle \frac{|\boldsymbol{D}|}{(I_{x0}^2 + I_{y0}^2)^{1/2}} \right\rangle_R$$

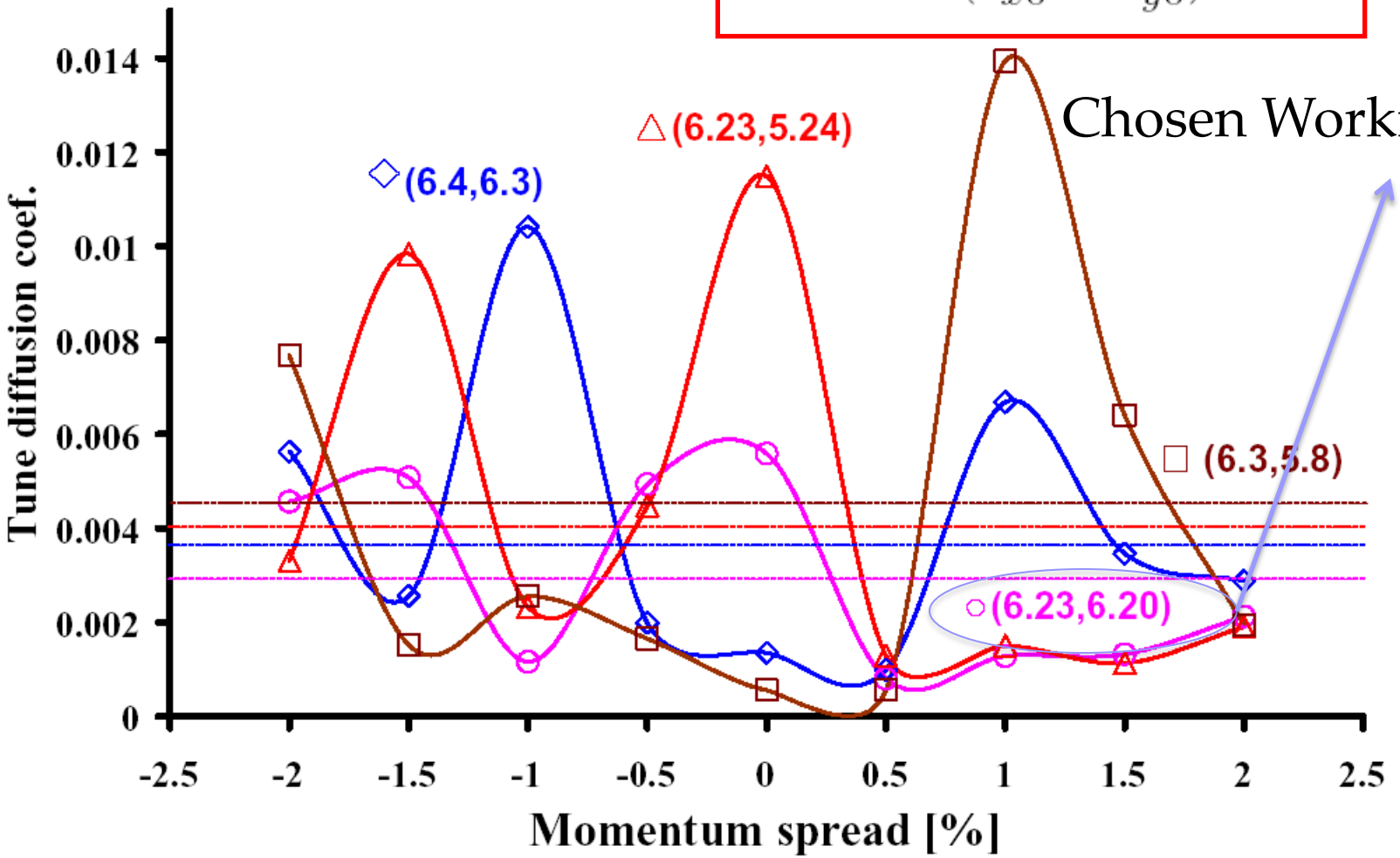

Global Working point choice

- Figure of merit for choosing best working point is sum of diffusion rates with a constant added for every lost particle
- Each point is produced after tracking 100 particles
- Nominal working point had to be moved towards “blue” area

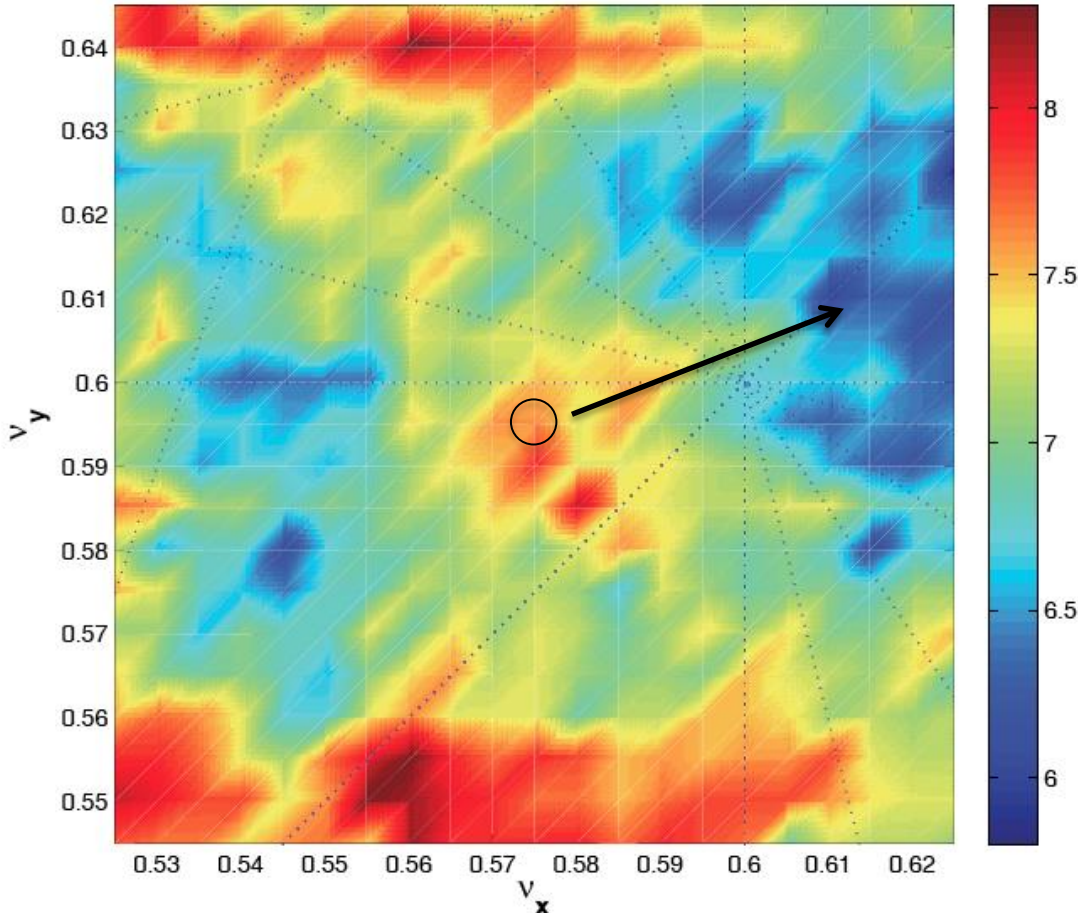

$$e^D = \sqrt{\frac{(\nu_{x,1} - \nu_{x,2})^2 + (\nu_{y,1} - \nu_{y,2})^2}{N/2}}$$

$$WPS = 0.1 N_{lost} + \sum e^D$$

Sextupole scheme optimization

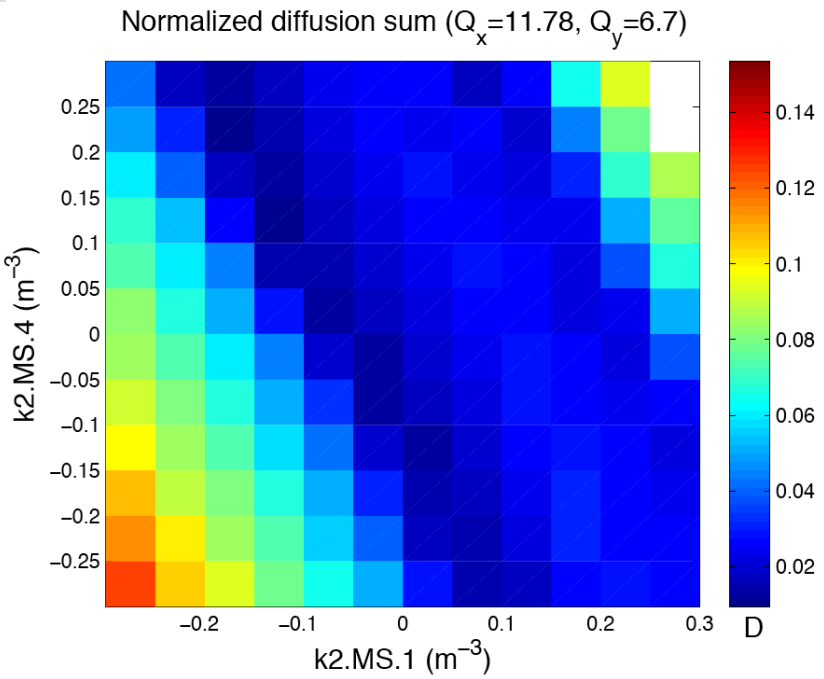

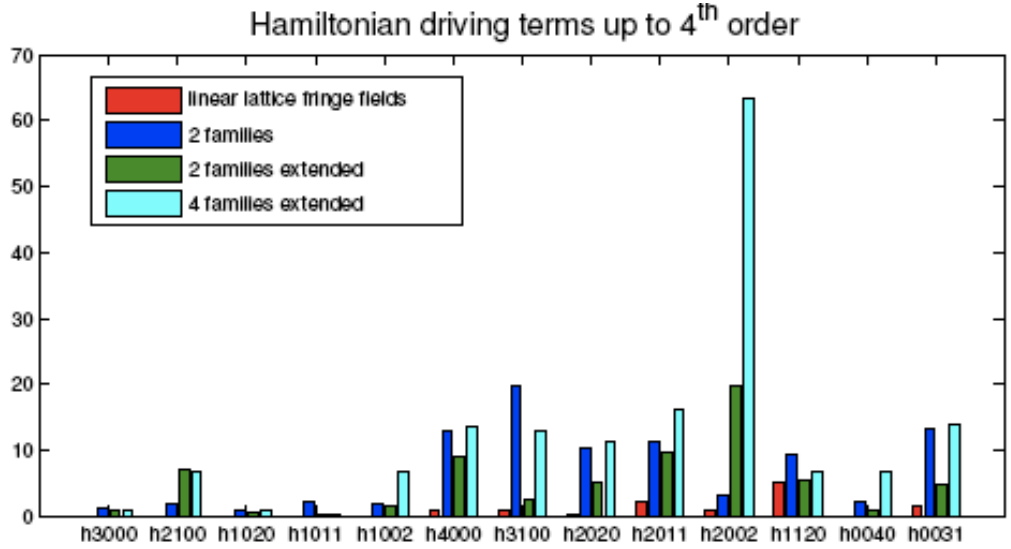

- Comparing different chromaticity sextupole correction schemes and working point optimization using normal form analysis, frequency maps and finally particle tracking
- Finding the adequate sextupole strengths through the tune diffusion coefficient

Beam-Beam interaction

Variable	Symbol	Value
Beam energy	E	7 TeV
Particle species	$\cdots$	protons
Full crossing angle	θ_c	300 μrad
rms beam divergence	σ'_x	31.7 μrad
rms beam size	σ_x	15.9 μm
Normalized transv. rms emittance	$\gamma\varepsilon$	3.75 μm
IP beta function	β^*	0.5 m
Bunch charge	N_b	$(1 \times 10^{11}-2 \times 10^{12})$
Betatron tune	Q_0	0.31

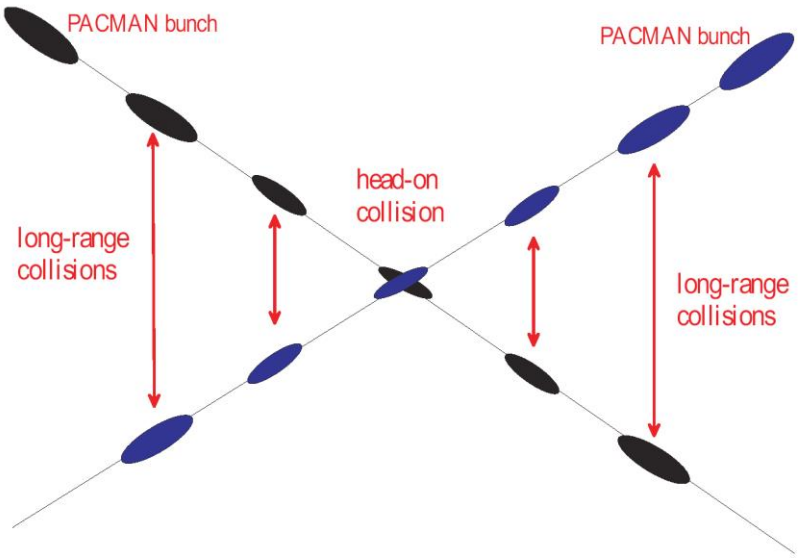

- Long range beam-beam interaction represented by a 4D kick-map

$$\Delta x = - n_{par} \frac{2 r_p N_b}{\gamma} \left[\frac{x' + \theta_c}{\theta_t^2} \left(1 - e^{-\frac{\theta_t^2}{2\theta_{x,y}^2}} \right) - \frac{1}{\theta_c} \left(1 - e^{-\frac{\theta_c^2}{2\theta_{x,y}^2}} \right) \right]$$

$$\Delta y = - n_{par} \frac{2 r_p N_b}{\gamma} \frac{y'}{\theta_t^2} \left(1 - e^{-\frac{\theta_t^2}{2\theta_{x,y}^2}} \right)$$

with $$\theta_t \equiv \left((x' + \theta_c)^2 + y'^2 \right)^{1/2}$$

Head-on vs Long range interaction

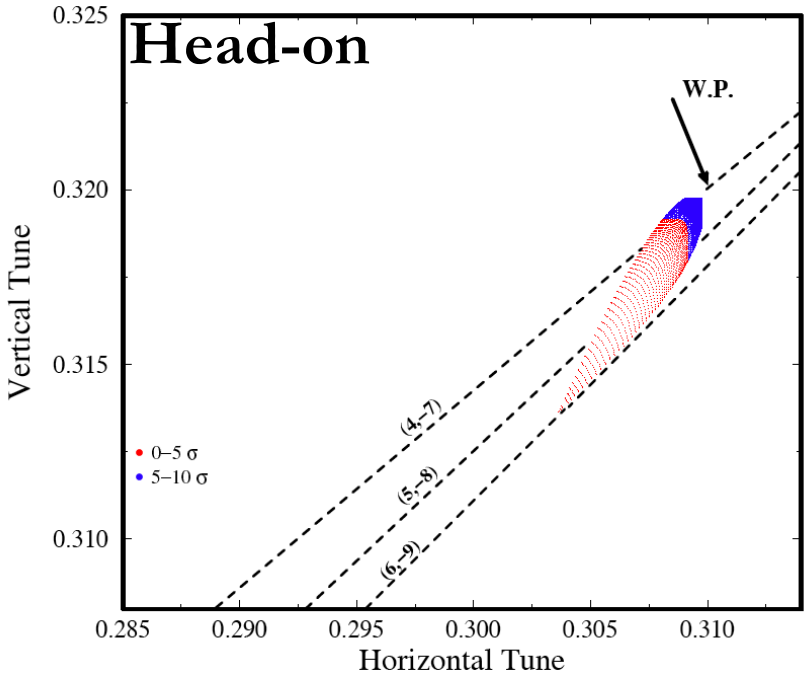

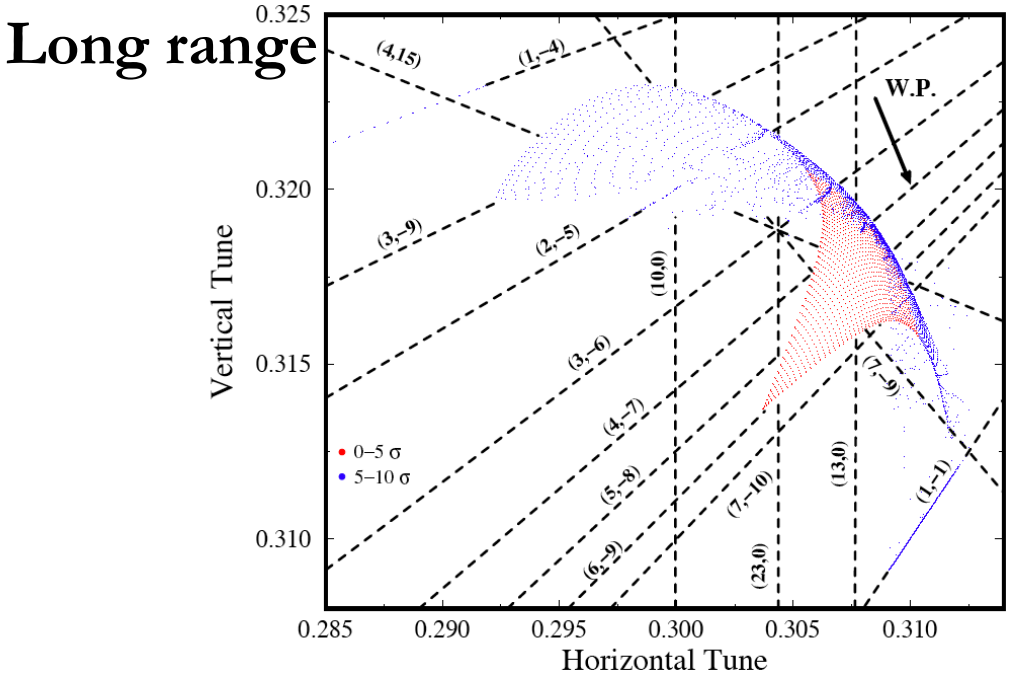

- Proved dominant effect of long range beam-beam effect
- Dynamic Aperture (around 6σ) located at the folding of the map (indefinite torsion)
- Experimental effort to compensate beam-beam long range effect with wires (1/r part of the force) or octupoles

Action variance

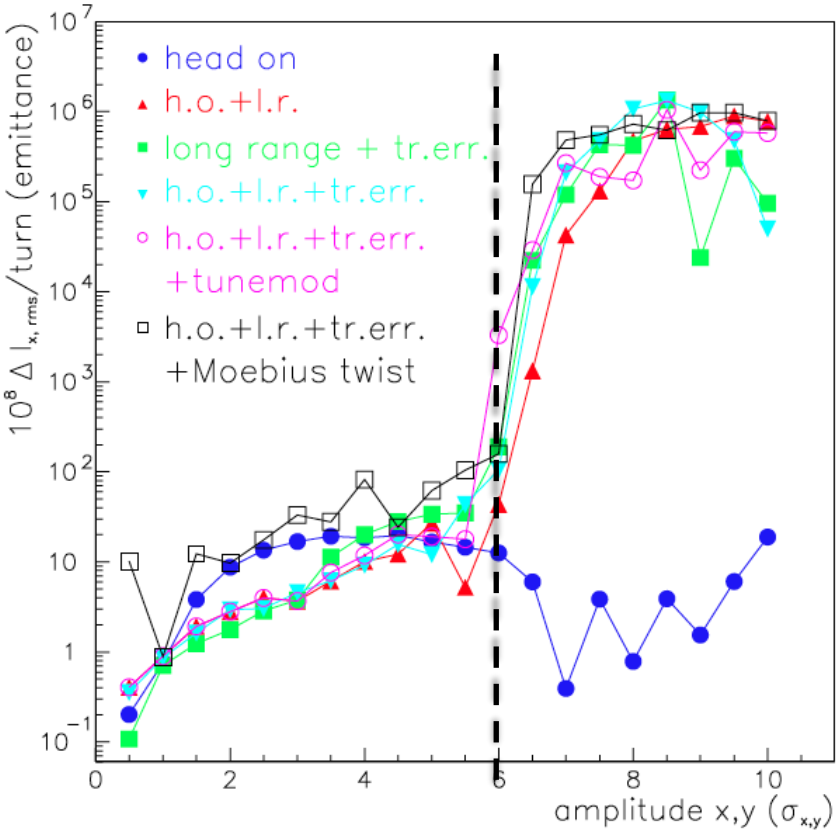

- In the chaotic region of phase space, the action diffusion coefficient per turn can be estimated by averaging over the quasi-randomly varying betatron phase variable as

$$D(J) = \frac{1}{2\pi}\int_0^{2\pi} d\phi\ [\Delta J(\phi)]^2$$

Action variance vs. frequency diffusion

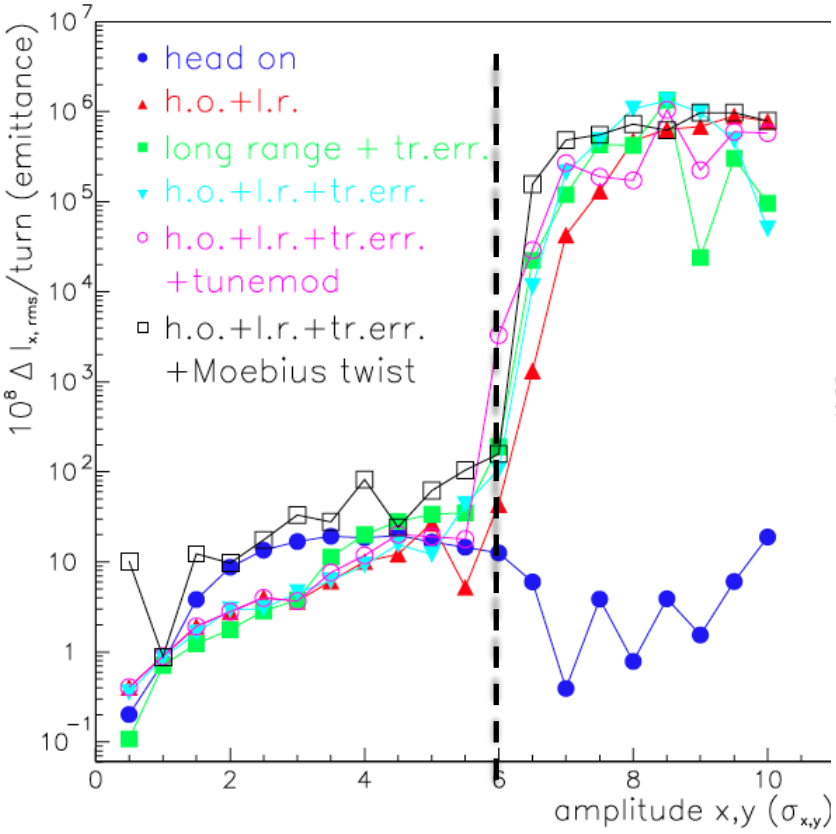

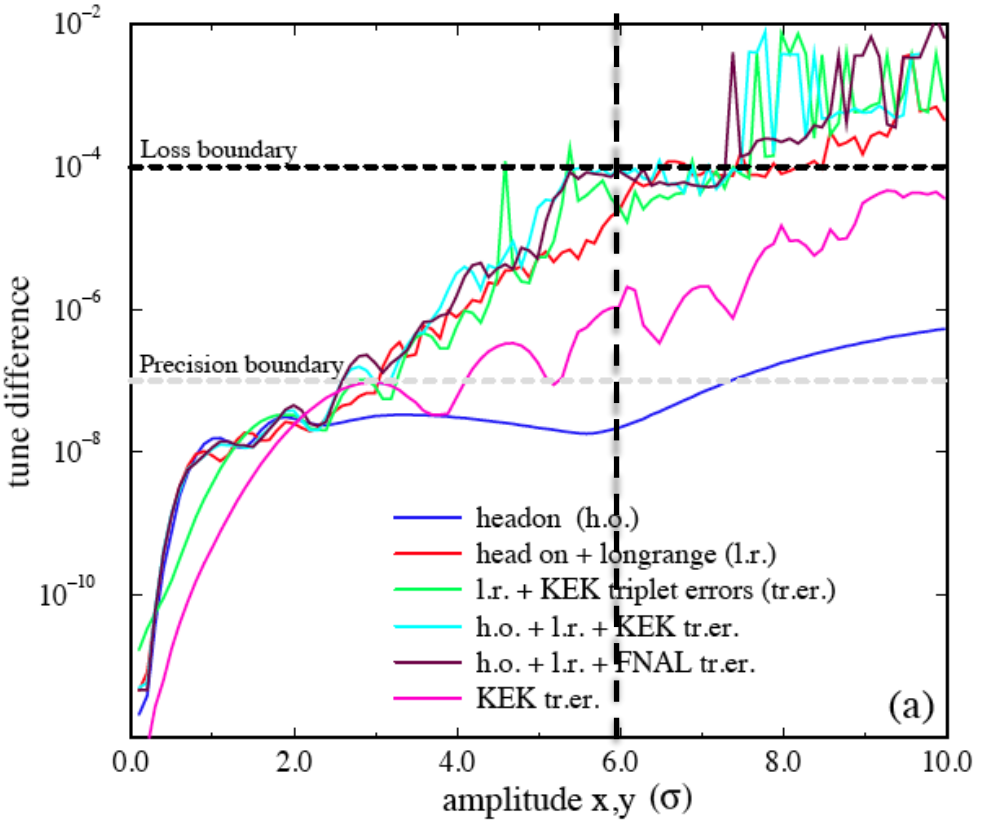

- Very good agreement of diffusive aperture boundary (action variance) with frequency variation (loss boundary corresponding to around 1 integer unit change in 10^7 turns)

Optimizing operational scenario

Tune scans color-coded with minimum DA for the selection of the best working point for operation.

S. Kostoglou et al.

Start of β*-leveling

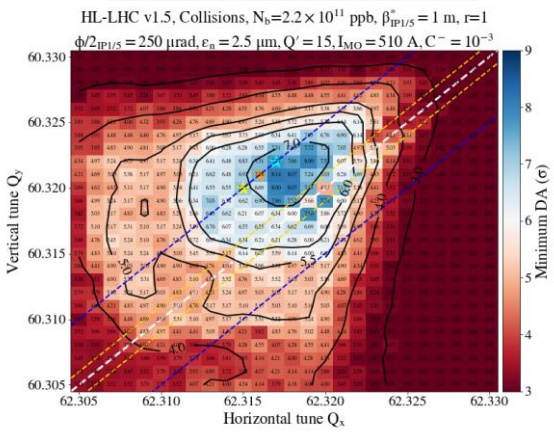

End of β*-leveling

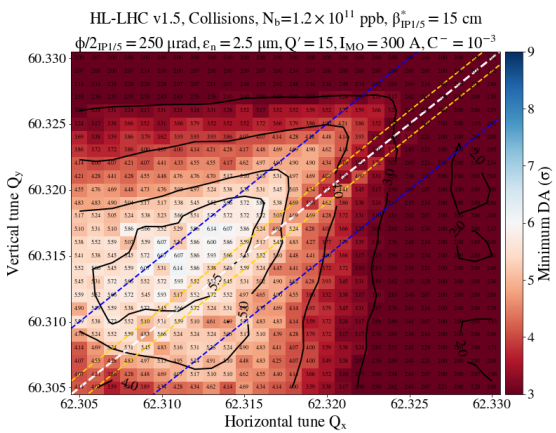

CC orbit bump non-closure

Impact of the non-closure of the CC orbit bump due to cavity voltage error: $V_{\mathrm{err}} = V_{\mathrm{nom}}(1-\varepsilon)$

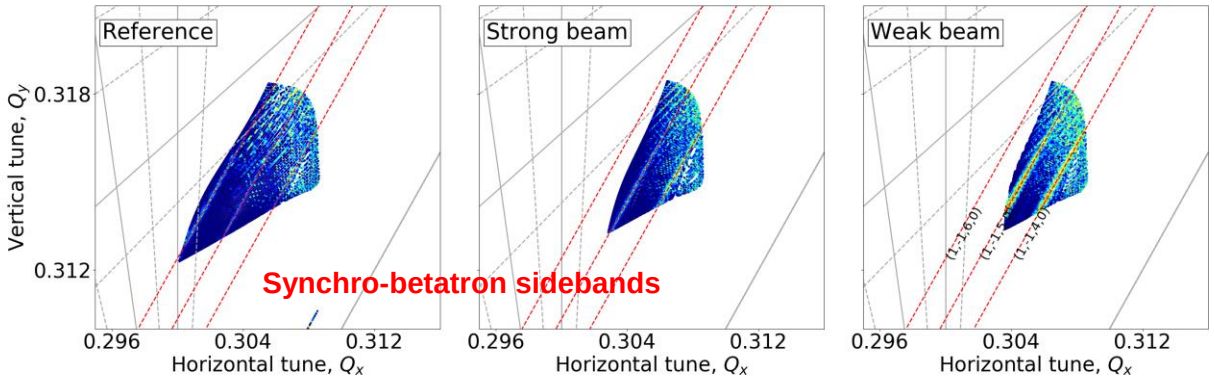

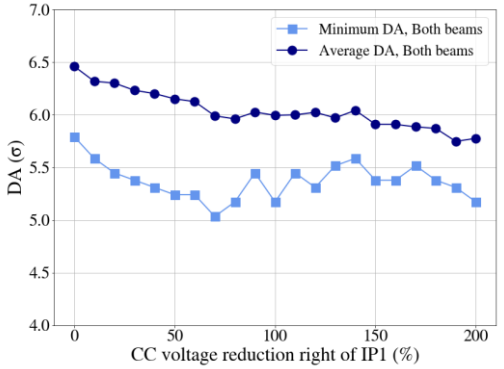

Wire compensation

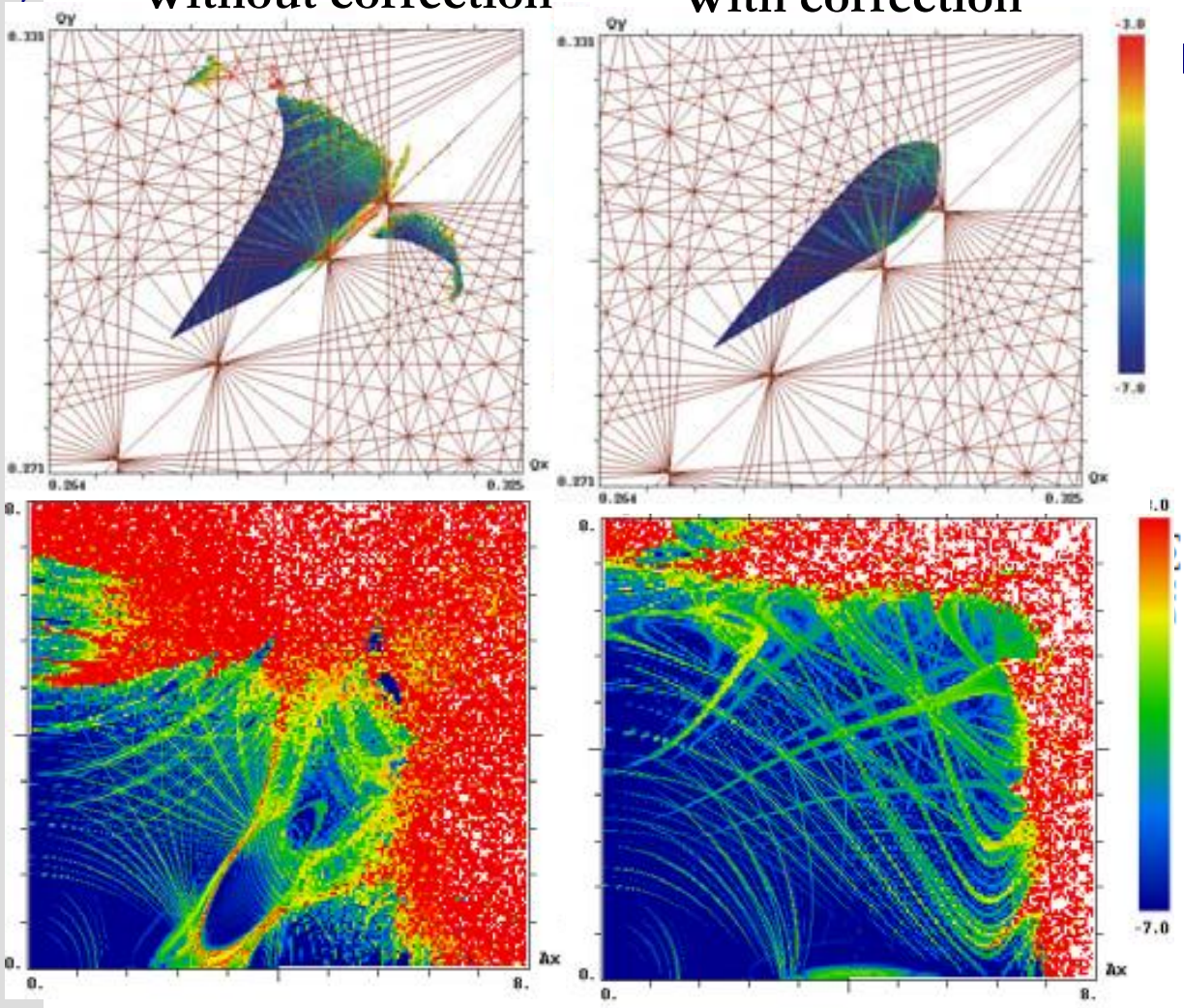

- Current baring wire can **improve DA by 1-2 σ**
- Tests in the LHC during 2017-2018

Reduced crossing angle of 450μrad @ 15cm

S. Fartoukh, YP et al., PRSTAB, 2015

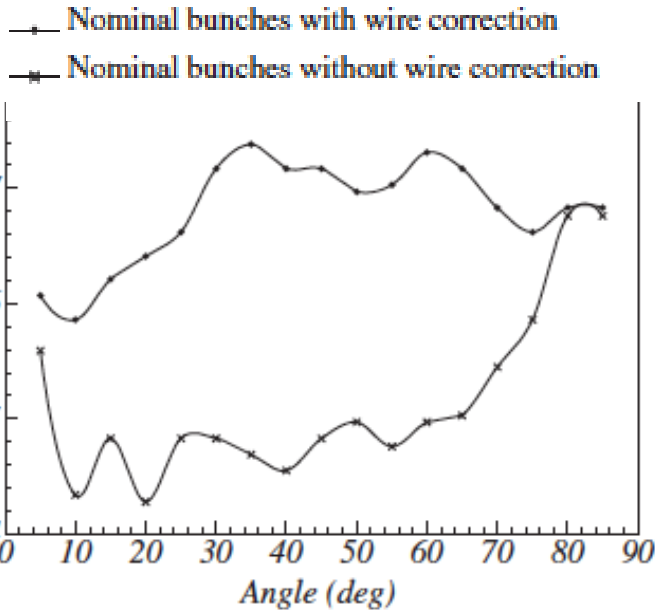

Beam-beam wire compensation

G. Sterbini, A. Poyet, A. Rossi, A. Bertarelli, et al.

- CHALLENGE: propose solutions to tackle the Beam Dynamics limitations

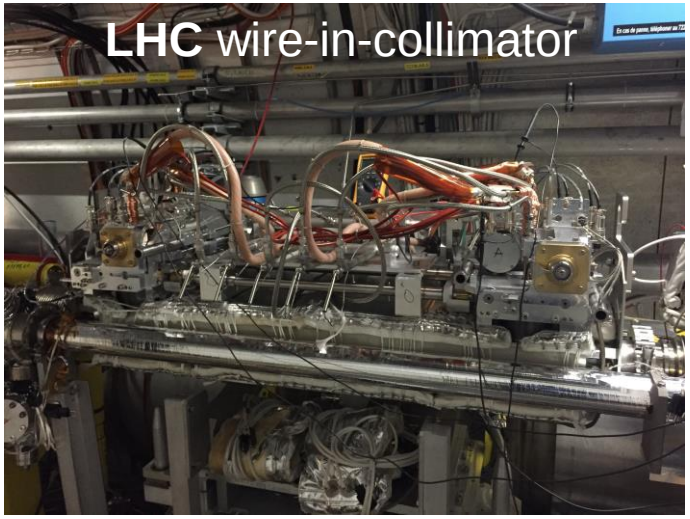

HL-LHC wires conceptual design

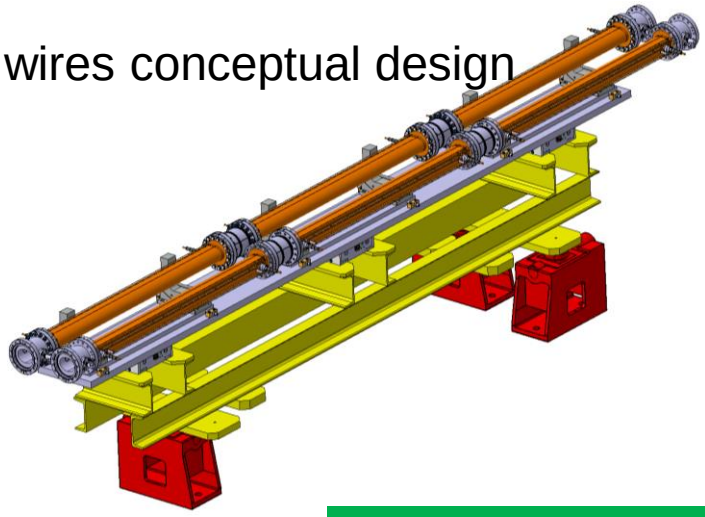

Experiments in Run 2

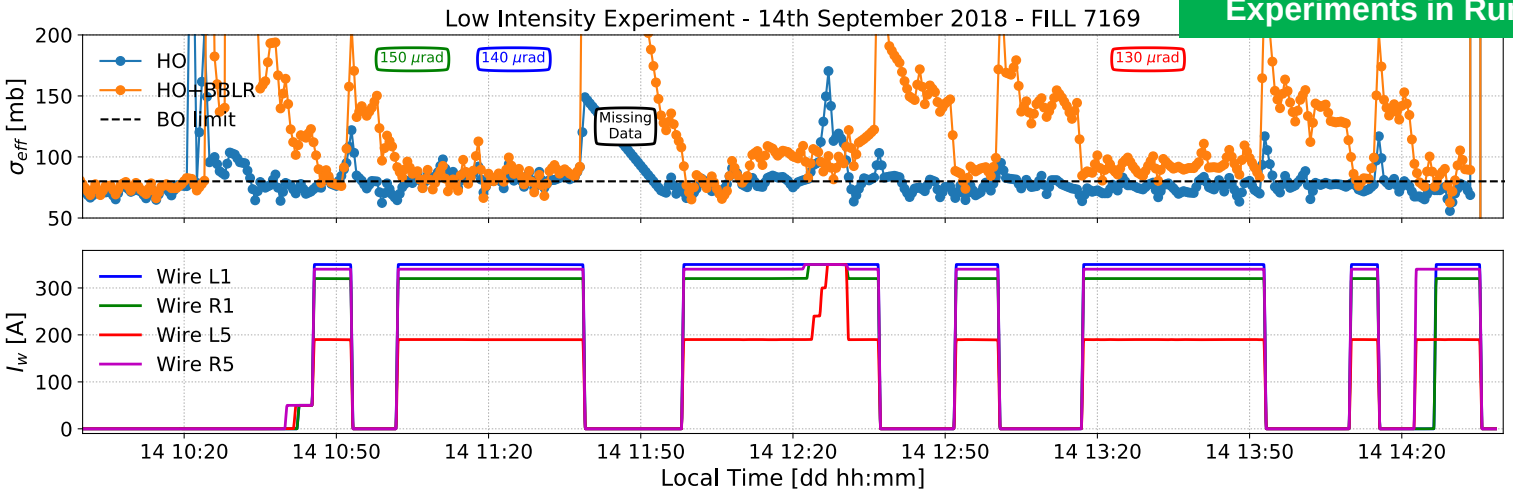

BBLR compensation

$$\sigma_{EFF} = -\frac{1}{\sum_{IP} L_{IP}} \frac{dN}{dt}$$

Instantaneous luminosity

Intensity loss-rate

- **Compensating effect** of the wires visible on **effective x-section**

Fill 10069, 29 August 2024

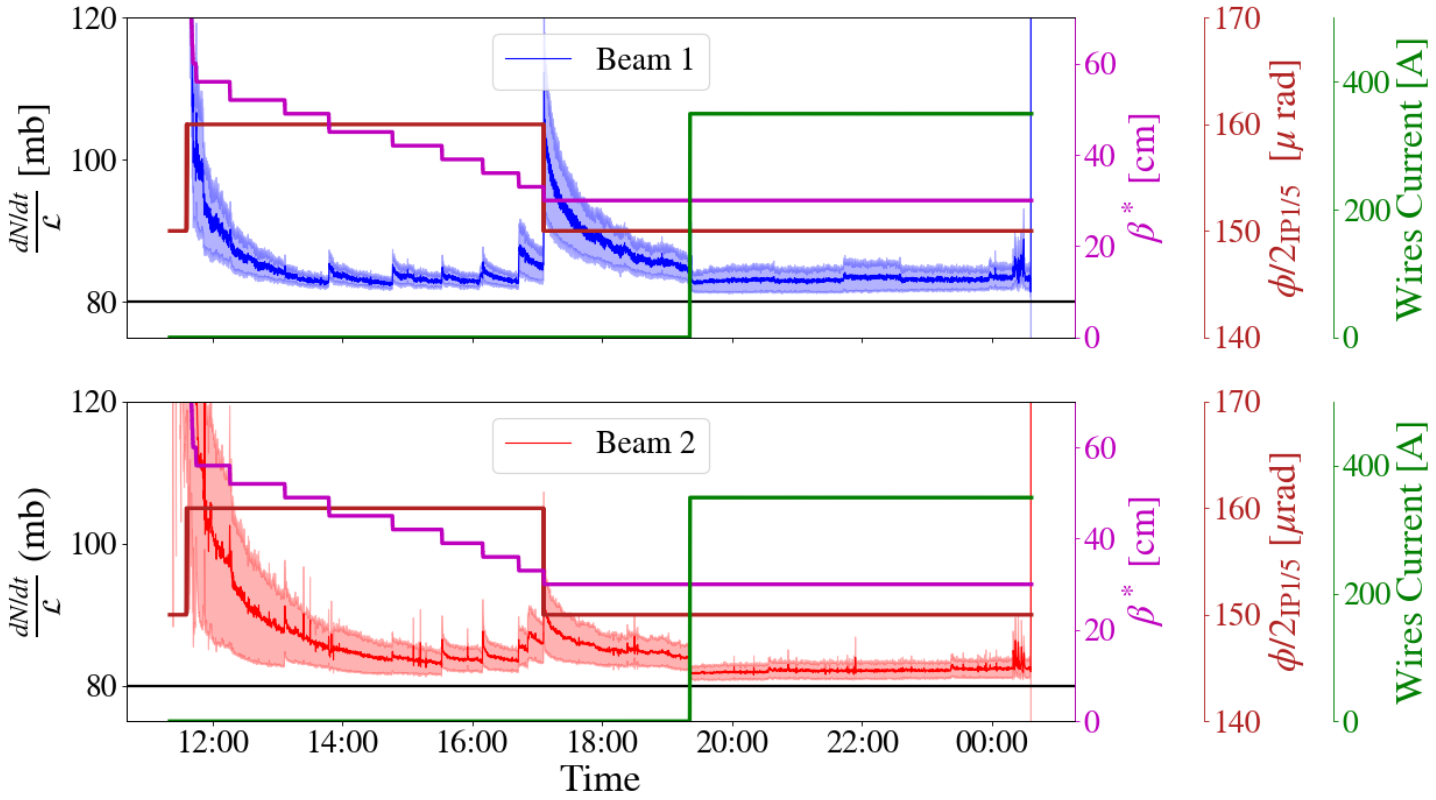

Wire compensation for HL-LHC

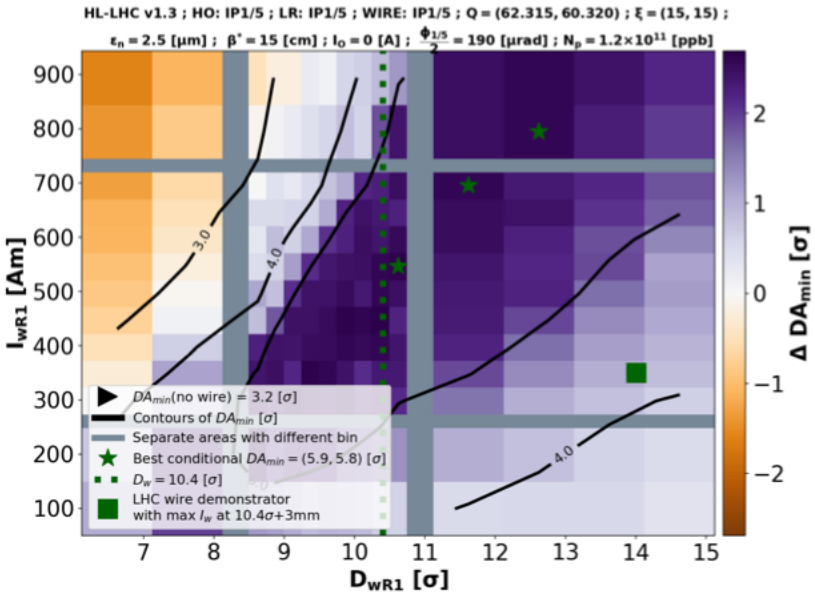

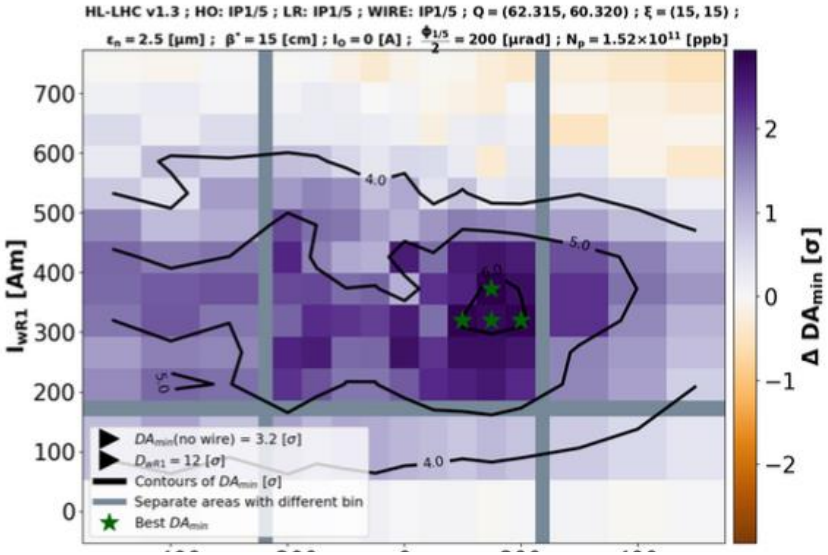

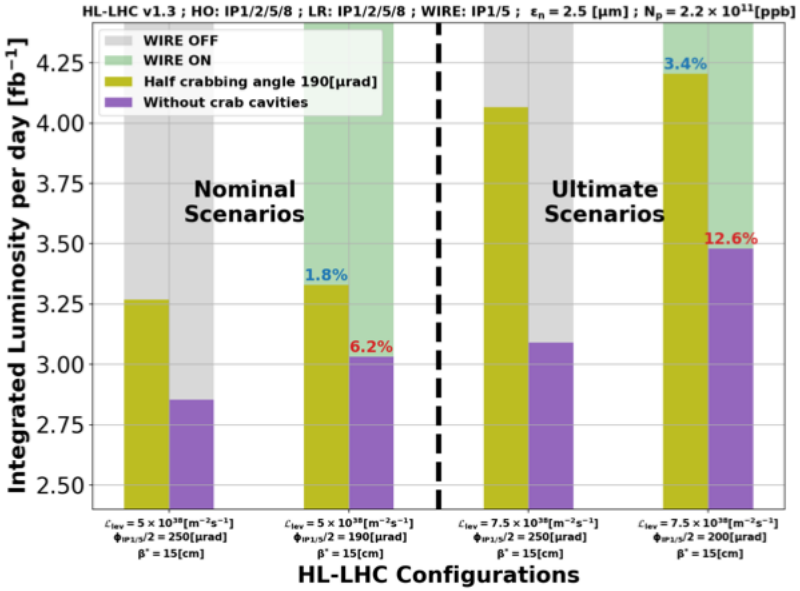

CHALLENGE: Predict and optimize the future (HL-LHC) by

- taking into account Machine Protection constraints and
- minimizing complexity, saving commissioning time and maximize machine availability.

K. Skoufaris, et al. PRAB 2022

Frequency Map Analysis with modulation

Frequency maps with space-charge

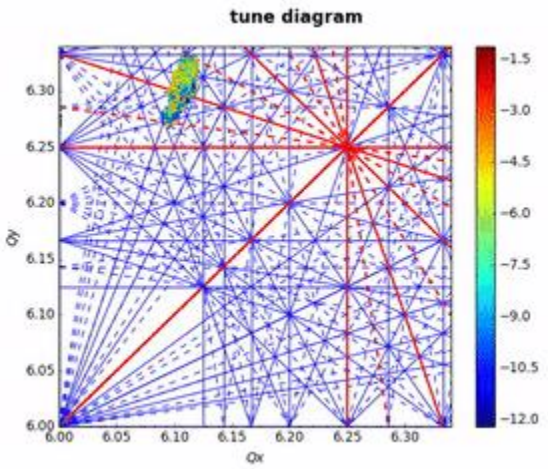

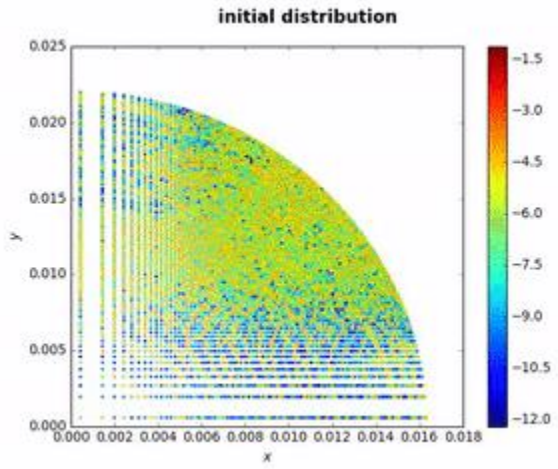

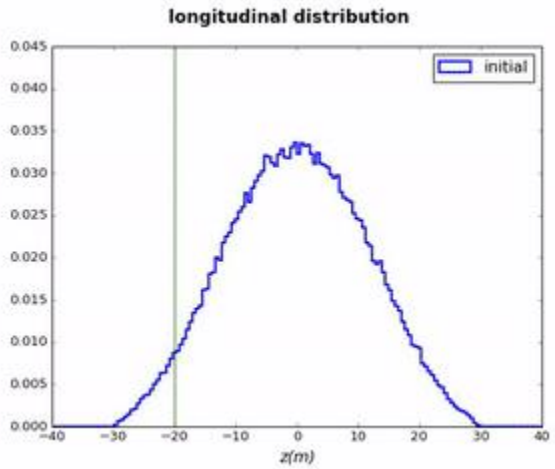

F.Asvesta, et al., 2017

- Evolution of frequency map over different longitudinal position
- Tunes acquired over each longitudinal period
- Particles with similar longitudinal offset but different amplitudes experience the resonance in different manne
- Particles with different longitudinal offset may experienc different resonances

LHC: Power supply ripples

- Quadrupoles of the **inner triplet** right and left **of IP1 and IP5**, **large beta-functions** increase the sensitivity to non-linear effects
- **Resonance conditions**: S. Kostoglou, et al., 2018

$$aQ_x + bQ_y + c\frac{f_{modulation}}{f_{revolution}} = k \text{ for } a, b, c, k \text{ integers}$$

-By increasing the modulation depth, sidebands start to appear in the FMAs

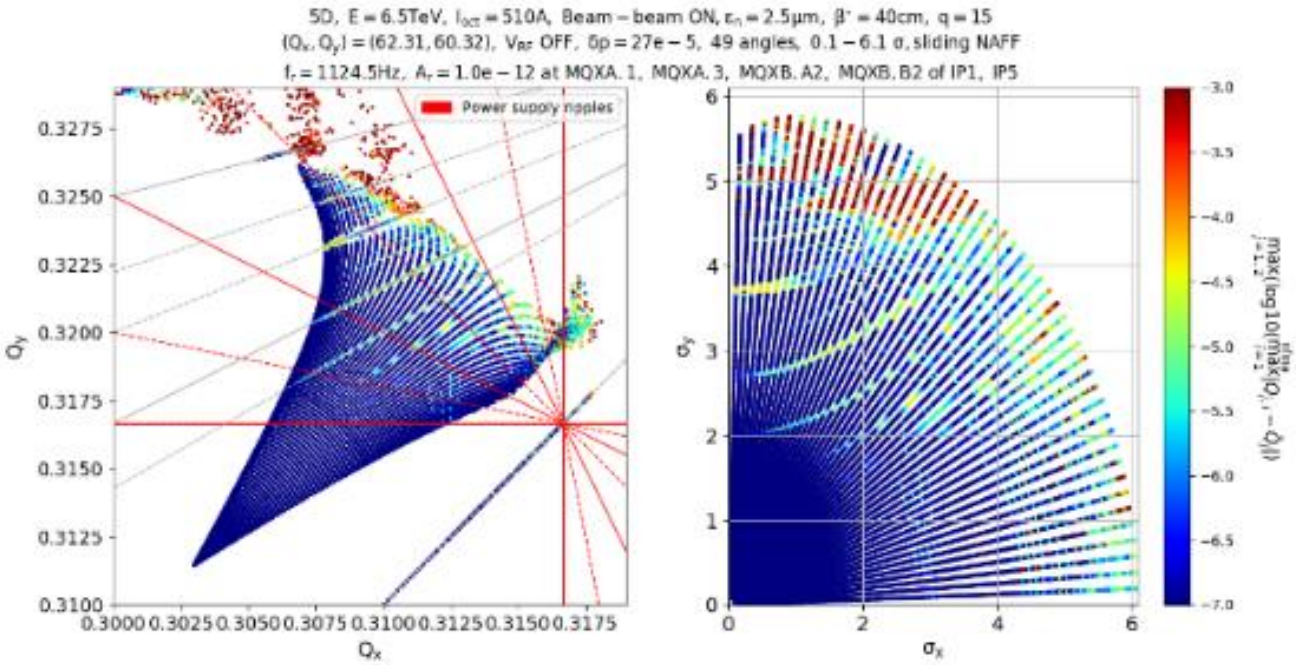

LHC: Power supply ripples

- Quadrupoles of the **inner triplet** right and left **of IP1 and IP5**, **large beta-functions** increase the sensitivity to non-linear effects
- **Resonance conditions**: S. Kostoglou, et al., 2018

$$aQ_x + bQ_y + c\frac{f_{modulation}}{f_{revolution}} = k \text{ for } a, b, c, k \text{ integers}$$

-By increasing the modulation depth, sidebands start to appear in the FMAs

ΔQ=1e-4

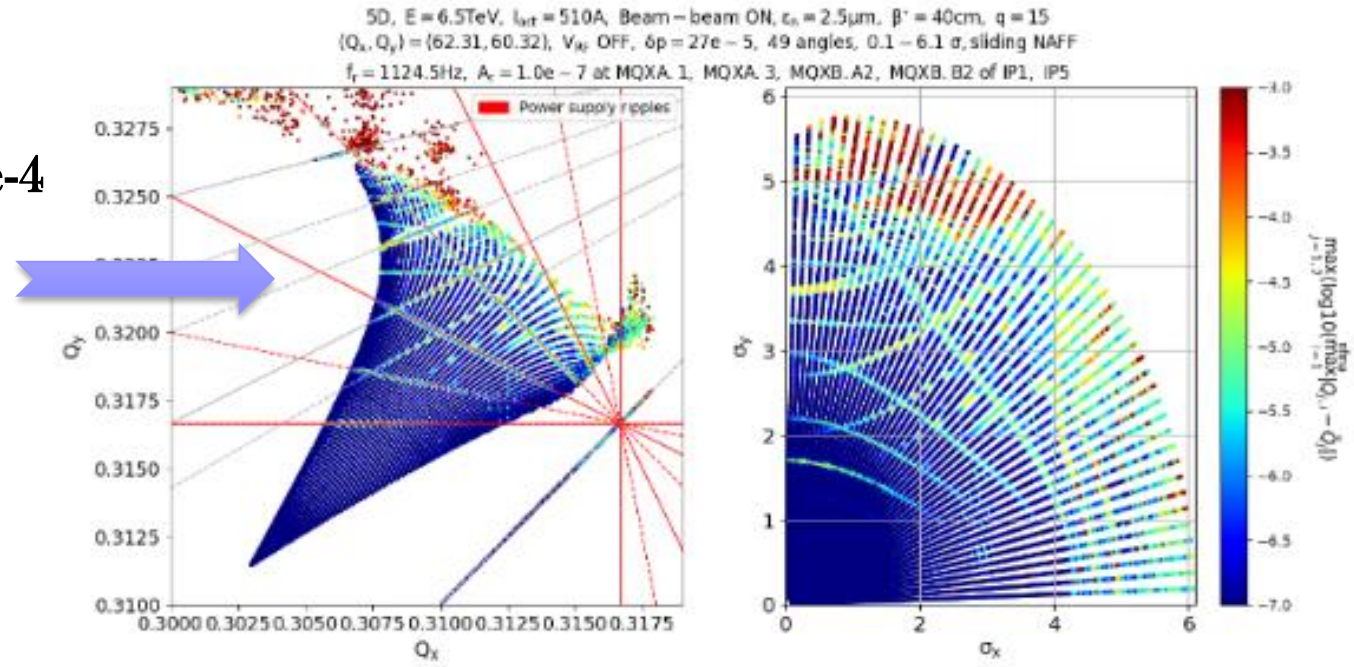

LHC: Power supply ripples

- Scan of different ripple frequencies **(50-900 Hz)**

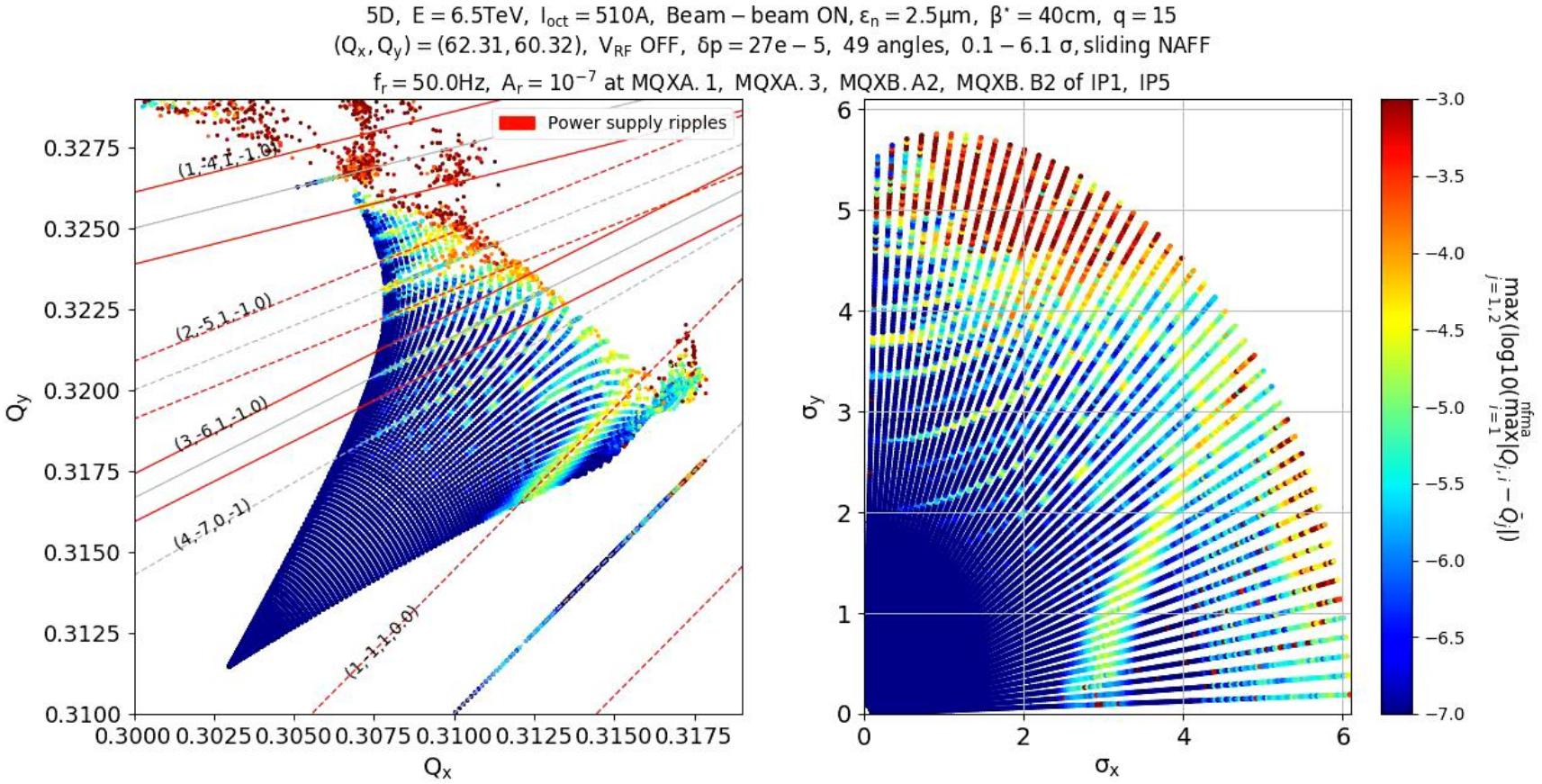

S. Kostoglou, YP et al., 2018

6D FMAs with power supply ripples

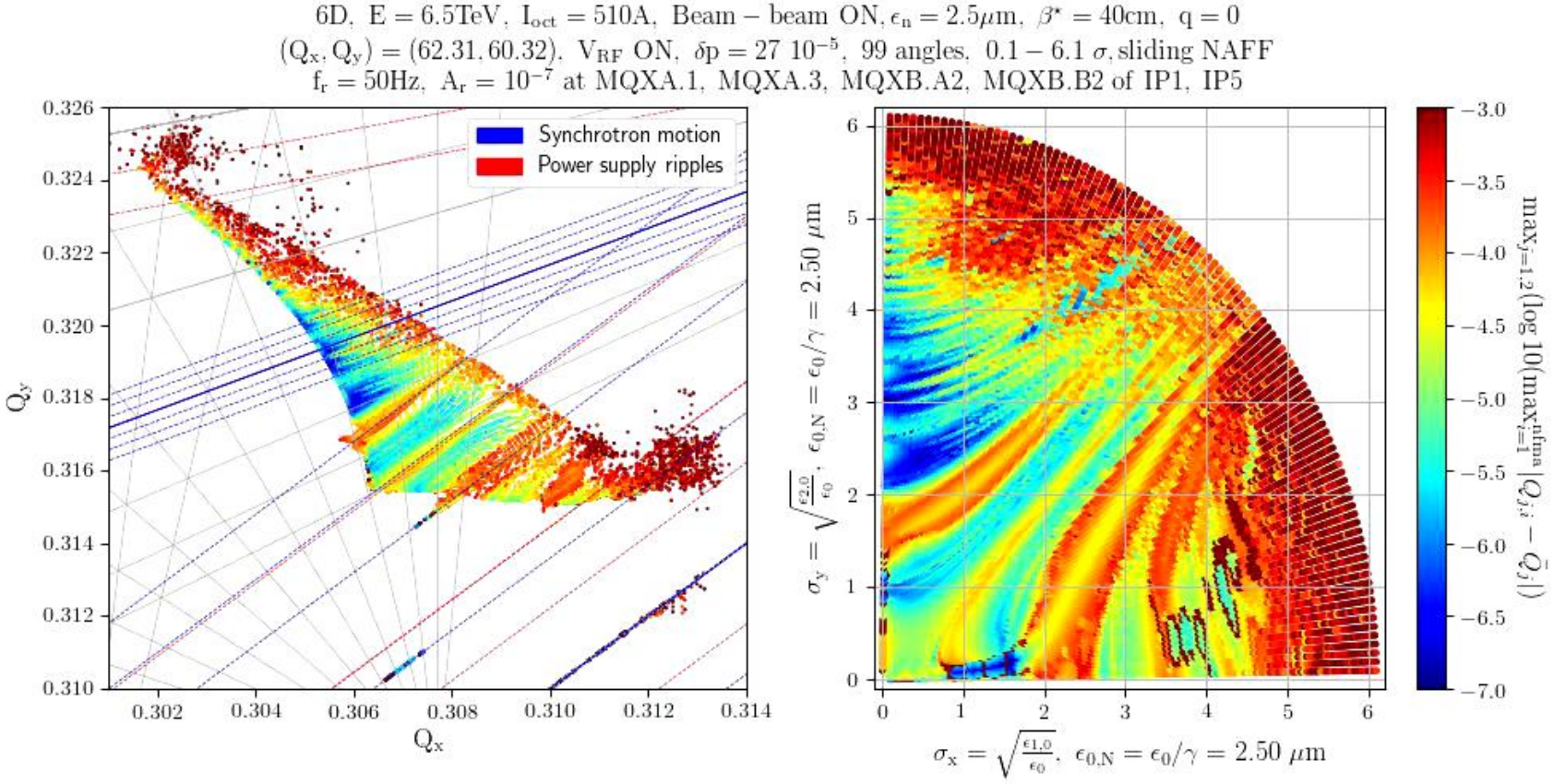

S. Kostoglou, YP et al., 2018

LHC & HL-LHC noise studies

CHALLENGE: chasing the source of the 10^{-3} σ beam oscillations and its impact on beam lifetime.

- 50 Hz harmonics on transverse beam spectrum.
- Harmonics of Beam 1 x2 larger amplitudes than Beam 2.

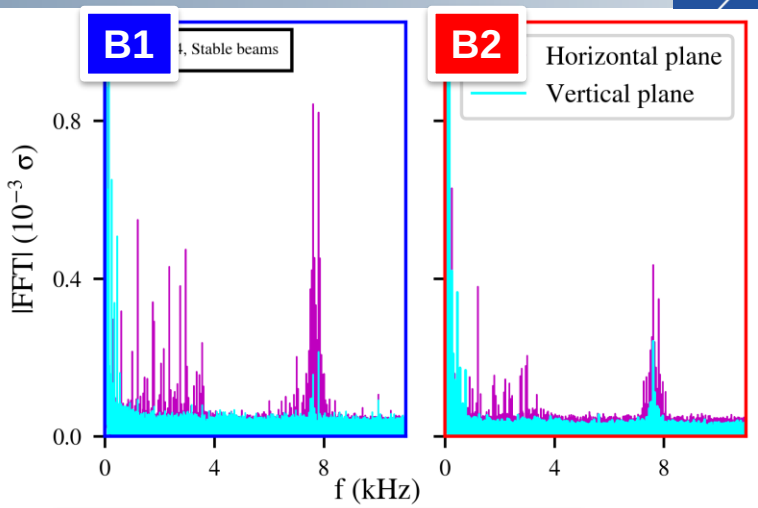

Perturbation source

Power converters of main dipoles: tests with active filters

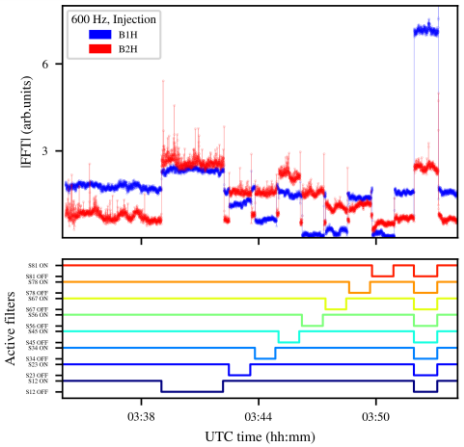

UPS voltage measurements, additional studies in Run 3

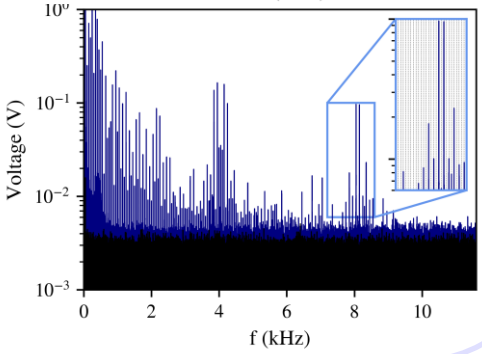

Impact on beam lifetime

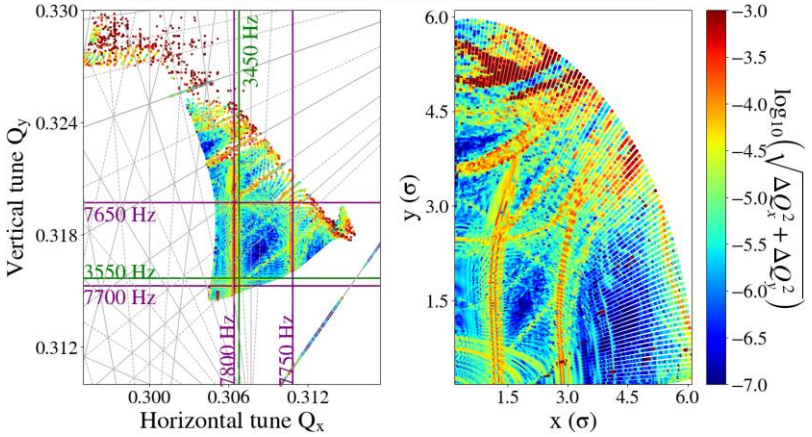

Single-particle tracking simulations: **22h** beam lifetime for Beam 1 and **27h** for Beam 2

S. Kostoglou, G. Sterbini, et al.

Incoherent e-cloud effects at (HL-)LHC

- Analysis of experimental data from **the LHC shows a slow beam degradation due to e-cloud both at injection and in collisions**
- A **development effort** was launched to acquire the **ability of simulating the effect of e-cloud forces within a symplectic tracking code** over the required long timescales (10M turns). The development included:
  - **Theoretical framework**
  - **Tricubic interpolator in sixtracklib tracking code** to apply forces from a recorded pinch in a symplectic way
  - **Software infrastructure to simulate and condition the electron pinches** and setup the simulation from the MAD-X description of the machine
- Presently capable of **simulating 10 M turns** (15 minutes of beam time) by exploiting the computational power of GPUs

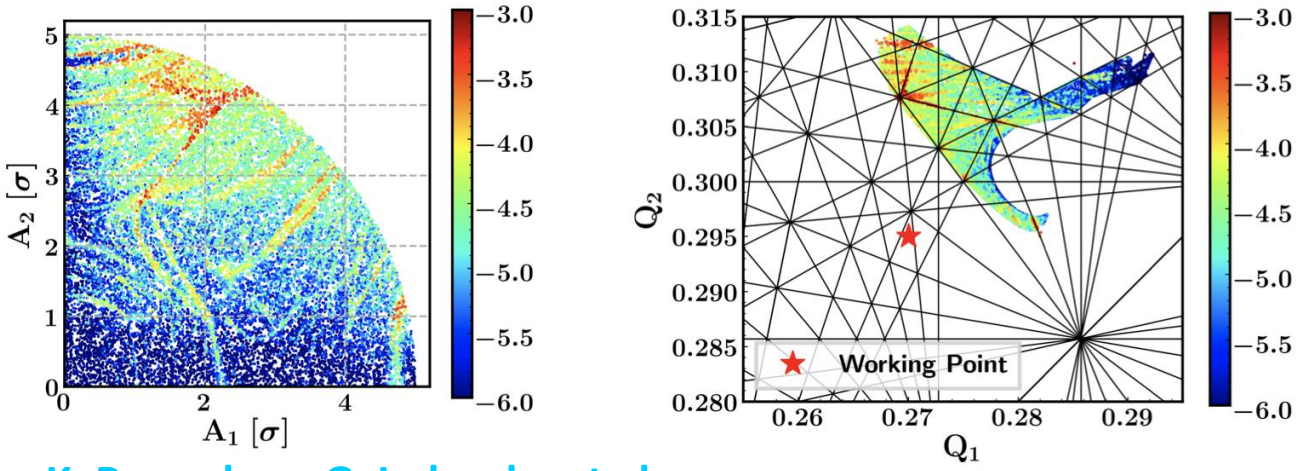

K. Paraschou, G. Iadarola, et al.

Summary

- Appearance of **fixed points** (periodic orbits) determine **topology** of the phase space
- **Perturbation** of unstable (hyperbolic points) opens the path to chaotic motion
- Resonance can overlap enabling the rapid diffusion of orbits
- **Dynamic aperture** by brute force tracking (with symplectic numerical integrators) is the usual quality criterion for evaluating non-linear dynamics performance of a machine
- **Frequency Map Analysis** is a numerical tool that enables to study in a global way the dynamics, by identifying the excited **resonances** and the extent of **chaotic** regions
- It can be directly applied to **tracking** and **experimental** data
- A combination of these modern methods enable a thorough analysis of non-linear dynamics and lead to a robust design

Acknowledgments

Thanks for the material to F. Antoniou, F. Asvesta, H.Bartosik, W. Herr, J. Laskar, N. Karastathis, S.Liuzzo, L.Nadolski, D. Pellegrini, D.Robin, C.Skokos, K. Skoufaris, C.Steier, F.Schmidt, G. Sterbini, A.Wolski, F.Zimmermann